2015

INVESTIGATION INTO THE COMPETITIVE PARTITIONING OF DISSOCIATED H_2 AND D_2 ON ACTIVATED FISCHER-TROPSCH CATALYSTS

Wilson D. Shafer
University of Kentucky, wilson.shafer@asbury.edu

STUDENT AGREEMENT:

I represent that my thesis or dissertation and abstract are my original work. Proper attribution has been given to all outside sources. I understand that I am solely responsible for obtaining any needed copyright permissions. I have obtained needed written permission statement(s) from the owner(s) of each third-party copyrighted matter to be included in my work, allowing electronic distribution (if such use is not permitted by the fair use doctrine) which will be submitted to UKnowledge as Additional File.

I hereby grant to The University of Kentucky and its agents the irrevocable, non-exclusive, and royalty-free license to archive and make accessible my work in whole or in part in all forms of media, now or hereafter known. I agree that the document mentioned above may be made available immediately for worldwide access unless an embargo applies.

I retain all other ownership rights to the copyright of my work. I also retain the right to use in future works (such as articles or books) all or part of my work. I understand that I am free to register the copyright to my work.

REVIEW, APPROVAL AND ACCEPTANCE

The document mentioned above has been reviewed and accepted by the student's advisor, on behalf of the advisory committee, and by the Director of Graduate Studies (DGS), on behalf of the program; we verify that this is the final, approved version of the student's thesis including all changes required by the advisory committee. The undersigned agree to abide by the statements above.

Wilson D. Shafer, Student

Dr. Jack Selegue, Major Professor

Dr. Dong-Sheng Yang, Director of Graduate Studies

INVESTIGATION INTO THE COMPETITIVE PARTITIONING OF DISSOCIATED H_2 AND D_2 ON ACTIVATED FISCHER-TROPSCH CATALYSTS

DISSERTATION

A dissertation submitted in partial fulfillment of the
requirements for the degree of Doctor of Philosophy in the
College of Chemistry
at the University of Kentucky

by
Wilson Davis Shafer
Lexington, Kentucky

Co-Directors: Dr. Burtron H. Davis, Adjunct Professor of Chemistry
Dr. John Selegue, Professor of Department of Chemistry
Lexington, Kentucky

2015

INVESTIGATION INTO THE COMPETITIVE PARTITIONING OF DISSOCIATED H_2 AND D_2 ON ACTIVATED FISCHER-TROPSCH CATALYSTS

By
Wilson Davis Shafer

Dr. Burtron H. Davis
Co-Director of Dissertation

Dr. John Selegue
Co-Director of Dissertation

Dr. Dong-Sheng Yang
Director of Graduate Studies

ABSTRACT OF DISSERTATION

INVESTIGATION INTO THE COMPETITIVE PARTITIONING OF DISSOCIATED H_2 AND D_2 ON ACTIVATED FISCHER-TROPSCH CATALYSTS

The Fischer-Tropsch process, discovered in the early to mid-1920s, still has researchers disputing the C_1 monomer, and the rate-determining step. A tremendous amount of work, over the years, has focused on how hydrogen plays a role in the pseudo-polymerization of chain initiation and propagation, in an attempt to reveal the mechanism. These investigations attempted to elucidate the debated issues through studying the kinetic isotopic effect (KIE) for CO hydrogenation by switching the syngas from CO/H_2 to CO/D_2 during a steady-state period. Applying this switching step could result in a deviation in the rate of CO hydrogenation, indicating a KIE. However, results for this process were still not fully clear as not all observations agreed, which indicated that the KIE could be the result of a combination of how hydrogen interacts thermodynamically (adsorption) and kinetically (CO hydrogenation) in FT synthesis. That is, hydrogen must be activated through dissociative adsorption before interacting in CO hydrogenation. Thus, the primary emphasis of this dissertation is to focus upon how the dissociatively adsorbed hydrogen and deuterium atoms are apportioned upon the surface of an active Fischer-Tropsch Catalyst, pinpointing whether competitive adsorption is muddling the KIE for CO hydrogenation.

Keywords: Fischer-Tropsch synthesis, H-D isotope effect, inverse kinetic isotope effect, cobalt catalyst, iron carbide, nickel catalyst, ruthenium catalyst

Wilson Davis Shafer

12/8/15

TO MY FAMILY AND MY LORD AND SAVIOR, JESUS CHRIST

Acknowledgments

I would first like to thank my mentor, Dr. Burtron H. Davis, for generously providing me this opportunity, permitting me to head back to school for the Ph.D. program while working full-time. I value his patience, encouragement, leadership, and prudence as I dove in to tread the unknown waters of the program. I truly never thought I would be given the opportunity to obtain a Ph.D. while in the hands of such a prestigious scientist.

I also want to thank Dr. John Selegue for his willingness and patience to take on the role of a co-chair of my committee. I absolutely enjoyed and appreciated his chemical erudition, bureaucratic wherewithal, and in-depth musical knowledge. If he had a nickel for every time I called/emailed him about something, he would have enough money to attend several concerts!

I would like to thank Dr. Dong Sheng Yang and Dr. David Atwood for their support and efforts in taking me on as a student, and in being part of my committee.

I want to thank Dr. Gary Jacobs for his continual leadership, pushing me to be better and strive further. I also want to thank him for the endless discussions of music, movies, life, faith, chemistry and… the ever mounting inside jokes!

I also want to acknowledge Dennis Sparks, the one who has to put up with me on a daily basis in the lab, for his willingness to take me in as soon as I got here and give me a wrench allowing me to start building. Being able to bounce ideas off of, and work alongside, one who has such a great amount of integrity and attention to detail has been a definite highpoint.

I also want to thank Dr. Muthu Kumaran Gnanamani and Dr. Venkat Ramana Rao Pendyala for their prudence and veracity as scientists. We started at nearly the same time and have been

working alongside each other for all these years, yet the pleasure is solely mine. Thanks are due for their continual scientific guidance and support even as I have come to distract both of them several times over these past 8 years.

In addition to all the others, my folks, Bubba and Weetie, as a continual force behind this decision and for all that they have sacrificed to get me to this point.

To my babies, Addison and Emery, for providing a joy with no bounds, adding so much enrichment to me life! Lastly, for providing evening entertainment while I studied for my cumulative exams.

Natalie, my partner in crime, you have gotten me through my Masters thesis at EKU and here we are again. I want to thank you for your strength, patience, love, encouragement, and "congrats" when I overcame each hurdle, staying up with me to keep me moving on the late nights, and taking the kids on days I had to keep my nose to the books. Love you baby doll!

Table of Contents

List of Tables

List of Figures

Chapter 1: A General Overview

1.1 A Historical Overview of the Fischer-Tropsch Process

1.1.1 The Groundwork (1899-1926)

In 1912, an incredibly well respected French chemist named Paul Sabatier (1854-1941), as a member of the Paris Academy of Sciences, was nominated and awarded, alongside Victor Grignard (1871-1935), the Nobel Prize in Chemistry [1, 2]. Dr. Sabatier won "for his method of hydrogenating organic compounds in the presence of finely disintegrated metals whereby the progress of organic chemistry has been greatly advanced in recent years [3, 4]."

The culmination of the Nobel Prize developed out of Sabatier's discovery, between 1899 and 1903, of nickel's capability to reduce a series of oxygenated materials (e.g. ketones and aldehydes) [5-7]. Applying the theory behind this new direction of heterogeneous catalysis allowed for a series of novel applications to be investigated, by means of this recently discovered hydrogenation process. The beautiful concept behind this experimentation was that a previously complicated experimental process (without the catalyst) could now be carried out in such a simple manner. The reaction itself consisted of passing an organic reactant as a vapor alongside pure H_2 through a glass tube holding a finely divided metal catalyst, normally heated above 100 ºC (i.e., creating cyclohexane by passing benzene with H_2 across a nickel catalyst) [8]. Sabatier's work also led to the first investigation into synthesizing methane by means of carbon monoxide and hydrogen [9].

Sabatier's work in catalytic hydrogenation swiftly achieved notoriety in the scientific community, which resulted in several nominations for the Nobel Prize in Chemistry: 1907, 1909, and 1911. The focus of his research paved [4, 10] a new route in chemistry that revolved

around the Sabatier-Senderens reduction [9, 11]. From the birth of catalytic hydrogenation came several important processes including the Fischer-Tropsch (FT) process [12].

A more complete historical account of FT can be found in Anderson [13] and Stranges [14]. Franz Fischer (1877-1947) received his PhD at Giessen in 1899, while studying under Karl Elbs (1858-1933), where his research focused upon electrochemistry applications. Subsequently, Fischer ended up working for Emil Fischer (1852-1919) in the field of electrochemistry until about 1911. He had planned on continuing this work by focusing his research in coal-to-electricity by direct means. However, WWI changed Franz Fischer's direction when Germany's lack of petroleum, due to absence of petroleum deposits, became obvious. Germany needed to conceive a new means for producing natural petroleum-based materials, to invent a synthesis process for fuel production from its abundant coal reserves. Though this forced a change in focus, Fischer began to examine the BASF process patented by Badische Anilin-und Soda-Fabrik, a process by which CO is catalytically reduced to hydrocarbon-based materials mainly comprised of alcohols, esters, ketones, and aldehydes. The BASF process, again because of WWI, was halted. However, Fischer decided to explore this process anyway, alongside Hans Tropsch (1889-1935), investigating this catalytic reaction at different pressures, temperatures (not going above CO decomposition, $2CO \rightarrow C + CO_2$), and different hydrogen/carbon monoxide (syngas) ratios. They began their process by reacting coal with steam to create syngas, then by passing the syngas across a catalyst at low pressures and temperatures (ranging from 180 to 200 ^{o}C), synthetically assembled hydrocarbon-based materials (synthetic fuels) with more than one carbon.

During the early 1920s, Fischer and Tropsch focused their work on a high-temperature range (above 400 °C), producing mainly oxygenated materials (esters, ketones, fatty acids, etc.),

coined as "synthol," and virtually no hydrocarbons. During the latter half of the 1920s, both the physical conditions and the catalyst were changed. Temperatures were dropped to less than 300 °C, and the primary active catalysts were first iron-cobalt-based and later iron-copper-based. This led to the synthesis of mainly hydrocarbon-based materials with virtually no oxygenated materials present in the product mixture [15, 16].

1.1.2 1926-1945

Fischer continued laboratory-scale research until the 1920's, when the dependence upon petroleum-based materials in Germany inflated, creating a continual escalation for the need of synthetic fuels and driving expanded research in the FT process. Fischer developed a small pilot-scale reaction in 1932, followed by a larger pilot plant in 1934. These plants were plagued by several issues, including heat removal, the catalysts' short lifespan (mainly due to sulfur poisoning), and significant loss of active metals. As a result, research shifted to focus on the more expensive cobalt-based catalyst and was based at Oberhausen-Holten. During the mid-1930s, a few years after the Nazi Party gained power, petroleum independence was at the forefront of the party's objectives. Given the importance of the FT process and direct coal liquefaction developments for Germany's energy independence, these processes became a major contribution to Adolf Hitler's Four Year Plan of 1936: *"Accordingly, German fuel production must now be stepped up with the utmost speed and be brought to final completion within 18 months. This task must be attacked and carried out with the same determination as the waging of a war; for on its solution depends the conduct of the future war and not on the laying in of stocks of petroleum* [17]." Germany's desire for energy independence allowed development of several large FT plants with annual production rates of 100,000-120,000 metric tons of material.

The standard FT catalyst, given its greater activity and lower reaction temperature, was the cobalt catalyst (100Co-5ThO_2.8MgO-200kieselguhr) developed by Otto Roelen (1897-1993). Overall production peaked at the outbreak of WWII in September 1939 at 5.4 million barrels per year (740,000 tons of liquids).

1.1.3 Post-WWII

Even though the Nazi Party wanted petroleum independence and did so by vastly increasing the amount of production, the Second World War took its toll. Bureaucratic confusion, material shortage, and lack of a workforce lowered production in the FT plants. In the end, when the German nation fell, production plunged because most of the plants were either completely dismantled or leveled by allied bombing. Synthetic fuel production was suspended because of the Potsdam (Babelsberg) Conference of July 16, 1945, which prohibited any production to occur [18]. Adding insult to injury, a short-lived agreement was made to dismantle 4 coal hydrogenation plants in the western zones by the British [19, 20].

During the 1950s and 1960s, the Fischer-Tropsch process was not heavily researched, as WWII had come to a close and petroleum research as a whole decreased. An exception to this trend was that in 1955, SASOL built one of the first main FT plants developed outside of Germany in Sasolburg, South Africa [21].

During the Arab-Israel War in the early 1970s, an oil embargo was placed on the United States and several other allied countries that supported the Nation of Israel [22]. This led to a shift in the global financial balance to the oil-producing countries, causing prices for petroleum-based materials to spike. This led to several economic issues related to the dependency upon petroleum, and shifted the focus to alternative measures. The sticker shock of the oil embargo

caused the German Document Retrieval Project, led by Richard Wainerdi and Kurt Irgolic with Texas A&M University's Center for Energy and Mineral Resources, to commence in October, 1975 [22-24]. The staff at the height of the project consisted of 12 full- and part-time members retrieving the documents. Interest came not only from universities, but from industries as well, i.e., Dow Chemical Company, Diamond-Shamrock Corporation, and Union Carbide. The undertaking, initially set as a three-year task, ended prematurely. The fact that the US, Canada, Russia, and England retrieved old process documentation 30-40 years later, in hopes to carry on Germany's previous research, is a sound indication that the Germans were well ahead of their time. Though most of the documentation remains uncovered, over 310,000 pages were found, and 75,000-100,000 pages refer directly to coal gasification.

The Fischer-Tropsch process is still alive and abundant today with large plants all over the world. Locations of current FT plants are displayed in Figure 1.1. The largest plant, put

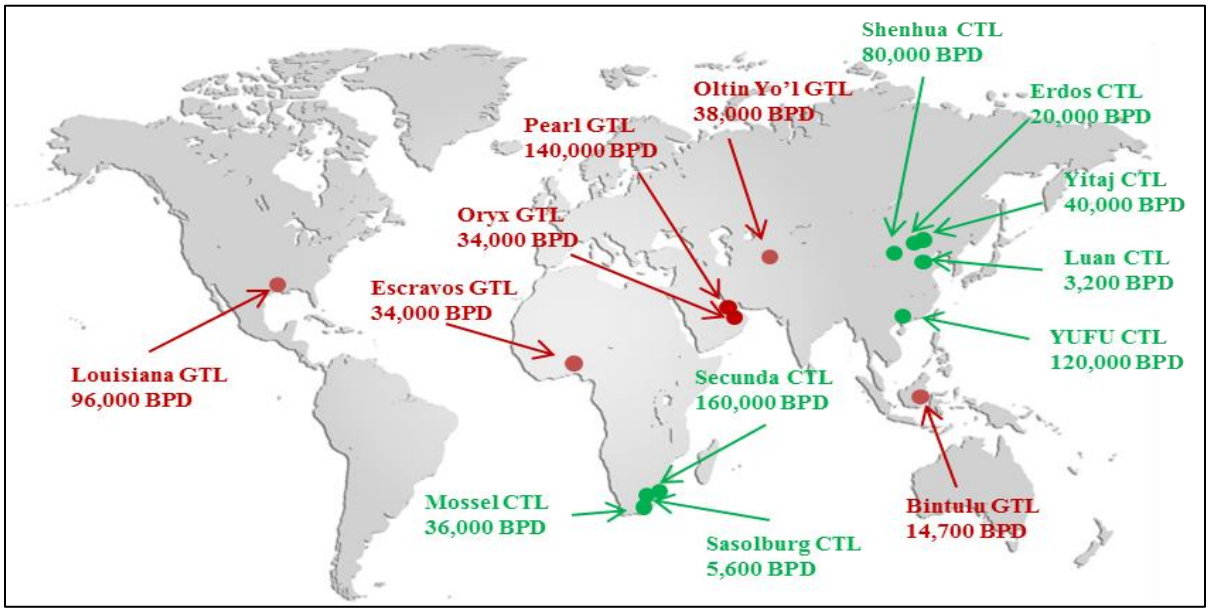

Figure 1.1: A global distribution of plants utilizing the FT process either by means of the CTL (coal-to-liquids) or GTL (gas-to-liquids) process measured in BPD (barrels per day) produced.

online in 2011, is the Pearl GTL (a partnership between Shell and Qatar), which produces 140,000 barrels per day of the FT synthetic fuels. SASOL now has multiple FT plants in South Africa, and several are coming online in China, as a means to convert coal to FT liquids. Provided above is a very brief account of the historical impacts attributed to this process over its 90 years of being online. Beyond the included references, there exists a vast amount of literature revolving around the historical impacts brought on by the FT process [25-29].

1.1.4 The Full Picture

The FT synthesis is a pseudo-polymerization process and one of the key steps in the Gas-to-Liquids (GTL) [30-32], Coal-to-Liquids (CTL) [33-36], and Bio-to-Liquid (BTL) [37-39] processes, as displayed in Figure 1.2. There are essentially three key steps for the entire

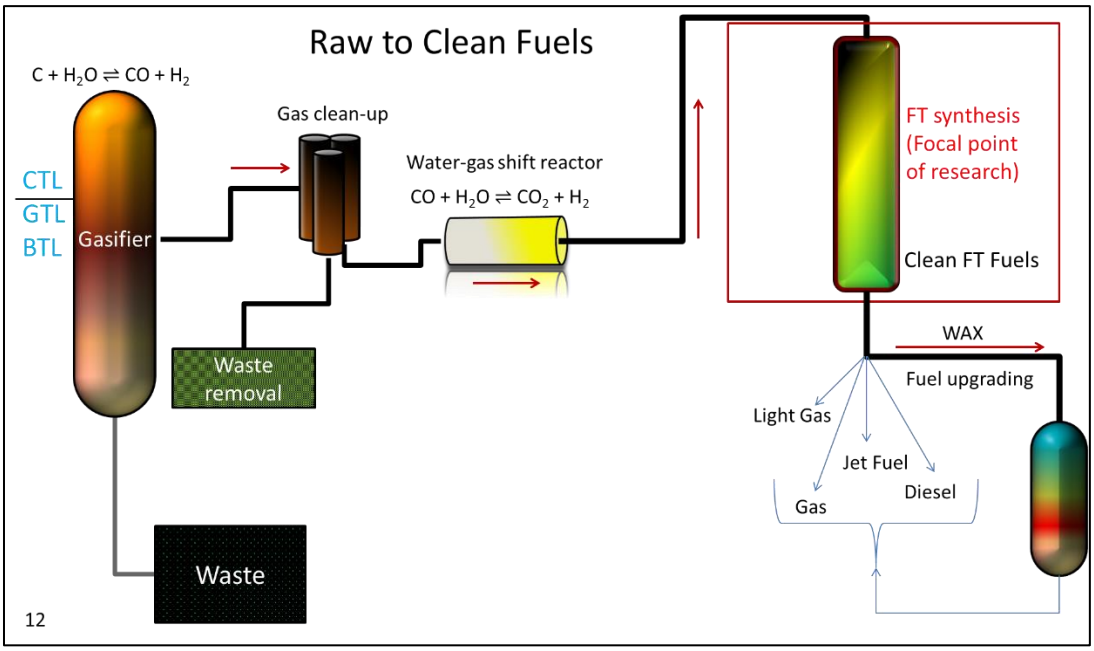

Figure 1.2: A simplified diagram of the CTL, GTL, and BTL processes.

process. The first step of these raw materials-to-liquid fuels (RTL) is the formation and cleaning of the syngas. The raw materials go through a process called pyrolysis, or gasification, to first generate the syngas. Unlike combustion, gasification is a very endothermic process ($\Delta H \approx 131.0$ kJ/mole) so to overcome the thermodynamic limitations, the procedure itself is conducted at around 1500 °C. The actual chemistry depends on which process is used. Discernibly, these equations, as they are displayed, do not include all of the extraneous components, such as

$$\text{CTL/BTL} = C + H_2O \rightleftharpoons CO + H_2 \text{ at a 0.7 ratio of } CO/H_2O$$

$$\text{GTL} = CH_4 + H_2O \rightleftharpoons CO + 2\ H_2$$

heteroatoms (i.e., sulfur, nitrogen), metals, and CO_2. Hence, to obtain the needed clean syngas, a cleanup procedure needs to be applied. Again, only a brief overview is given here as there is a vast amount of literature involving the specific experimental gasification conditions and procedures [40, 41].

Depending on the original carbon source, the off-gas from the gasification process could contain several components that need to be removed, including metals, sulfur compounds (i.e., COS, H_2S), CO_2, and nitrogen compounds (i.e., HCN, NH_3). The primary factors for the syngas cleanup are the unwanted sulfur molecules and CO_2. Sulfur is most important to eliminate as it irreversibly binds to the FT catalyst and thus becomes detrimental to the entire RTL process. The CO_2 needs to be removed for two main reasons: environmental concerns and the fact that its presence will affect the Water-Gas-Shift (WGS) conversions.

The WGS shift system (if needed) is a hydrogen-upgrading process that is needed to

$$H_2O + CO \rightleftharpoons H_2 + CO_2 \qquad \Delta H = -34 \text{ kJ/mole}$$

boost the overall H_2/CO ratio, mainly in a CTL/BTL process. The chemical reaction is an equilibrium synthesis. Therefore, the more CO_2 that is allowed to pass from the gasification process and gas cleanup, the more the WGS reaction will be driven back to the reactants, suppressing the overall yield. This process, though an important step, is not always needed; e.g., when natural gas is used as the carbon source in the GTL process. This is also the case in the CTL/BTL process, when iron is used as the active component, since iron performs WGS and FT synthesis simultaneously. Again, as there is a tremendous amount of information regarding the WGS system and conditions in the literature, the intent here was mainly to give an overview of one place it is commonly used [42-44].

Once the syngas has been made, cleaned, and upgraded (if needed), it passes into the FT system to create a large range of hydrocarbons, depending on the catalyst utilized in the process. The next few sections will go into further detail about the FT process, so this will be omitted here.

The last component in the RTL process is the fuel upgrading, mostly by means of hydrocracking of the waxes down to higher-octane-based materials. The raw synthetic resources that are derived from the FT synthesis are very high-cetane-based materials. This is a high-quality, clean fuel for diesel engines, but in turn, very low-octane. The hydrocracking process can turn these high-cetane waxes, which are created from the FT synthesis, to higher-octane material, as normally hydrocracking and hydroisomerization go hand-in-hand [45].

This simple overview has highlighted not only the significance of the history of the FT process, but also the important role it plays in the overall production of synthetic fuels today.

1.2 Fischer-Tropsch Overview

1.2.1 The Basic Chemistry

As mentioned previously, the FT synthesis is a pseudo-polymerization process [15, 16], where the starting materials are two simple diatomic molecules, hydrogen and carbon monoxide.

$$(2n+2)\ H_2\ (g) + CO\ (g) \rightarrow C_nH_{2n+2} + n\ H_20\ (l)$$

The span of materials that are synthetically produced from the FT process, however, is quite large, with hydrocarbon products typically ranging from methane up to C_{70} [46, 47]. The severity of the conditions (temperature, pressure, space, and velocity), the type of reactor, and the catalyst composition can deviate the range of products to solely methane or can produce methane as less than 5 mole % of the product, where the bulk of the product is wax. Though FT synthesis generally follows a polymerization process, the known reactants are not the building block, as the C_1 monomer is still unknown [48-51]. Otherwise, the FT process stepwise relates closely to the polymerization process:

1. During chemisorption of the reactants (the syngas), the H_2 goes through a dissociative adsorption (will be discussed later as this is the main portion of the thesis) and CO does dissociate, but this is another point of contention between scientists.
2. An initiation of chain growth starting from the $*C_1$ monomer occurs.

3. The carbon chain is then propagated (again, length will depend on several factors).
4. The chain is eventually terminated.
5. The final product irreversibly desorbs from the metal (disregarding secondary reactions).

The scope of the polymerization process for a product range can be described by a simple polymerization model developed by Anderson et al. [52] and independently developed by Schulz [53] and Flory [54] called an Anderson-Shultz-Flory (ASF) plot. The ideal distribution can be expressed by the following equation (equation 1) and is the most conventional model used to date:

$$\frac{M_n}{n} = (1-\alpha)^2 \alpha^{n-} \quad (1)$$

where M_n/n is the mole fraction of a hydrocarbon with carbon number n and α is defined as the chain growth probability. Alpha (α, equation 2) is defined by the rate at which the chain propagates (r_p) versus the rate at which it terminates (r_t).

$$\alpha = \frac{r_p}{(r_p + r_t)} \quad (2)$$

The basis for the ASF polymerization model assumes the hydrocarbon chain lengths are independent of one another, and, thus, solely depend on r_p and r_t. Therefore, the distribution of FT products can then be theoretically created in a linear fashion by plotting the natural log of

the mole fraction as the dependent variable *y*, and the carbon number as the independent variable *x*, as displayed in Figure 1.3 for a typical cobalt catalyst.

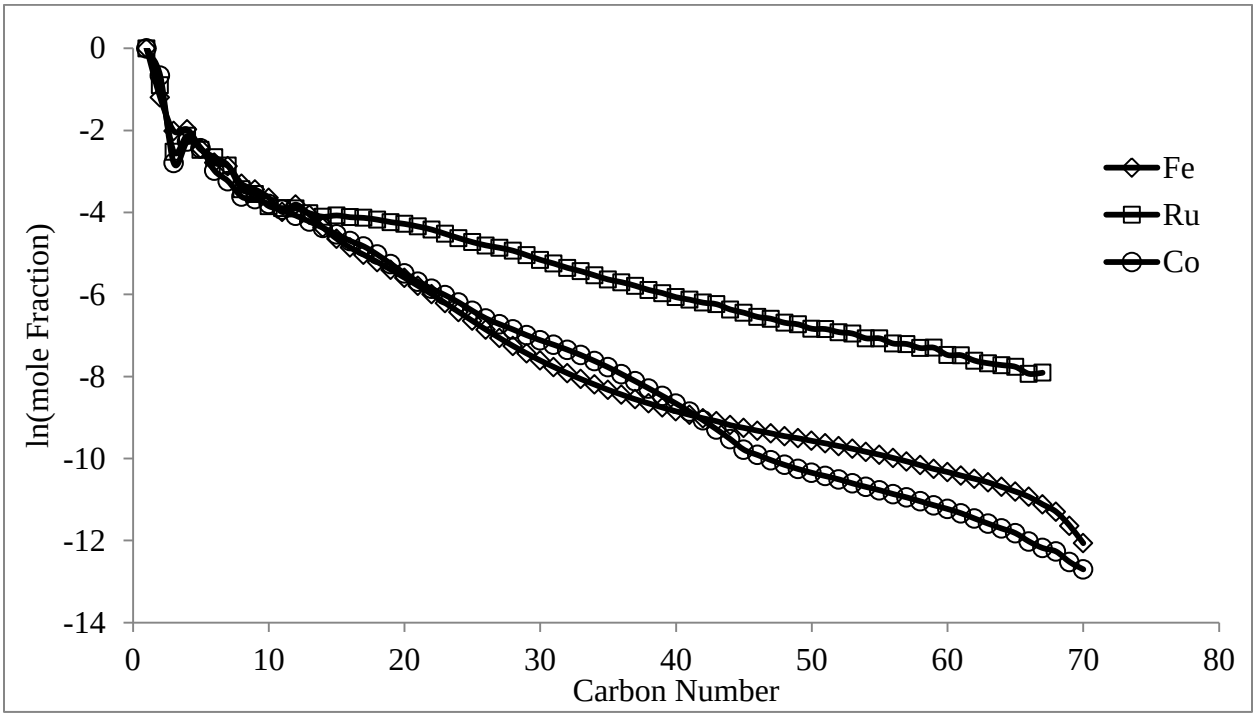

Figure 1.3: An ASF plotted by the natural logarithm of the mole fraction for a cobalt, ruthenium, and iron FT product distribution.

The ASF polymerization model can be a great tool when theoretically ascribing a range of hydrocarbons to assess transversely through a series of catalysts portraying certain characteristics. More importantly, trends can be displayed in attempting to understand promoter, support, and reactor effects on the FT synthesis through the deviation provided by the ASF model. Figure 1.4 provides an overall viewpoint for an expected distribution for specific alpha values, and creation of this plot is now common practice.

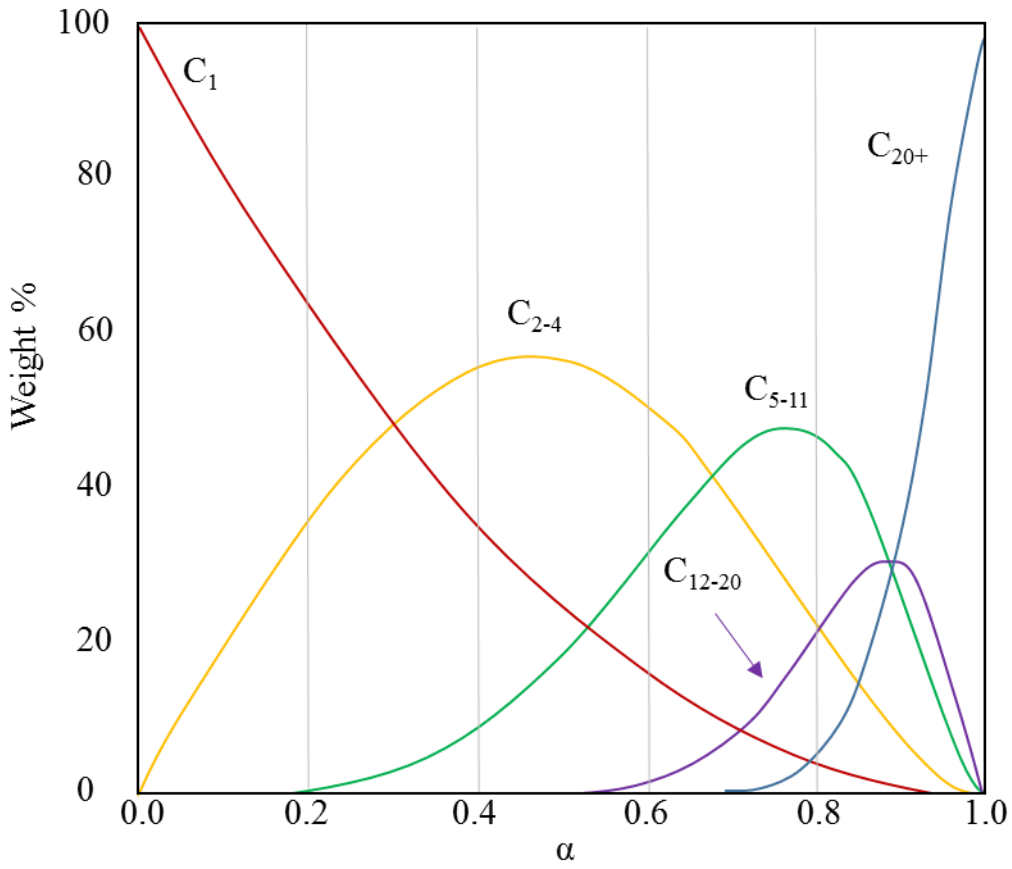

Figure 1.4: A distribution of products based upon α.

Depending on the active metal, most active FT processes are fashioned to be in a range where the bulk of the materials produced fall at or above α = 0.8. Considering that the idea behind this process is to create longer-chain hydrocarbons, there is essentially no reason to create a very low-α catalyst where the bulk of the products are simple natural gas.

1.2.2 Common FT Active Metals

As mentioned, the four most active metals for the FT synthesis are cobalt, iron, ruthenium, and nickel. However, cobalt and iron are the only two viable for practical operating

conditions due to nickel's excessive methane production and the high price/low availability of ruthenium [55].

Iron has the highest earthly abundance and is therefore the cheapest at around $97 per ton. Of the different active metals, iron is the preferred choice for industrial use when coal and biomass are the carbon source. During the gasification process, given the high abundance of naphthalene-based materials, the CO/H_2 ratio effluent is less than one, and typically closer to 0.7. The low level of H_2 in the exhaust of the gasification is sufficient for iron, because unlike any of the other FT metals, iron can increase the H_2 ratio through in-situ WGS. Iron is also different in that iron carbide, not the metal itself, is the active species. In addition, iron carbide alone is a very low-α catalyst, and normally an alkali promoter, such as potassium, is added to increase the dissociation of CO, allowing the alpha to increase [56-57]. Copper is normally added as a promoter as well, to enhance the reducibility of the iron catalyst [58].

Cobalt is the other primary active metal for a large-scale RTL process, namely the GTL process. Cobalt, unlike iron, does not have the intrinsic capabilities for WGS and cannot handle the low H_2/CO ratios. The pyrolytic degradation of natural gas (CH_4) allows for a 2:1 H_2/CO ratio, ordinarily required for FT synthesis when cobalt is employed as the active FT component. Cobalt is typically supported on materials such as Al_2O_3, SiO_2, and TiO_2 [59], where good interactions between that active metal and supports exist. This is a fine balancing act, since a poor interaction can cause the cobalt particles to sinter, leading to a decrease in surface area, an increase in the unwanted product of methane, and a decrease in the overall activity. However, if the interaction between the support and the cobalt is suitable and the particles are fine, much higher temperatures are required for reduction. Given the importance of the interaction between the active cobalt metal and its support in determining the longevity of the synthesis, promoters

such as platinum are commonly used to alleviate the high temperatures required for cobalt reduction [61].

1.2.3 Mechanism

Primary products per carbon number accounting for greater than 95 mole of C% for the products synthesized from the FT process are as follows: the terminal alcohol, 1-olefin, paraffin, trans-2-olefin, and cis-2-olefin. To give an idea of the considerable arrangement of products, Figure 1.5 displays a chromatographic picture of merely the oil phase (excluding gas, aqueous, and wax) for the distribution of products for cobalt, iron, and ruthenium FT catalysts. As noted in the flame ionization detector (FID) scan, the relative amounts of each major component vary significantly depending on the catalyst used. Compounding the selectivity is the sensitivity to the physical properties of the process (e.g., temperature, pressure, H_2/CO ratio) and the type of reactor (slurry or fixed-bed). Deviations in the product distribution between these conditions can complicate the olefin/paraffin (O/P) ratio [61-65] through reinsertion to hydrogenate, isomerize or to initiate chain growth [47, 66, 67].

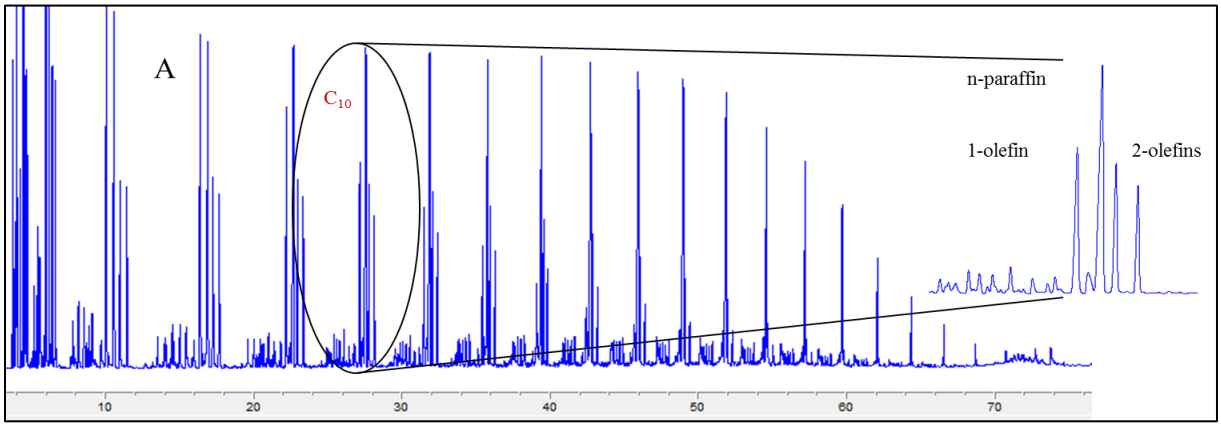

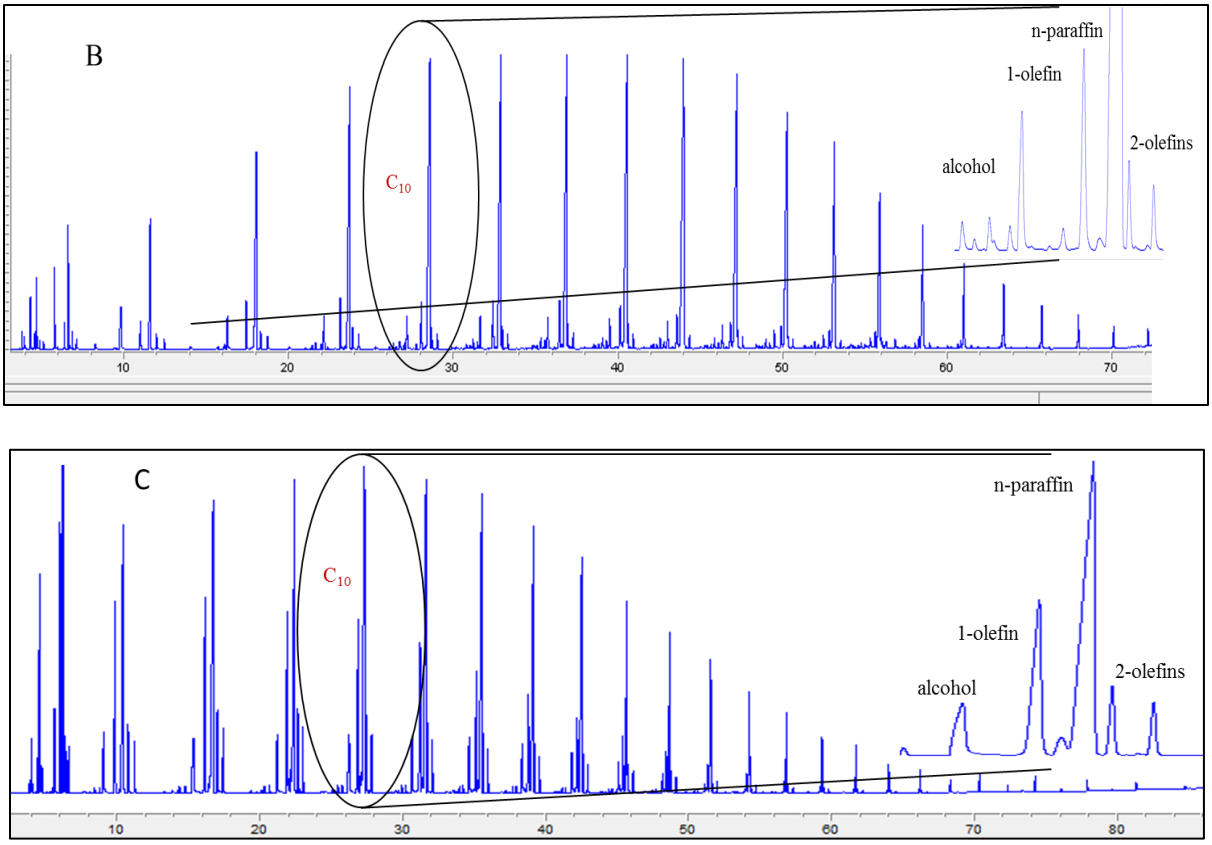

Figure 1.5: FID chromatographs for the products of the oil phase for cobalt (A), iron (B) and ruthenium (C) FT catalysts.

Hydrocarbon chain lengths also vary the olefin/paraffin ratio as heavier products accumulate due to decreasing vapor pressure, in slurry-based FT systems. As residence time increases proportionally so does reinsertion; thus, an inverse relationship arises where the longer the hydrocarbon chain, the lower the O/P ratio (as *n* increases, O/P decreases). This attribute can be visually described by Figure 1.5, principally in iron, where the olefin material decreases more rapidly in the FID chromatograph.

Bearing in mind the lengthy products consisting of aliphatic molecules, the FT synthesis could be investigated as the building of molecules through a multi-step reaction. However, all the intermediates remain bonded to the surface and can only be observed, and if surface specific

compounds are noted, they could be considered intermediates, or just onlookers. As mentioned prior, several steps need to occur in the synthesis route by the addition of hydrogen, going from a CO bond(s) to a C-C bond:

- associative/dissociative adsorption of CO (remains a point of contention)
- dissociative adsorption of hydrogen (the subject of this thesis)
- splitting of the CO bonds
- transfer of 2 H* atoms to O* to form H_2O
- allocation of 2 H* to C* to form (CH_2)
- formation of a new C–C bond (unless methane is formed)
- desorption of H_2O
- desorption of aliphatic product

This list is a guide, but the specific order for all the given steps still eludes researchers. Obviously, for aliphatic materials to be synthesized, CO will need to dissociate. A case in point is the following, describing complications of certain steps in the CO adsorption [68]:

1. Does CO molecularly adsorb, or dissociatively adsorb?
2. If CO does molecularly adsorb, does dissociation require hydrogen assistance?

Adsorption studies of carbon monoxide on metal surfaces are vast given these complications, and this is arguably the most studied catalytic reaction [69-83].

Fischer, discerning that the synthetic route involved formation of aliphatic carbon hydrogen bonds, and knowing the carbide tendencies of iron, first proposed the carbide mechanism as seen in Figure 1.6.

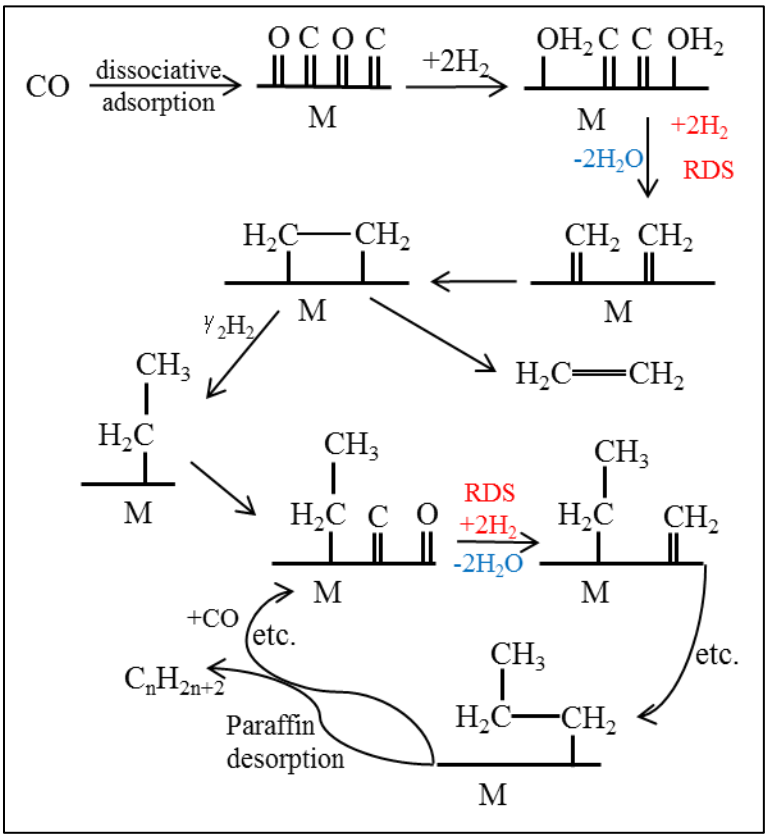

Figure 1.6: A proposed synthetic route for FT by means of the carbide mechanism.

Although this mechanism was promoted by Fischer, this was not his first choice; he did not favor the carbide mechanism until results displayed hydrocarbons as the primary products for FT synthesis [84]. Although this mechanism was set aside for a brief period, recent advances in surface science displaying ample surface carbon and no surface oxygen revived the idea that hydrocarbon products could be built through the combination of methylene groups [85-89].

The carbide mechanism follows the idea that CO dissociatively adsorbs upon the active FT metal, covering the surface with carbon and oxygen atoms. The adatoms are sequentially hydrogenated, forming water and the methylene monomers. The quasi-equilibrium assumption for the dissociation and hydrogenation of CO lies within the first hydrogenation step; the second is rate-limiting. [90].

Fischer first proposed an oxygenated mechanistic route for the FT synthesis as very little aliphatic material was generated; i.e., products were mostly comprised of alcohols. Although the carbide mechanism gained ground after being proposed by Fischer, work done by Kummer and Emmett [91, 92], noted more in Section 1.3.1, gave rise again to the oxygenated mechanism [93]. A detailed example within Figure 1.7 is currently known as the enol mechanism.

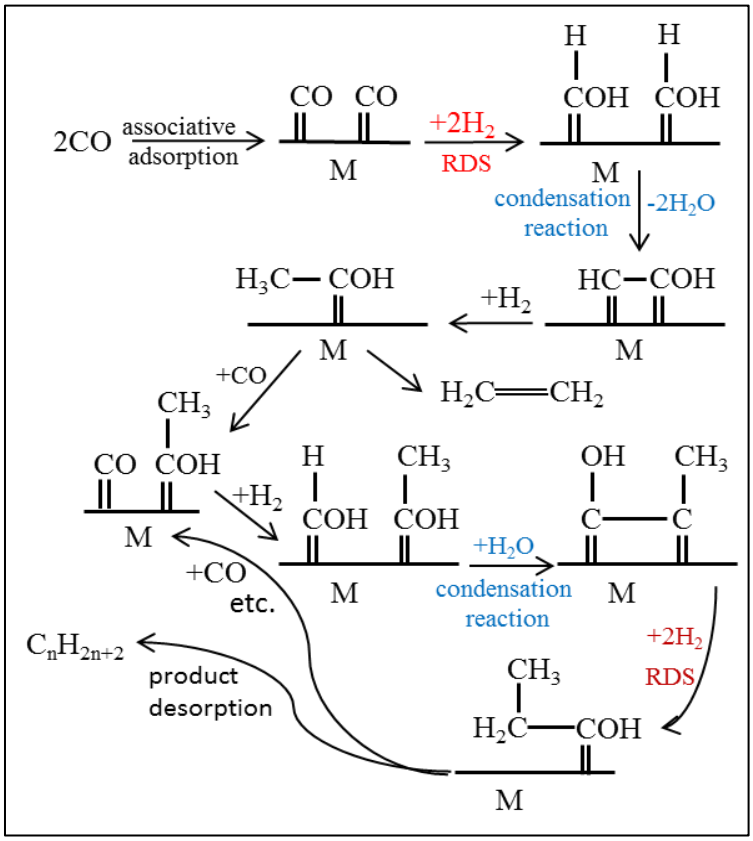

Figure 1.7: The proposed enol mechanism.

This mechanism describes CO adsorbing without dissociating upon the FT active metal surface. After chemisorption, CO reacts with adsorbed H atoms to create hydroxymethylene (M-CHOH). The enol structure grows by a sequence of condensation steps using adjacent groups. This mechanism describes a route where the rate-controlling step is the first carbon hydrogenation, whereas the other mechanisms are the assumed at a quasi-equilibrium state.

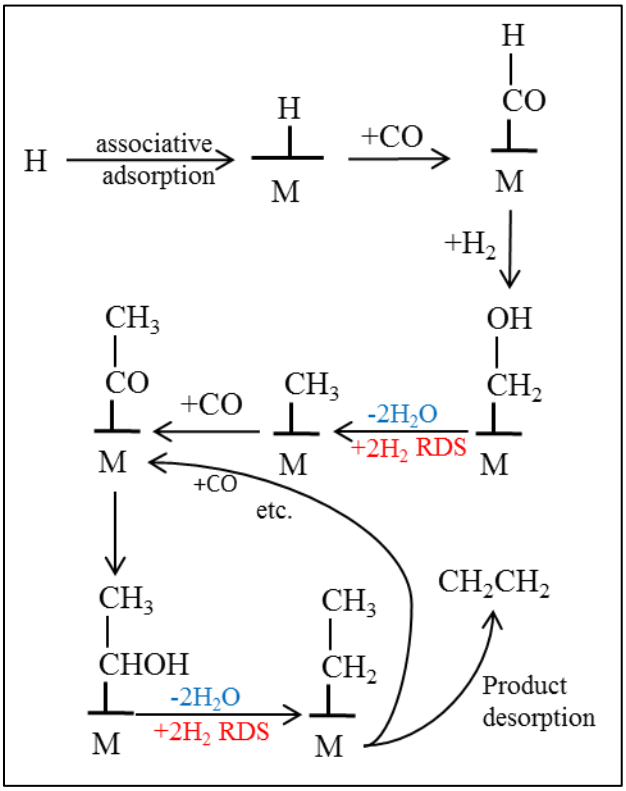

Figure 1.8: The CO insertion proposed mechanism.

Another commonly proposed mechanism is CO insertion [94]; displayed above in Figure 1.8. Unlike the previously mentioned synthesis route, CO is molecularly adsorbed onto the active catalyst and goes through hydrogen-assisted dissociation only after chain incorporation. Again, the proposed rate-limiting step is the hydrogenation of CO to the CH_2 methylene group. The

assumed monomer for this mechanism is simply CO through insertion into metal-carbon bonds. Adding vigor to this mechanism, migratory CO insertion is a common step in homogenously catalyzed reactions such as hydroformylation [95].

1.3 Isotopic Tracers

1.3.1 Carbon

To elucidate the complete FT mechanism, researchers employed isotopes such as ^{2}H, ^{18}O, and ^{14}C as tracers. As mentioned, some of the earliest ideas about chain growth came from the carbide characteristics of the active metal, e.g. iron. This practice was followed as an attempt to understand the FT mechanism, until some work done by Kummer et al., while working under Dr. Paul Emmett, disputed this route. Their work changed the mechanistic ideology of FT by experimentally demonstrating the assumed intermediate was not the metal carbide [91, 92].

Emmett came across ^{14}C during his tenure on the Manhattan Project, and in the late 1940s started using this carbon radioisotope to probe the FT mechanism. The experimental idea was relatively simple and could be used to determine if CO proceeds through a metal carbide intermediate before being reduced to methylene groups, where hydrocarbons are built by the combination of methylene monomers across the metal. Given the presupposed hypothesis where carbide was presumed as the intermediate, creating a radiolabeled carbide surface with ^{14}C followed by running FT with unlabeled syngas ($^{12}CO/H_2$) would reveal the surface participation if the FT process [91].

Four catalysts were screened: three were iron (two pure iron oxide prepared by two different methods, and the third $Zr/Fe/Al_2O_3$) and the last was a cobalt-thoria-kieselguhr

(100:18:100) catalyst. The catalysts were first reduced under H_2 at specific temperatures, followed by the carburization with the labeled carbon monoxide at 200–270°C, and then the monitoring of the CO_2 (used to determine CO consumption). The FT system was set up in a batch mode at atmospheric pressure, allowing the consumption of syngas to occur, and the pressure was held constant by raising the mercury in the burette. Methane, hydrogen, and carbon monoxide were measured separately. The methane was burned to CO_2 and converted to barium carbonate to be counted in a scintillation counter. The radioactivity that was evident in the product stream (i.e., methane) was found to be less than that of the radioactive gas used in the carburization process. Additional work was completed to ensure the results were not affected by exchange between the products and the carbide phase. In these sets of experiments, using ^{14}C as a tracer, the bulk of the aliphatic materials were assembled through an "unknown" process, though a small portion could possibly have been assembled through the carbide intermediate (Figure 1.9).

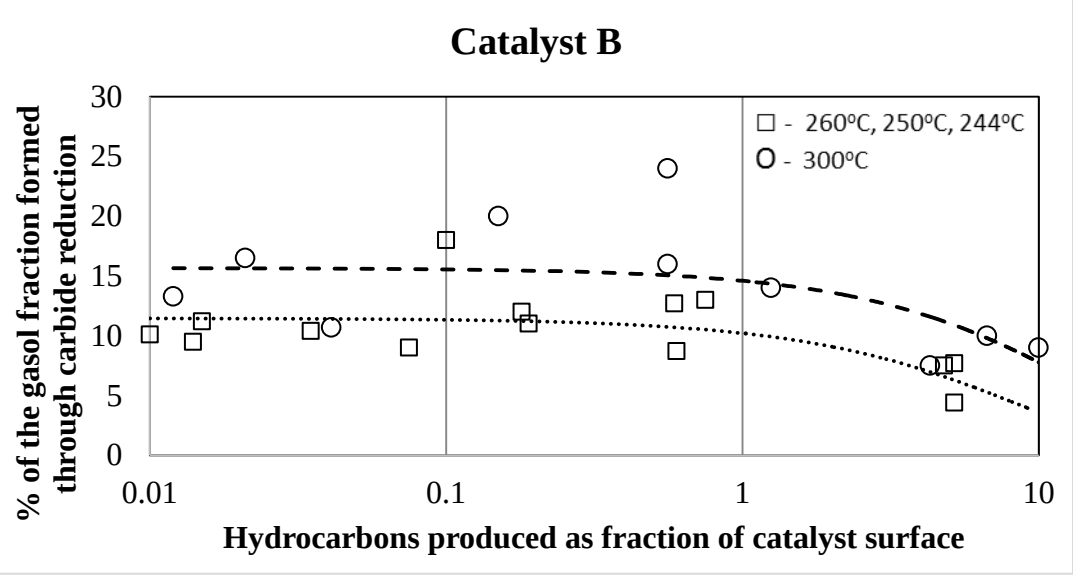

Figure 1.9: The percent of ^{14}C formed through carbide reduction;
redrawn from Emmett et al. [91].

This work set forth a vast number of experiments that are still being undertaken today as a means of understanding the complicated process of CO adsorption and hydrogenation. The fact that there are still competing proposed mechanisms more than 90 years after the introduction of the FT process demonstrates how truly complex it is.

This work provided information that agreed more with some of the ideas set forth by Elvins and Nash, as the C_1 monomer is more of a C-H-O (formyl) complex at the surface site [96, 97]. Their reasoning for this is the carbide by means of CH_2 additions across the metal, where C and O dissociating first could not explain the alcohols that were forming from the FT reaction. In turn, Emmett and co-workers again used ^{14}C as a tracer, not with CO but with ethanol. If the complex, as described by Elvins and Nash, revolved around C-H-O, then incorporation of simple oxygenated materials such as ethanol would allow for one to trace reaction products. The incorporation of ethanol with the syngas allowed for a description of products to be observed [92]. Ethanol adsorbed into the chain growth process and affected a range of C_3 to C_{10}, as noted in Figure 1.10.

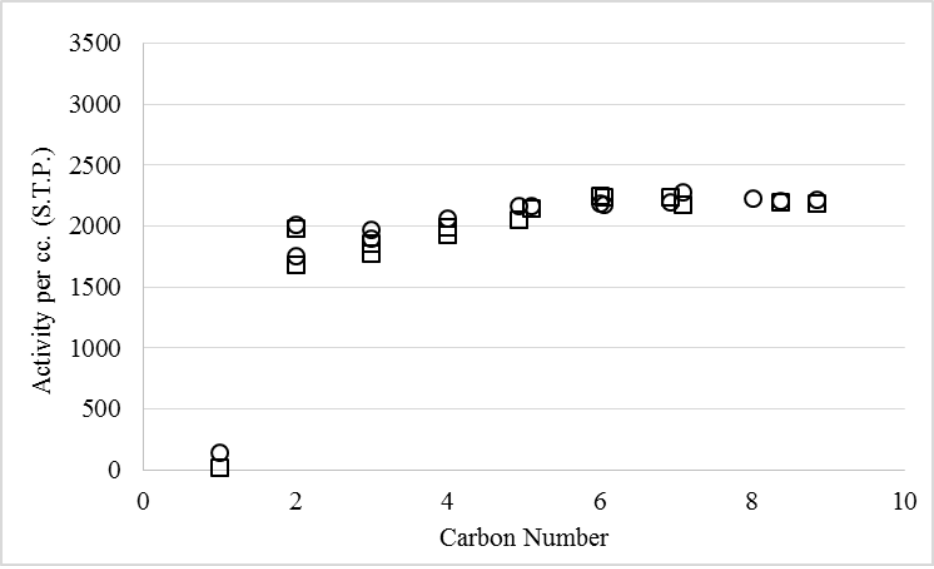

Figure 1.10: Results from the adsorption of the ethanol species, redrawn from Emmett et al. [92].

Ethanol (the adsorbed compound resulting from ethanol) is incorporated into the FT process as a chain initiator. This work by Emmett using isotopic tracers gave a window into the occurrences of the FT process. In addition, the consistency of activity provided per carbon number revealed that this process is not random between the adsorbed ethanol species and the carbon species on the metal surface. Note that this incorporation is an alcohol onto an iron catalyst, and alcohol does not incorporate as readily into a cobalt FT system. In turn, olefins incorporation also became evident, but is more active with the cobalt-based FT catalyst than with iron. As before, the work led to a vast host of other isotopic tracer incorporation experiments using carbon-14 and carbon-13, more so than can be described here [51].

1.3.2 Hydrogen

Considering the focal point of this thesis, in the interpretation of hydrogen and its stable isotope deuterium, the remaining discussions will revolve around this topic. Two main experimental designs have utilized hydrogen as a means to probe the FT mechanism. The first revolves around the ASF plot, in an attempt to understand the polymerization process, i.e., primary versus secondary reactions. Certain reactors, such as laboratory-scale continuously stirred tank reactors and plant-sized slurry reactors, are known to accumulate products (Figure 1.11), causing deviations from the known ASF plot. The second main experimental design for the utilization of hydrogen and its isotope also peers into the mechanism by probing the rate-limiting step for the kinetic process of CO hydrogenation.

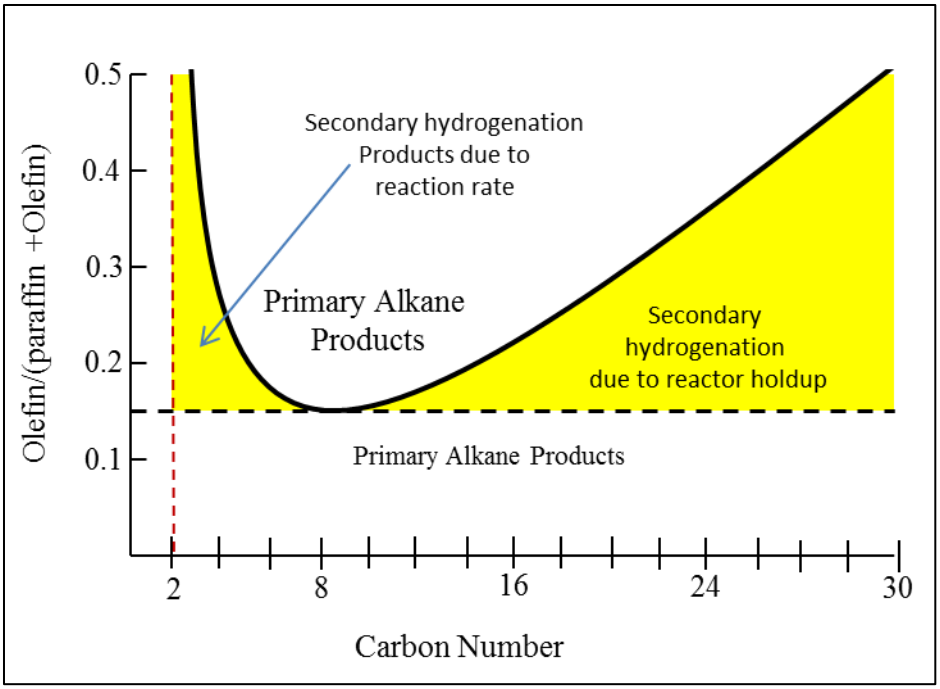

Figure 1.11: Comparison of the olefin versus total hydrocarbon production, redrawn from Buchang et al. [47].

1.3.2.1 Primary Product Distribution

As mentioned, FT products theoretically follow the ASF model described by equation 1. A semi-logarithmic plot of the mole fraction as the independent variable versus the carbon number will give a linear plot with a negative slope. However, experimental evidence has shown several variances from the theoretical model, deviating from a straight line, as displayed in Figure 1.12. These types of deviations are normally only seen in a slurry-based reactor system, where the products will only leave as a vapor and the heavier liquids need to be extracted online. Some H_2/D_2 exchange work has been performed to specifically describe this type of issue for a slurry-based FT system. [98-100].

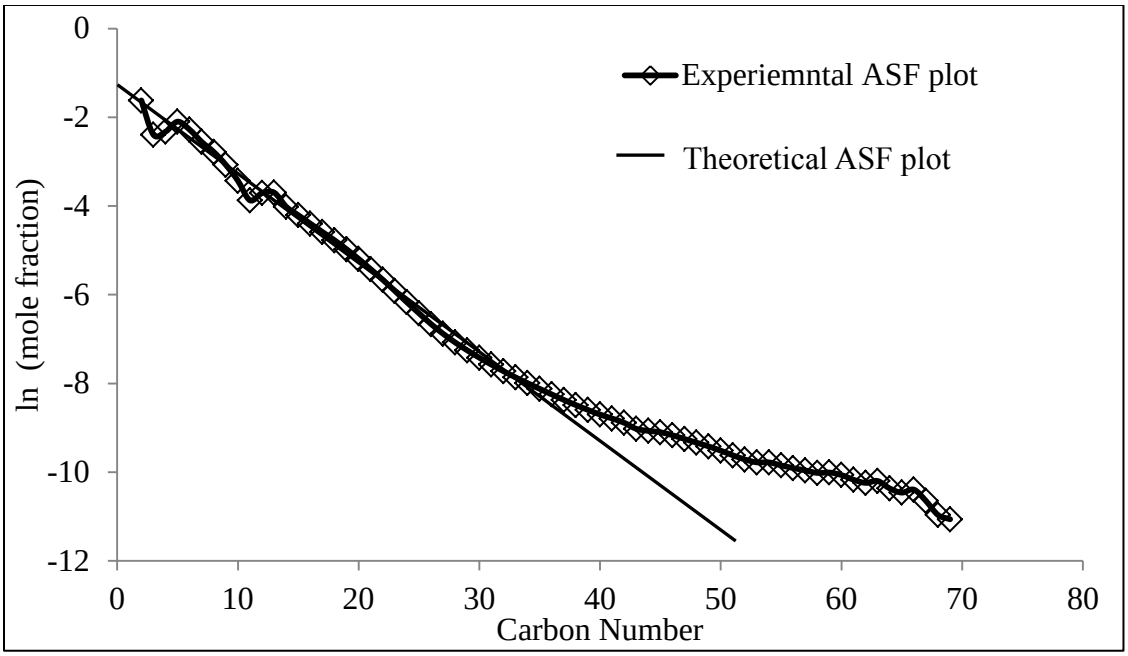

Figure 1.12: The comparison between a theoretical and experimental ASF plot to display experimental deviations from the ASF model.

The primary thermodynamic product for the FT process is methane, though several irreversibly formed products throughout the entire distribution (i.e., the *n*-paraffin, C_nH_{2n+2}) can be considered additional primary products. In addition to the primary products, secondary products exist, such as oxygenated materials, olefins, and some branched hydrocarbons. For example, as displayed in Figure 1.12, the line for the entire distribution at C_3 and above, C_1 and C_2 products normally deviate where C_1 is high and C_2 is low. C_1, as the main thermodynamic product, has been described as forming at different active sites for all the longer C-C bonded hydrocarbons [101, 102]. The reason given for the unusual decrease in the C_2 is ethylene's ability to reincorporate back into the FT chain growth process. These types of deviations from the theoretical ASF model have been attributed to a flurry of theories:

- Two chain growth probabilities [103-105]
- Vapor phase equilibrium (VLE) [100, 106, 107]
- Olefin reabsorption [107]
- Chain length desorption issues [108-110]
- Intensive observables
    - Pressure
    - Temperature
    - SV

Given the variety of proposed theories, a method for uncovering the true reason for this deviation includes the use of hydrogen isotopic tracers. Allowing a switch from H_2 to D_2 during the time-on-stream (TOS), for a brief period, has brought some insight into the FT product distribution [98-100].

1.3.2.2 Kinetic Isotopic effect

The present research utilizes the idea of switching between H_2 and D_2 during the FT reaction, while monitoring the rate at which CO is converted to hydrocarbons. This experimental design, in an attempt to understand the kinetic isotope effect (KIE, which will be defined in the next section) for CO hydrogenation, has been performed several times; though most describe an inverse kinetic isotope effect (IKIE), not all have agreed [111-124]. The confusion brought upon these experiments by the difference in the KIE is not something that this work is attempting to solve. Yet, discovering if a KIE is present in the competitive

adsorption could be a means to potentially understand if the thermodynamic process of adsorption is affecting the results for the KIE in CO hydrogenation.

1.4 Kinetic Isotopic Effect

1.4.1 Theoretical Concept

The KIE can be an invaluable tool to aid in the understanding of specific reaction rates, mechanisms, and solvent effects. Specifically, the KIE can be defined as the dependence of the reaction rate upon a reacting molecule's isotopic composition. There are several different classifications of KIEs:

1. Primary kinetic isotope effect – This occurs when the isotopic bond (either made or broken) is involved with the rate-determining step
2. Secondary kinetic isotope effect – This occurs when the isotopic bond (either made or broken) is not involved with the rate-determining step (this could be more correlated to a change in hybridization, i.e., a sp^2 carbon to a sp^3 as displayed by the Diels-Alder reaction)
3. Normal Kinetic Isotopic Effect – This occurs when the rate of the lighter isotope is faster, e.g. $k_H > k_D$.
4. Inverse Kinetic Isotopic Effect – This occurs when the rate of the heavier isotope is faster, e.g. $k_H < k_D$.

These rates can be dependent upon the isotopic difference within a phenomenon called zero point energy (ZPE). The ZPE is the lowest possible energy a quantum mechanical, physical

system may contain. From this, the energy difference between the lowest energy level (where n = 0) and the lowest point on its isotopic-specific effective point (based upon the Born-Oppenheimer approximation, or BOA) can be calculated. Essentially all bonds have a series of quantized vibration levels with specific energies (E_n) given in equation 3, where n is the

$$E_n = (n + 1/2)\, h\nu \tag{3}$$

quantum level, and h is Planck's constant. These are dependent upon the frequency ν of the bond stretch as given in equation 4, where μ is the reduced mass and k is the force constant.

$$\nu = \frac{1}{2\pi}\sqrt{k/\mu} \tag{4}$$

In turn, equation 4 is dependent upon the atomic mass given in equation 5, connected at each end (assuming a diatomic molecule like H_2 or D_2), where m_1 and m_2 are atomic masses (H, D, or

$$\mu = \frac{m_1 m_2}{m_1 + m_2} \tag{5}$$

M). Theoretically the ZPE (Figure 1.13) is where n = 0, thus from equation 1, E_n = 1/2 hν. Even at the ground state, molecules such as H_2 and D_2 will vibrate at a certain frequency, as given by the experimental ZPE for H_2 = 4161 cm^{-1} and D_2 = 2993 cm^{-1}[115].

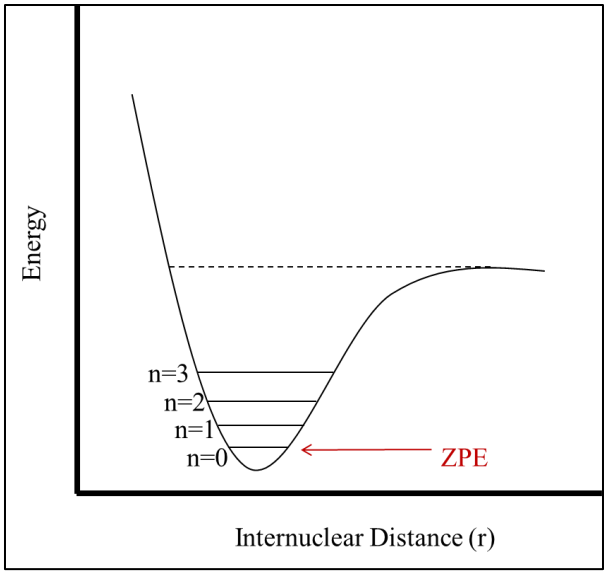

Figure 1.13: The location of the ZPE in a potential energy well.

As displayed by the experimental frequency mentioned, the ZPE energy for deuterium would be lower, since this energy can be related directly to the atomic mass, where ν is inversely proportional to mass. Adding this concept to Figure 1.13, Figure 1.14 theoretically describes the ZPE energy levels for both isotopes.

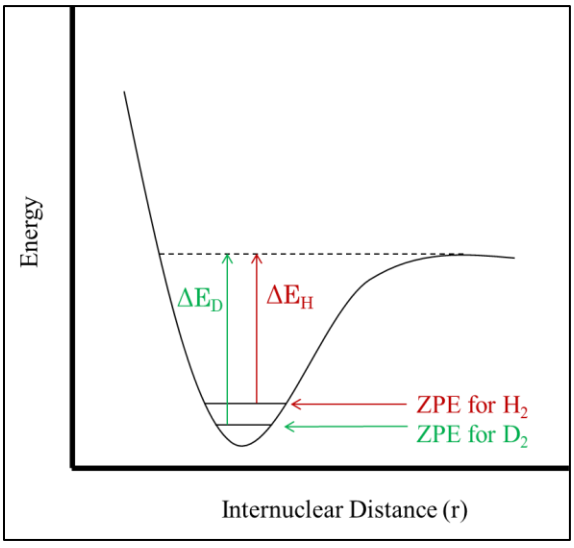

Figure 1.14: A theoretical plot illustrating the potential energies of deuterium versus hydrogen.

Although Figure 1.14 provides a theoretical difference between the H and D ZPE energy curves, it does not display the full picture. The bond formation for the hydrogen is also needed; in this case the formation will be to carbon.

Figure 1.15 provides a graphical analysis of this potential energy expression and portrays the basic isotope effect analysis. Superimposing the ZPEs (Figure 1.14) allow for the two isotopically substituted reactants to be displayed on the potential energy surface of the reaction. This surface gives the activation energies of the two reactions, which help in finding the rate constants.

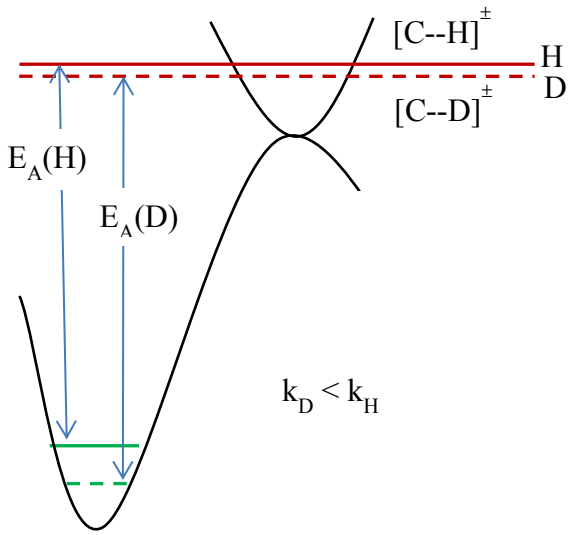

Figure 1.15: A theoretical plot providing a full picture of the difference in ZPEs between the ground state and the transition states for competitive hydrogen/deuterium adsorption.

Lastly, taken from Figure 1.15, the KIE can be used to determine where the ZPEs are playing more of a role, either through the formation of the bonds or the breaking. Specifically, the KIE is defined by the rates of H (k_H) and D (k_D) during the process either though the bond

breaking or formation, given by equation 6 where k_H and k_D are the rate constants for H and D, respectively.

$$KIE = \frac{k_H}{k_D} \tag{6}$$

From this, the given energy barrier between the ground state and the transition state can be ascribed to the Arrhenius equation for the activation barrier for each separate isotope (equations 7 and 8), where A represents the Arrhenius constant, E is the activation energy, R is the ideal gas constant, and T is temperature.

$$k_D = A_D e^{-Ead/RT} \tag{7}$$

$$k_H = A_H e^{-Eah/RT} \tag{8}$$

Next, by substituting equations 7 and 8 into equation 4 and making the simplifying assumption that the Arrhenius constant for H and D is equal, i.e., $A_H = A_D$, we can start defining the KIE by the separate activation barriers for each isotope.

$$KIE = \frac{e^{-E_{aH}/RT}}{e^{-E_{aD}/RT}} \tag{9}$$

Equation 9 can then be simplified further by using an essential identity for the exponential where $e^x/e^y = e^{(x-y)}$. Thus, equation 9 can be rewritten as

$$KIE = e^{-(E_{aH} - E_{aD}) / RT} \quad (10)$$

The energy described in equation 8 is the potential energy given by a bond formed by two atoms vibrating together. This relationship can be described by the quantum approximation called the harmonic oscillator. The energy equation that is used to describe this relationship is equation 1, where *n* must be equal to zero. It is important to remember the energy given in equation 8 is the activation energy, and therefore can be described as the difference in ZPE for the reactant and the transition state. Lastly, the potential energy given can be separated by isotopes for H_2 (equation 11) and D_2 (equation 12) accordingly,

$$E_D = (1/2)h\,(\upsilon^{\dagger}_D - \upsilon^{0}_D) \quad (11)$$

$$E_H = (1/2)h\,(\upsilon^{\dagger}_H - \upsilon^{0}_H) \quad (12)$$

where $\upsilon^{\dagger}$ is the ZPE transition state frequency and υ° is the ZPE for the ground state frequency. Lastly, equations 11 and 12 can then be substituted into equation 8 to give equation 13 a

$$KIE = e^{[-(1/2)h(\upsilon^{\dagger}_D - \upsilon^{\circ}_D) - (1/2)h(\upsilon^{\dagger}_H - \upsilon^{\circ}_H)] / kT} \quad (13)$$

frequency relationship for each isotope where Planck's constant can be converted to Boltzmann's constant *k* (not to be confused with the spring constant *k* or the rate constant in

future discussions). This in turn can then finally be simplified down to equation 14, as a way to

$$KIE = e^{[-(1/2)h(\upsilon^{\ddagger}_{H} - \upsilon^{\ddagger}_{D}) - (\upsilon^{o}_{H} - \upsilon^{o}_{D})] / kT} \quad (14)$$

the describe difference in the expected IKIE and the normal kinetic isotope effect (NKIE) where the over all KIE equation can be illustrated.

Consequently, by disseminating equation 14 down to the frequency components, it can be shown that if $\Delta\upsilon^{\neq} > \Delta\upsilon^{o}$ the entire equation would end with the KIE = $e^{-x} < 1$. However if $\Delta\upsilon^{\neq} < \Delta\upsilon^{o}$ then the KIE = $e^{x} > 1$. Thus, if the frequency difference in the transition state is larger than in the ground state, equation 14 would be positive, displaying a normal KIE. However, if the opposite is observed, then the exponential will be negative, displaying a value less than one as described by the IKIE. Figure 1.16, a basic visual representation of this concept, displays the theoretical potential energy well activation energy (E_a) and the transition step.

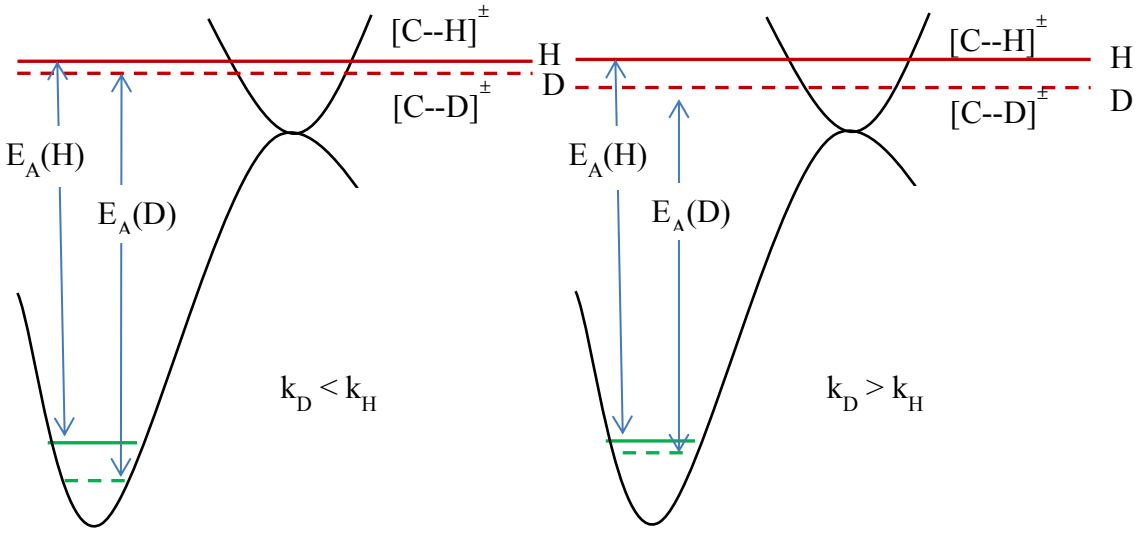

Figure 1.16: Visual representation of the difference between an NKIE (left) and IKIE (right).

These transition steps can be locally applied to different steps along the FT mechanistic pathway, such as H_2/D_2 to the adsorbed H^*/D^*, or the H^*/D^* to the CH/CD bonding from C*O.

Lastly, based upon the Hammond postulate, the transition state will most resemble the molecule where the smallest energy difference occurs. Therefore, the position of the transition state on the reaction coordinate, thus the KIE, will depend upon the thermodynamic difference in energy between the products and reactants. However, given that the focus of this work is with the FT process, Figure 1.16 displays an exothermic process where the reactants more resemble the transition state.

1.4.2 KIE of Hydrogen Isotopic with an FT System

Experimentally, the concept behind the H_2/D_2 switching experiment is to synthetically keep all of the components of the FT system as a control, allowing the only variable to be a switching between hydrogen and deuterium. An example route is displayed in Figure 1.17.

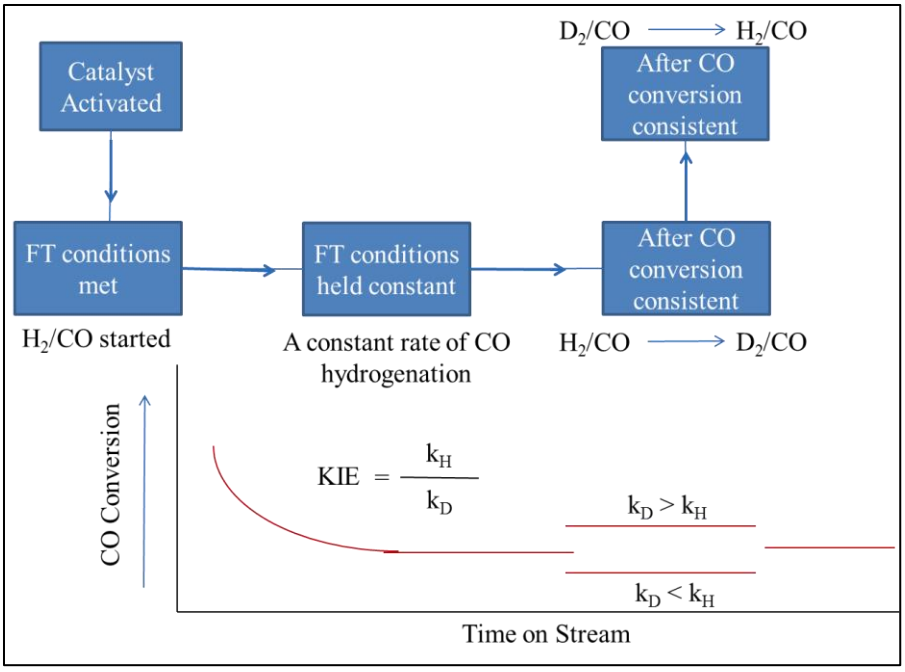

Figure 1.17: A general cartoon describing the experimental KIE switching investigation for CO hydrogenation.

The experimental design in Figure 1.17 can be conducted separately for each of the active FT metals, as long as the conditions remain the same throughout the switching process. For example, if a cobalt catalyst is to be used for the KIE switching; several steps need to be taken before switching can occur. Activations and FT schemes for pressure and temperature, space velocity (SV), will vary pending on the reactor system, the active metal, and the catalyst characteristics (i.e., the supports and promoters used). A platinum-promoted cobalt/alumina would be activated by H_2 at 350 $^{\circ}$C and atmospheric pressure. After activation, the catalyst needs to be brought up to FT conditions and held for a period of time. Care must be taken when switching from activation conditions, especially regarding the temperature of the FT system.

After the period of activation, the system can be cooled to below the FT-active temperature range and switched to syngas, where in a cobalt system the H_2/CO ratio would need

to be 2. The FT reactor can then be slowly brought up to the desired pressures and temperatures for an effective FT range. Care is then taken to monitor the CO hydrogenation rate, by examining the methane content and then changing SV accordingly to ensure CO conversion remains low. The cobalt system is more active in the first 24 hours and then will drop for a brief period of time, after which the cobalt FT rate (the rate at which CO is converted to hydrocarbons) becomes consistent. The SV needs to be decreased allowing CO conversion to be close to 50%. Considering the exchange possibilities, WGS, and secondary reactions, the rate of FT is monitored by CO, not hydrogen. The CO conversion can be calculated by equation 15, where CO_{in} is the inlet flow, and CO_{out} is the flow of CO in the effluent.

$$\text{CO Conversion} = \frac{CO_{in} - CO_{out}}{CO_{in}} \qquad (15)$$

After a period of Time-on-Stream (TOS), say 24 hours, has occurred and the FT system is stable (i.e., the CO conversion for H_2/CO, the pressures, the temperatures, and SV are all consistent) then the switch to deuterium from hydrogen can occur. The switch to deuterium only needs to occur for a brief period of time, enough for the desired number of reactor turnovers, allowing for a few samples to be taken at these conditions before switching back to hydrogen. This ensures that if a change in the FT rate is noted, the only variable is the change between hydrogen to deuterium. If the FT rate has dropped, then once the switch back to hydrogen occurs, the rate should increase back to the previous results.

1.5 Competitive Adsorption

1.5.1 Hydrogen Adsorption

Given hydrogen as a single-electron system, one should expect this atom could provide a straightforward chemical-reacting adsorbate. Even the overall reaction, essentially the adsorption of hydrogen upon a fixed metal surface (M), seems to be straightforward. Yet the

$$M + {}^{1}/_{2}\, H_2 \rightleftharpoons MH$$

amount of surface science literature describing the process for hydrogen adsorption poses considerable complexity. As a case in point, data provided solely for three transition metals (Ru [125-139], Ni [140-157], Fe [158-167]) display a tremendous amount of effort in attempting to understand the progression of H adsorption. Yet, before a discussion of adsorption can take place, a few details need to be put into place to distinguish it from the other molecular solids:

1. The small size of the molecule (H–H distance is 0.74 Å)
2. The spherical shape of the atom
3. The existence of two stable isotopes with masses differing by a factor of 2
4. The two spin states of hydrogen; ortho (symmetric) and para (antisymmetric)
5. The low electron density.

The adsorption of H_2 upon the metal surface can be portrayed visually with Figure 1.18.

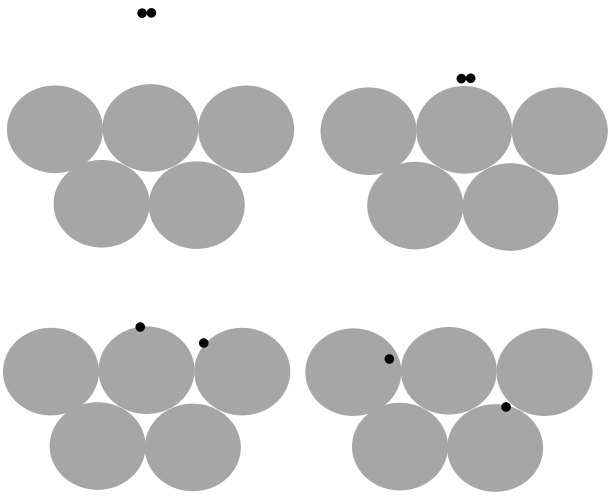

Figure 1.18: A series of diagrams depicting the possible route for H_2(two small circles) as it interacts with the metal.

Upon dissociation (chemisorption), the hydrogen atoms can interact independently with the metal. Once the hydrogen atom chemically adsorbs, its atomic properties allow for different types of interactions with the metal surfaces. Adsorption can be described through a two-state process for H_2. The first is physisorption, which occurs with a weaker attraction without dissociation, and the second is chemisorption (where H_2 dissociation occurs). The adsorption process is far more complicated than the discussion herein, and can be affected by:

1. the attraction of hydrogen to specific metal surfaces (pure element, alloys);
2. surface defects;
3. isotopic effects due to tunneling or diffraction;
4. molecular directionality as the distance between the molecule and the metal surface decreases.

These factors will create small changes in the activation energy for the chemisorption process on a single-crystal metal plane, which plays a role in determining trapping versus sticking phenomena. Future discussion will revolve around the two previously mentioned adsorption processes.

1.5.1.1 Physisorption

As previously mentioned, this process is weaker in energy and hydrogen dissociation does not occur. The driving influence is small interactive forces called van der Waals forces, directed by attraction of the H_2 molecule as it approaches the metal surface. The prospective binding energies are low, ranging from 3.5 kJ/mol to 15 kJ/mol. Therefore, for the sake of experimentation, it can be carried out at very low temperatures. This process can be described through a general energy level diagram, as previously described for the KIE. Taking into account the previously mentioned factors, the adsorption process can be portrayed by Figure 1.19, where the H_2 molecule, in its ground state infinitely far from the metal lattice, approaches the metal plane from the *z*-axis, perpendicular to the surface plane.

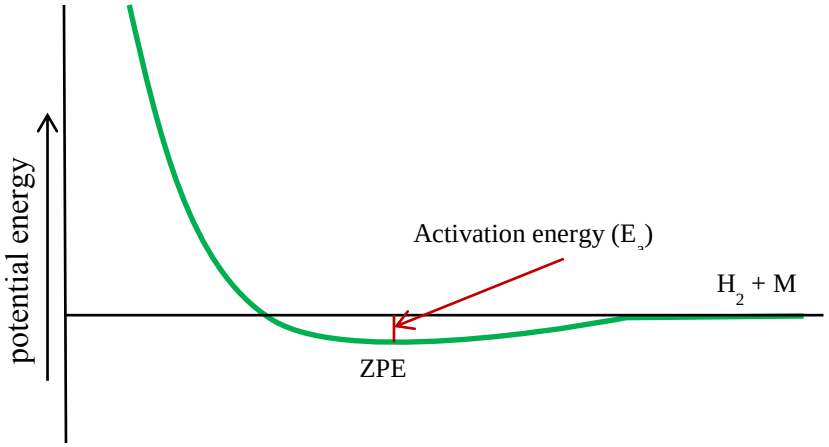

Figure 1.19: Potential Energy diagram for the physisorption of H_2 as it approaches a metal surface.

1.5.1.2 Chemisorption

With chemisorption, a completely different interaction pattern is observed as the hydrogen atom moves along the *z*-axis toward the metal surface. This is because, unlike before, the hydrogen molecule dissociates and becomes atomically bound to the metal surface. Again this can be displayed by sketching a potential energy diagram (Figure 1:20) to display the

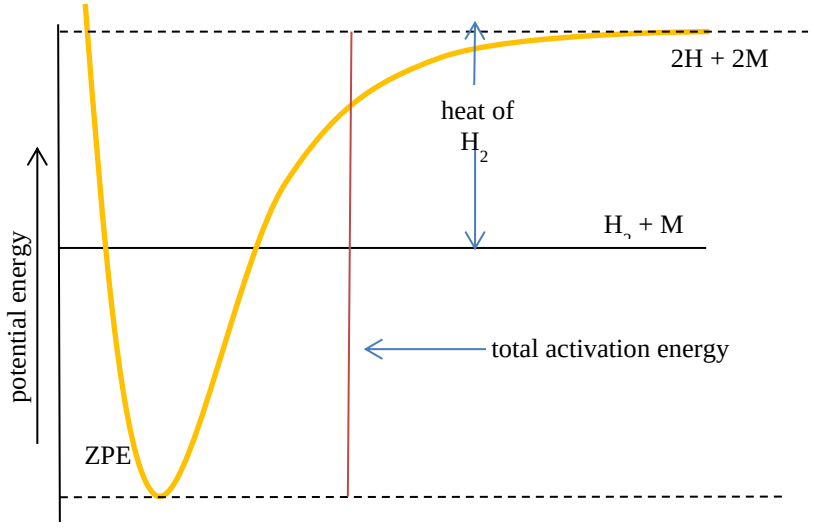

Figure 1.20: Potential Energy diagram for the chemisorbed (pre-dissociated) hydrogen with the metal surface.

interaction as a whole. The potential energy wells will range between 500 and 600 kJ due to the strong interactive forces as the hydrogen atoms are brought close to the surface.

Superimposing Figure 1.19 and Figure 1.20 can be used to describe the adsorption process as slightly spontaneous or activated (Figure 1.21). Given the attraction of transitional

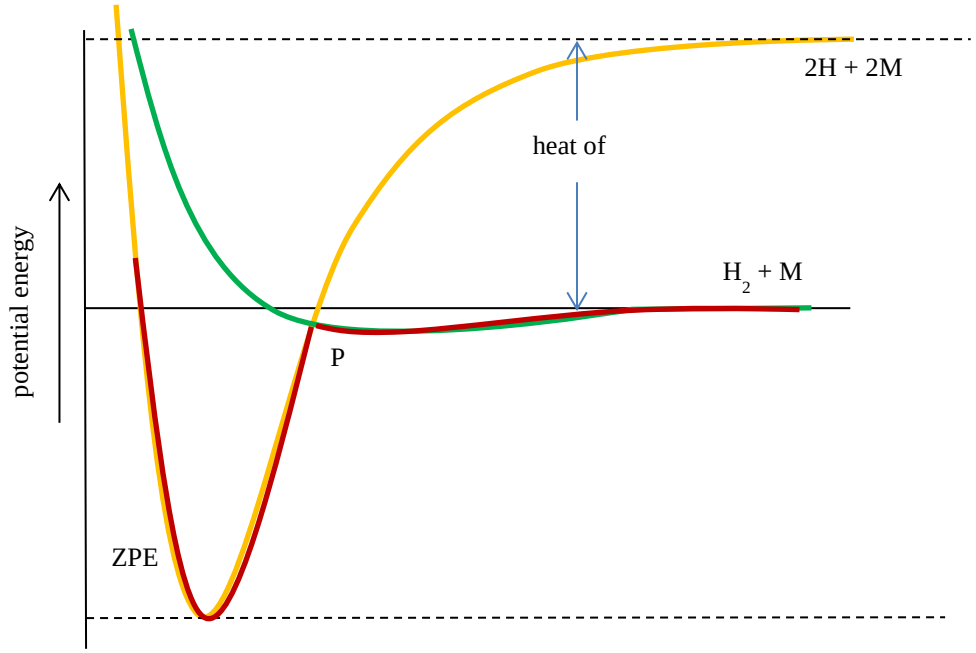

Figure 1.21: Superposition of the physisorptive and the atomic interaction potential energy curves yields a crossover point P.

metals toward hydrogen and the subject of this current work, only the spontaneous process of adsorption will be considered. This simplistic viewpoint only considers adsorption upon a single pure metal crystal [168], yet the real system is far more complicated, as the active metal is not in a pure crystalline state, and is placed upon a support. For more information, the reader is directed to the helpful paper by Bartholomew, which “emphasizes concepts and fundamentals

relating to the kinetics, energetics, and stoichiometries of adsorption of hydrogen on supported cobalt, iron and nickel," [169].

1.5.2 Theoretical Concept in the Dissociation of Hydrogen Isotopes

Theoretical evidence through known vibration frequency has provided a possible means to understand the concept of adsorption for H_2 (D_2). Potentially providing a theoretical route to calculate the KIE for hydrogen adsorption on an FT metal. Exploring the harmonic oscillator equation for the ZPE (equation 1), we set $n = 0$ and υ is the frequency from equation 2 using the reduced mass (equation 3). Considering the reduced mass (i.e., not in real dimensions), solving equation 3 for various bonds yields the results (Table 1.1), which reveals M-H ≈ 2, and M-D ≈ 1.

Table 1.1: Theoretical ratios for the reduced masses

Bond	μ
D_2	0.50
H_2	1.00
NiD	0.98
NiH	1.93
CoD	0.98
CoH	1.93
FeD	0.98
FeH	1.93
RuD	0.99
RuH	1.96

Taking this into account for equation 2 reveals the following equations (where M represents each metal), which give the frequency for each bond accordingly.

$$D_2 = 1/2\pi \sqrt{2}\, k \qquad (16)$$

$$H_2 = 1/2\pi \sqrt{k} \qquad (17)$$

$$MH = 1/2\pi \sqrt{k}/2 \qquad (18)$$

$$MD = 1/2\pi \sqrt{k} \qquad (19)$$

According to the hypothesis in the previous section, the KIE is dependent upon the difference in frequencies (equation 14, Figure 1.16) between the ground state, i.e., H_2 or D_2, and MH or MD. Given the equations 16-17, calculated values reveal that the spring constant *k* is the same for both equations. Knowing this, the set of equations (i.e., 16-17) can then be simplified and compared as shown by equation 20. Though calculated values exist for the constant k for

$$\upsilon_H = \sqrt{2}\, \upsilon_D \qquad (20)$$

both H_2 and D_2, none (of which the author is aware) exist for the metal hydride for M–H. Thus, knowing that the spring force constant is the same for both H_2 and D_2, where $k_{HH} = k_{DD}$, it follows that with M (e.g., Co, Ni, Ru, and Fe) bound to either isotope, the spring constants should also be the same, i.e., $k_{MH} = k_{DH}$. Given this, equations 18 and 19 can then also be simplified accordingly as shown in equation 21. Thus in both cases, the reactants (H_2, D_2) and

$$\upsilon_{MH} = \sqrt{2}\, \upsilon_{MD} \qquad (21)$$

the products (MH, MD) should have frequencies that will display a commonality. Though equations 20 and 21 are the same in ratio, they do not equal one another. The mass of the metal is obviously significantly more, and therefore *k* for the MH/MD bond will be significantly lower in energy and thus have a lower frequency. If $k_{HH} > k_{MH}$ and $k_{DD} > k_{MD}$, then the difference in the ratio will also follow suit, where $\Delta\upsilon^{o} > \Delta\upsilon^{\dagger}$. Take for example in Table 1.2, frequency values are displayed for each of the bonds necessary to calculate the KIE in hydrogen adsorption.

Table 1.2: Frequencies in cm^{-1} for the bonds needed for adsorption (asterisks refer to Figure 1.22).

H_2	4161	D_2	2993
MH	*2250 **1700	MD	*1591 **1202
	*800 **600		*566 **424

The difference between the two frequencies for H_2 and D_2 match the value given by equation 21. This distinction can be applied across the board for the transition frequencies. However, the difference between the transition frequencies is much less since the *k* (force constant) values are considerably lower. To further this concept, where $\Delta\upsilon^{o} > \Delta\upsilon^{\dagger}$, if combined with the previous discussion in the overall KIE and placed back into equation 14, $\Delta\upsilon^{o}$ would display a larger difference in the frequencies for the reactants ZPE. Thus, as displayed in Figure 1.16, the thermodynamic desorption process would display a NKIE, which agrees with others [117].

Lastly, taking the frequencies in Table 1.2 and applying them into equation 12 to calculate the expected values for KIE in hydrogen/deuterium adsorption, in agreement with

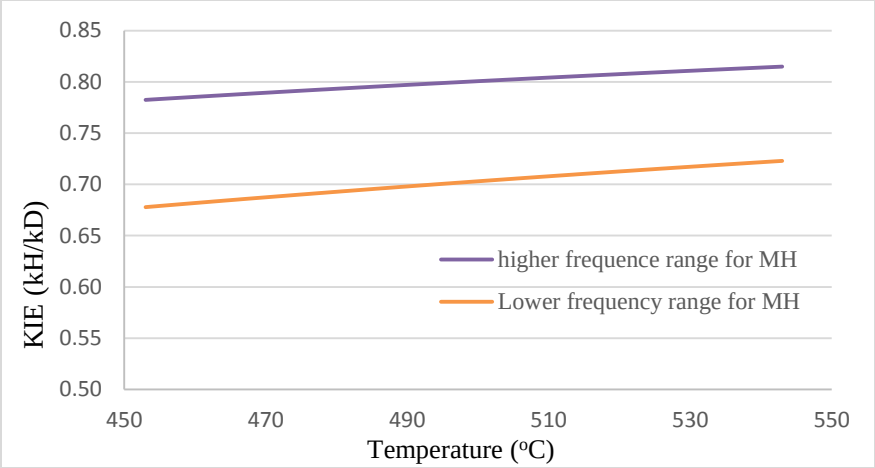

Figure 1.22: The KIE description for competitive hydrogen/deuterium adsorption in a temperature range of 450–550 ^{o}C, for the higher frequencies*, and lower frequencies** provided in Table 1.2.

others [112, 117], obtains values for k_D/k_H ranging from 0.68 to 0.80 (k_H/k_D = 1.23-1.48). This is seen above in Figure 1.22, which gives values that agree with the previous discussions where $k_H > k_D$ for the competitive hydrogen/deuterium adsorption process. The theoretical competitive adsorption displays an overall NKIE; incorporating this idea into the FT synthesis is important for theoretical and experimental purposes.

1.5.3 Dissociation of Hydrogen Reasoning

Based upon the reaction mechanisms given from section 1.2.3, general reaction networks could be generated. This would allow for some reasoning on the order of the reactions based upon the evidence given by the reaction mechanism. The first, which is based upon the carbide (CH_2) insertion mechanism, could go as follows, where M is the active metal:

Carbide mechanism proposed:

1. $CO + M \rightleftharpoons CO_M + M \rightleftharpoons C_M + O_M$
2. $H_2 + 2\ M \rightleftharpoons 2\ H_M$
3. $H_2 + O_M \rightleftharpoons H_2O + M$
4. $C_M + H_M \rightleftharpoons CH_M + H_M \rightleftharpoons {}^{\neq}CH_{2M} + H_M \rightleftharpoons CH_3 - \neq$ possible monomer for FT
5. CH_3
    a. $CH_3 + H_M \rightarrow CH_4$
    b. $CH_3 + CH_2 \rightleftharpoons C_2H_5$ * either desorbed or chain growth continues

Reaction network based upon the proposed enol mechanism

1. $H_2 + 2\ M \rightleftharpoons 2H_M$
2. $2\ CO + M_2 \rightleftharpoons 2\ CO_M + 2\ H_M \rightleftharpoons 2\ C_MHOH_2$
3. $2\ CHOH_2 \leftrightarrow H_2O + HC_MC_MOH$
4. $HC_MC_MOH + 2\ H_M \rightleftharpoons CH_3C_MOH + M$
5. CH_3C_MOH
    a. $CH_3C_MOH + 2\ H_M \rightleftharpoons CH_2CH_2 + H_2O$
    b. $CH_2C_MOH + CO_M + 2\ H_M \rightleftharpoons C_MHOH + CH_2C_MOH \rightleftharpoons C_MOHC_MCH_2 + H_2O$

Reaction network based upon the proposed CO insertion mechanism

1. $H_2 + 2\ M \rightleftharpoons 2\ H_M$
2. $2\ CO + 2H_M \rightleftharpoons 2\ C_MOH$
3. $C_MOH + 2\ H_M \rightleftharpoons C_MH_2OH$

4. $C_MH_2OH + 2\ H_M \rightleftharpoons C_MH_3 + H_2O$
5. $C_MH_3 + CO \rightleftharpoons C_MCH_3$ continued through CO insertion followed by H addition

These proposed reaction networks display some common generalities. Specifically, before any H atoms can interact with the C from CO, the hydrogen itself must be adsorbed upon the active metal. Thus the measurement of the KIE for CO hydrogenation by means of the previously proposed route must not only include the rate at which hydrogen affects the CO, but also the rate at which hydrogen interacts with the active sites. Based upon the previous experimentation, a common understanding from the switching experiment reveals that the FT reaction displays an IKIE for the H_2/D_2 switching experiment. This outcome could be indicative of the actual result for CO hydrogenation, or a concentration of surface D atoms on the active sites.

The calculated results from the previous section disclose a KIE value of more than 1 for H_2/D_2 adsorption. Not all of the calculations for the competitive hydrogen adsorption agreed with the one presented; regardless, a value for the KIE was very biased. Based upon the calculations, this would seem to indicate that the competitive adsorption of hydrogen isotopes could play a role in the KIE of CO hydrogenation. As far as the author is aware, no experimental work revolving around this subject has been published.

The next chapter discusses the reactor and the analytical equipment used for the experimentation. Chapters 3–6 discuss specifics regarding each of the FT catalysts, including the analysis, results, and conclusions.

Chapter 2 : Experimentation

2.1 Reactor System

This chapter will focus on the overall experimental work done for all of the catalyst analyzed. Given the overall analytical work will remain the same for all the runs applied, a general overview of the process leading to the actual run will be appropriate. In addition, the reactor system (other than the reactor itself) was reused for all the experimentation so a general overview will be discussed in this chapter 2 where specifics of the reduction and TPD process will be tailored in each specific chapter depending on the metal analyzed.

In order to perform this experimentation, a closed reactor system was needed to contain a catalyst at atmospheric pressure and high temperature under a reduced environment. The catalyst needs to be prepared ex-situ, then placed into the system for analysis. The temperatures will need to be precise given the idea behind this study is to understand coverage at very specific temperatures. Lastly, given the difficulty in the separation of the products (H_2/HD/D_2) a tremendous amount of analytical work will need to occur to ensure that not only is the separation of the gases is possible, but the quantification as well.

In addition, the overall process for instrumentation for catalytic characterization will be added in chapter 2, including XRD, BET, and TPR. Results from the characterization will however be placed into the separate chapters.

The reactor setup (Figure 2.1) utilized for the competitive adsorption was created as a

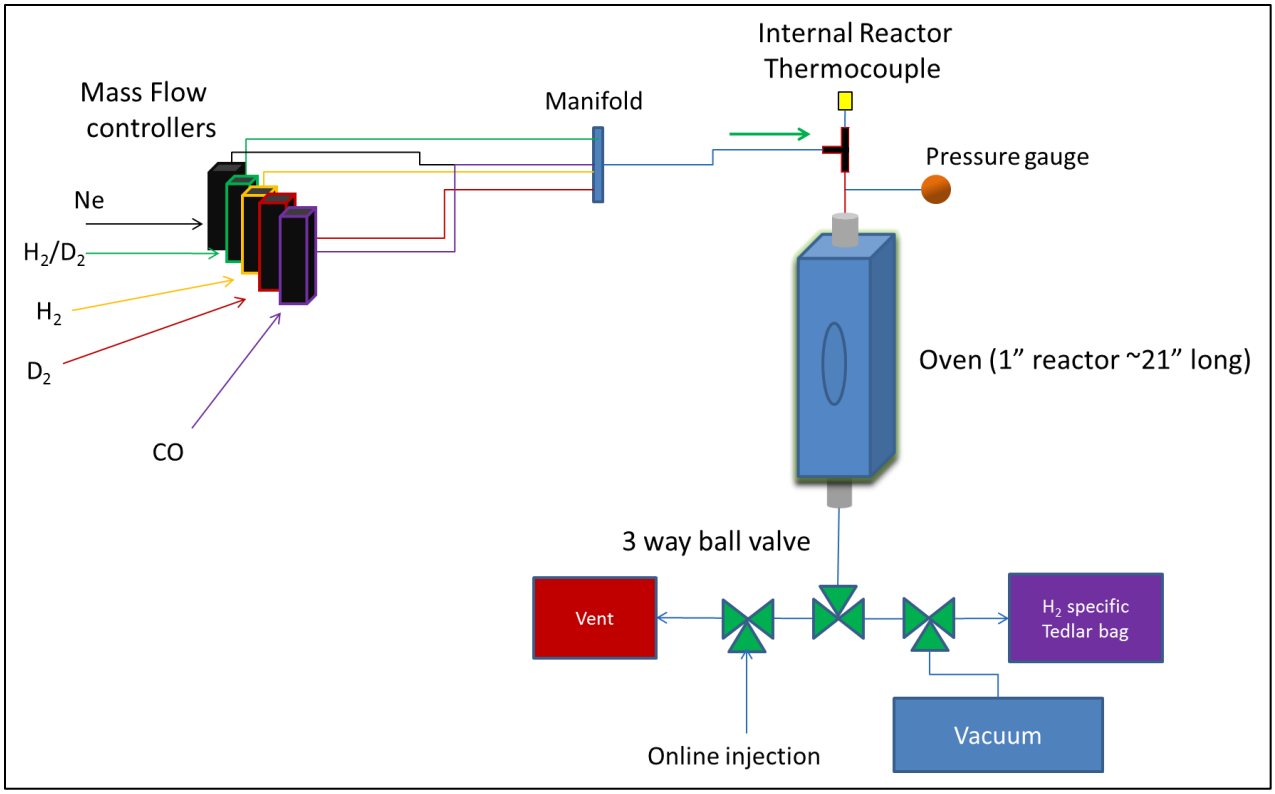

Figure 2.1: A representative cartoon of the plug flow fixed-bed reactor used for the adsorption experiments.

straightforward plug flow system. Five separate Brooks (Hatfield, PA) mass flow controllers (MFC) were used to govern the flow for each specific gas. This was done by controlling the rate through a percentage of the total flow that is had been calibrated. A specific voltage is applied across the MFC based upon the percentage and from this a certain flow is allowed across. However since this is based upon the thermal conductance of a specific gas, if another is passed across, the flow rate vs. the specific percentage will not be accurate. Therefore, each MFC needs to be calibrated for each specific gas used, so that the amount passed across the catalyst bed will be precisely known.

The bulk of the stainless steel used for the system was ¼" o.d. 316 stainless steel, while the reactor itself was 1" o.d. 316 ss. The thermocouple was a 1/32" o.d. thermocouple that was given the ability to slide along the *z*-axis of the reactor inside a fixed 1/8" o.d. thermal well. The

reason for the capability was to insure that the temperature gradient along the *z*-axis of the bed inside the reactor was less than ±5 °C, and overall temperature was at the required temperature for each specific catalyst. The pressure gauge was a low-pressure gauge (0–100 psi) and was only set as a means to ensure the bed was run at atmospheric pressure, where the bed pressure does not create an issue. The low-pressure regulator could also ensure bed pressure consistency as an iron catalyst could coke during the carburization process causing unnecessary high bed pressures.

The oven was a Lindberg (Riverside, MI) clamshell oven with a 1" bore for a reactor capable of 1200 watts of power (~10 A), allowing temperatures to maximize at 1000 °C. The oven was controlled by an Omega CN3254R ramp/soak controller, and powered by a 25 A Omega solid-state relay. The controller allocates power the system applying heat in a very systematic fashion allowing no inconsistencies between the different activations for each metal.

After the furnace a series of Swagelok (Solon, OH) 3-way ¼" ball valves were used as a means to divert the flow without interrupting the experiment. During the bulk of the experiment the flow was diverted to a fume hood. During the last section of the first three approaches (explained later), flow is diverted to the gas collection bag for catalysts. The online injection port was set up as a ¼" port connector with an 11 mm septum set inside the ¼" nut. The needle is then inserted into the system, directly in line with the flow of gas, allowing sampling during the experiment and direct injection onto the column. Lastly, the pump was a ¾ HP Edwards (Albany, NY) high-vacuum roughing pump placed to allow the system have a vacuum of up to 30" of water.

2.2 Instrumentation

2.2.1 Catalyst Surface Analysis

2.2.1.1 Brunauer-Emmett-Teller (BET)

The surface area, pore volume, and average pore radius of each ruthenium catalyst were measured using a Micromeritics Tri-Star 3000 gas adsorption analyzer system. Approximately 0.3–0.4 g of sample was weighed and loaded into a 3/8″ o.d. sample tube. Nitrogen was used as the adsorption gas and sample analysis was performed at the boiling temperature of liquid nitrogen. The sample was evacuated at ambient temperature overnight to approximately 6.7 Pa. The physisorption results were quantified using the Barrett-Joyner-Halenda (BJH) desorption model, which provides a relationship between the amount of the adsorbate lost and each pore emptying step of the desorption process.

2.2.1.2 Temperature Programmed Reduction

Temperature programmed reduction (TPR) was recorded using a Zeton-Altamira AMI-200 unit which makes use of a TCD detector. The sample was first ramped to 350 ºC in pure Ar to remove residual H_2O from the sample, prior to cooling to 50 ºC to begin the TPR. The test was performed using 10% H_2/Ar mixture referenced to Ar at a flow rate of 30 cm^3/min (sccm). The sample was heated to 800 ºC at a ramp rate of 10 ºC /min.

2.2.1.3 Temperature Programmed Reduction

Hydrogen chemisorption was conducted using temperature-programmed desorption (TPD) with the Zeton-Altamira AMI-200 instrument. The catalyst sample was activated using a flow of 10 cm^3/min of H_2 mixed with 20 cm^3/min of argon at 350 ºC for 10 h and then cooled

under flowing H_2 to 373 K. The sample was held at 50 ºC under flowing argon to remove and/or prevent adsorption of weakly bound species prior to increasing the temperature slowly to 350 ºC. The TPD spectrum was integrated and the number of moles of desorbed hydrogen determined by comparing its area to the areas of calibrated hydrogen pulses. The loop volume was first determined by establishing a calibration curve with syringe injections of nitrogen into a helium flow. Dispersion calculations were based on the assumption of a 1:1 H: atomic molar composition (AMC) stoichiometric ratio and a spherical cluster morphology.

2.2.2 Chromatography

Each gas sample (0.5 mL) was manually injected into an Agilent (Santa Clara CA) 6890 cryogenic gas chromatograph with an attached thermal conductivity detector (GC-TCD) containing two 90 m Agilent molecular sieve columns fashioned with column connectors to create one 180 m column. The temperature program was isothermal at -80 ^{o}C, with a 4 mL/min flow rate. Neon was chosen because of the inability to adequately separate the H_2/D_2 mixture with Ar and N_2, and because of the small thermal conductivity difference between H_2 and He.

Five-point calibration curves were made for H_2, HD, and D_2, using an evenly mixed standard bought from Cambridge Isotope Laboratories (Figure 2.2). The standard was manually

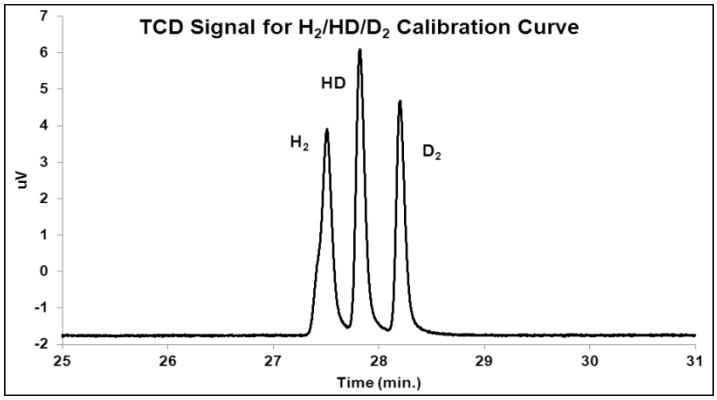

Figure 2.2: A standard TCD chromatogram of the standard mixture

injected using a 100 μL Hamilton syringe (Franklin, MA) to inject volumes ranging from 5 μL to 100 μL. Several injections were made for each concentration to obtain a constant linear curve with a correlation coefficient above 0.99 (Figure 2.3 – Figure 2.5). The hydrogen diffusion-

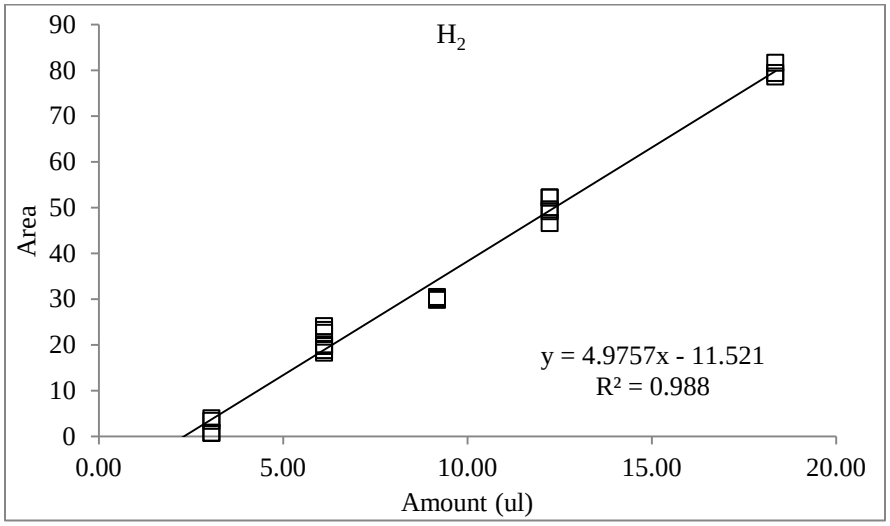

Figure 2.3: The calibration curve built from the standard for H_2.

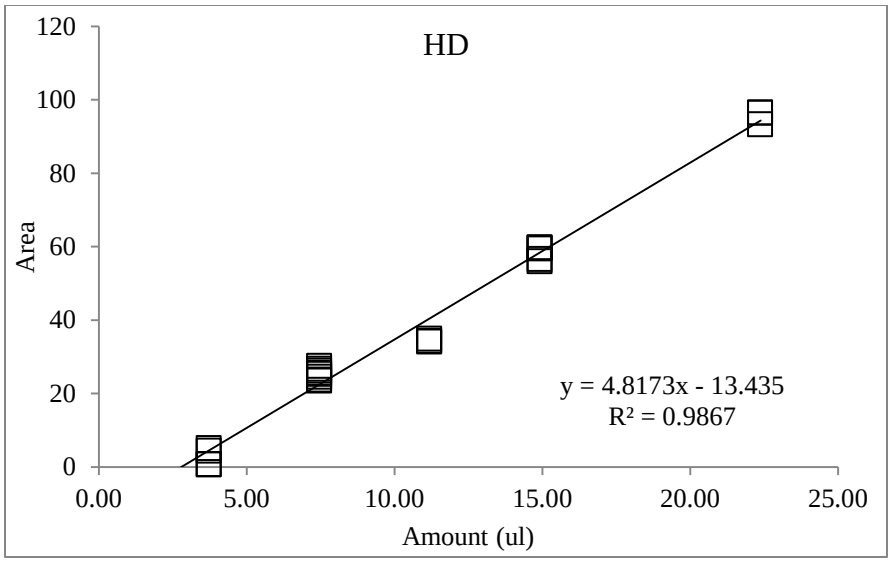

Figure 2.4: The calibration curve built from the standard for HD.

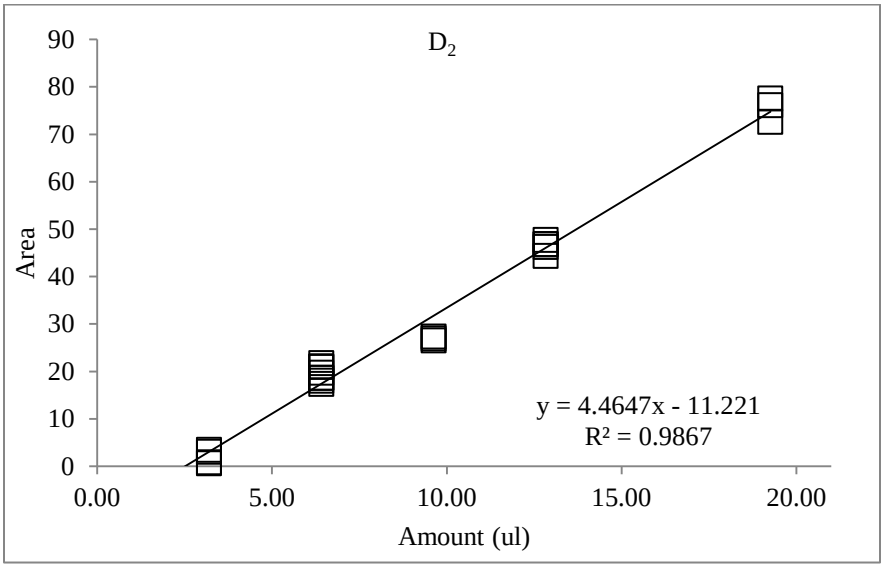

Figure 2.5: The calibration curve built from the standard for D_2.

resistant gas bag bought from SKC (Eighty Four, PA) obtained from the TPD mainly contained neon; therefore, a 1 mL syringe was used for multiple 500 μL injections of sample obtained

from reduction of the specific catalyst to the GC. Since neon was used during the TPD and also used as the carrier gas for the GC, there should be no contribution by neon in the TCD signal.

Chapter 3 : Cobalt

3.1. Introduction

Cobalt is one of the most commonly used active metals for the Fischer-Tropsch (FT) synthesis. The main source for FT production using cobalt is through the GTL process as conversion of methane through steam reforming leads to a greater than 2/1 ratio of H_2/CO

$$H_2O + CH_4 \rightarrow 3H_2 + CO$$

(syngas). This ratio is required for cobalt as a decrease in ratio, lower than about 1.5, can cause coking upon the catalyst prematurely decreasing the activity. The FT mechanism occurring on the catalyst, as mentioned, is still under scrutiny. While some authors prefer a CH_2 insertion mechanism [1] and suggest that chain addition is the rate-determining step, others claim a CO insertion mechanism and argue that the rate-determining step is where CO insertion occurs [2]. Controversy has also arisen from this where some researchers have argued that if CH_2 insertion was the favored mechanism, then no oxygenated material could be produced. From this controversy, Dry et al. [3] argued for a mechanism that involves both CH_2 and CO as active surface intermediates. Since the rate-determining step remains a point of contention, a number of H_2/D_2 studies have been performed, but, unfortunately, with no clear conclusion [4-8].

Briefly, in switching from H_2 to D_2, the rate of CO conversion increased, suggesting an overall negative kinetic isotope effect. This chapter examines whether preferential partitioning of either H or D on the cobalt metal surface occurs such that it may influence data when measuring the kinetic isotope effect. Moreover, by examining both unsupported cobalt and alumina or silica supported cobalt catalyst, the potential for spillover influencing the results was also examined.

3.2 Experimental

3.2.1 Catalysis Preparation

25% Co/Al_2O_3 catalyst was prepared by a slurry impregnation method using Catalox 150 (high purity γ-alumina, ~150 m^2/g) as the support. Al_2O_3 was calcined for 10 h before impregnation and then cooled under an inert gas to room temperature. $Co(NO_3)_2 \cdot 6H_2O$ (99.9 % purity) was used as the precursor for Co. In this method, which follows a Sasol patent [9], the ratio of the volume of solution used to the weight of alumina was 1:1, such that approximately 2.5 times the pore volume of solution was used to prepare the loading solution. Two impregnation steps were used, each to load about 12.5% of Co by weight. Between each step the catalyst was dried under vacuum using a rotary evaporator at 100 $^{\circ}$C and the temperature was slowly increased to 95 ºC. After the second impregnation/drying step, the catalyst was calcined under airflow at 350 ºC for 4 h.

The 15%Co/SiO_2 catalyst was also prepared using the aqueous slurry-phase impregnation method, with cobalt nitrate. The support was PQ-SiO_2 CS-2133, surface area about 352 m^2/g). The catalyst was calcined in flowing air or flowing 5% nitric oxide [10-13] in nitrogen at a rate of 1 L/min for 4 h at 350 $^{\circ}$C. The NO-calcined catalyst was used for isotopic

studies, since the particle was expected to be smaller and one of the aims of the paper is to explore the possibility of reverse spillover from the support.

3.2.2 BET Surface Area and Porosity Measurements

The surface area, pore volume, and average pore radius of the catalyst calcined at 350 °C was measured by BET using a Micromeritics Tri-Star 3000 gas adsorption analyzer system. Approximately 0.35 g of sample was weighed out and loaded into a 3/8″ o.d. sample tube. Nitrogen was used as the adsorption gas and sample analysis was performed at the boiling temperature of liquid nitrogen. Prior to the measurement, the sample was slowly ramped to 433 K and evacuated overnight to approximately 6.7 Pa.

3.2.3 Temperature-Programmed Reduction

Temperature-programmed reduction (TPR) was recorded using a Zeton-Altamira AMI-200 unit, which makes use of a TCD detector. The sample was first ramped to 350 ºC in pure Ar to remove any residual H_2O from the sample, prior to cooling to 100 °C to begin the TPR. The test was performed using 10%H_2/Ar mixture referenced to Ar at a flow rate of 30 cm^3/min. (sccm). The sample was heated to 1100 °C at a ramp rate of 10 °C per min.

3.2.4 Hydrogen Chemisorption by TPD

The Co/Al_2O_3 (~0.22 g) was activated in a flow of 10 cm^3/min of H_2 mixed with 20 cm^3/min of argon at 270 °C for 10 h and then cooled under flowing H_2 to 100 °C. The sample was held at 100 °C under flowing argon to remove and/or prevent adsorption of weakly bound species prior to increasing the temperature slowly to 350 °C, the temperature at which oxidation

of the catalyst occurs. The TPD spectrum was integrated and the number of moles of desorbed hydrogen determined by comparing its area to the areas of calibrated hydrogen pulses. The loop volume was determined by establishing a calibration curve with syringe injections of hydrogen into a helium flow. Dispersion calculations were based on the assumption of a 1:1 H:Co stoichiometric ratio and a spherical cobalt cluster morphology. After TPD of hydrogen, the sample was reoxidized at 350 °C using pulses of oxygen. The percentage of reduction was calculated by assuming that the metal reoxidized to Co_3O_4.

3.2.5 Reduction and Desorption using the H_2/D_2 Mixture

30 g of the 25%Co/Al_2O_3 catalyst, 15 g of CoO, and 15 g of the 15% Co/SiO_2 were loaded into the plug flow reactor and three separate approaches were set up to run each catalyst.

(1) Each cobalt catalyst was reduced under 15 sccm of the 1:1 H_2/D_2 mixture. The bed was heated at 1 ºC /min to 350 °C and held for 48 hours. The system was cooled to 100 °C at 1 °C /min., where neon was introduced and the fixed bed system was held at this condition for one hour. The reactor was heated to 350 °C under 15 mL/min. of neon. The hydrogen/deuterium remaining on the catalyst desorbed and was collected into a hydrogen specific gasbag using neon as the carrier gas.

(2) The cobalt catalyst was heated to 350 °C and held for 44 h under 15 sccm of H_2 flow. After 44 hours of flow, an uninterrupted switch occurred to allow the 1:1 H_2/D_2 to flow for four hours at the same temperature. The system was then cooled to 100 °C at 1 °C /min., where neon was introduced

and the fixed bed system was held at this condition for one hour. The reactor was heated to 350°C under 15 mL/min of neon. The hydrogen/deuterium remaining on the catalyst desorbed and was collected into a hydrogen specific gasbag using neon as the carrier gas.

(3) The cobalt catalyst was heated to 350 °C and held for 44 hours under 15 sccm of D_2 flow. After the 44-hour period the D_2 was stopped and the H_2/D_2 mixture was introduced at the same flow rate of 15 sccm. The system was then cooled to 100 °C at 1 °C /min, where neon was introduced and the fixed bed system was held at this condition for one hour. The reactor was heated to 350 °C under 15 mL/min of neon. The hydrogen/deuterium remaining on the catalyst desorbed and was collected into the hydrogen-specific gasbag using neon as the carrier gas.

Each approach was repeated for each catalyst to ensure the repeatability of the experiments.

3.3 Results and Discussion

3.3.1 Surface Area Measurements

The catalyst was prepared by a slurry impregnation as opposed to incipient wetness impregnation [14] to maintain the cluster size about 10 nm while increasing the homogeneity of the catalyst particles. The BET surface area measurements by adsorption of N_2 showed that the surface area for the 25%Co/Al_2O_3 catalyst was around 103 m^2/g. A 25% Co metal loading by wt % is equivalent to 34% Co_3O_4. If Al_2O_3 is the only contributor to the surface area, then the surface area should be close to $0.66 \times 150 = 99$ m^2/g. The actual surface area measurement is

approximately the calculated value, suggesting that pore blocking should not be a significant problem. The results from the BJH adsorption tests (Table 3.1) of this catalyst were in agreement with the previous report [14].

Table 3.1: Summary of BET surface area and porosity measurements.

Catalyst ID	BET SA (m^2/g)	Average Single Point Pore Volume (mL/g)	Average Pore Radius (nm)
Catalox 150 γ-Al_2O_3	149	0.493	6.9
15%Co/PQ-SiO_2, calc. in NO	298	1.06	7.1
15%Co/PQ-SiO_2, calc. in air	263	1.04	7.7
25%Co/Al_2O_3	103	0.258	5.0

For the SiO_2-supported cobalt catalysts, if SiO_2 is the sole contribution to surface area, then the surface area should close to $0.80 \times 352\ m^2/g = 282\ m^2/g$. That the surface area of the air-calcined catalyst is less than this (Table 3.1) suggests some pore blocking by larger particles. As shown in Table 1, this was not observed for the case of the catalyst calcined in nitric oxide, where smaller particles – expected to alleviate pore blocking – were obtained.

3.3.2 Reduction/ TPD

The TPR from Jacobs et al. [15] for the 25% Co/Al_2O_3 displays a two-step reduction of Co_3O_4 particles (Figure 3.1), a sharp peak at around 600 $^{\circ}$C (Co_3O_4 – CoO) and a broader peak

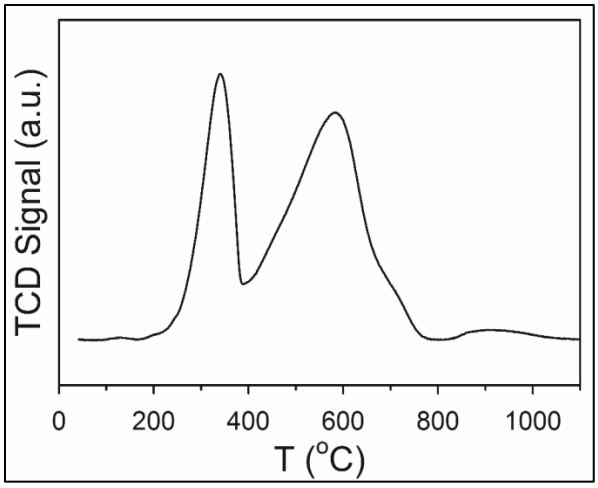

Figure 3.1: TPR profile of 25%Co/Al_2O_3.

ranging from 700 °C to 1050 °C (CoO – Co^0). After running two separate TPR experiments, one directly after calcination and the other after 10 hours of reduction at 350 °C, only a fraction of the Co surface species responsible for the broad peak was reduced. The reduction of Co_3O_4 was completed at this temperature; hence, the focus was upon the reduction of the CoO particles to Co^0, as shown for this specific catalyst where, at 350 °C, 42% was reduced [15]. Considering that 30 g of catalyst were loaded into the reactor, a 48 h period at 350 °C for was used to ensure a significant (e.g., > 42%) extent of cobalt reduction. The reduction temperature was kept below 400°C to prevent sintering of Co atoms. Based on the calculations given from [15], Table 3.2

Table 3.2: Hydrogen chemisorption by TPD with pulse reoxidation after reduction for 10 h at 350 °C.

Catalyst ID	H_2 evolved (mol/g_{cat})	Uncorr. % Disp.	Uncorr. Diam. (nm)	O_2 uptake (mol/g_{cat})	% Red.	Corr. % Disp.	Corr. Diam. (nm)
25%Co/Al_2O_3	89.2	4.2	24.5	1058	37	11.2	9.2
15%Co/PQ-SiO_2, calc. in NO	39.8	3.1	33.0	791	56	5.3	19.2
15%Co/PQ-SiO_2, calc. in air	38.0	3.0	34.5	1436	85	2.7	38.5

summarizes the chemisorption results and shows that a satisfactory active-site density was obtained for carrying out the isotopic studies.

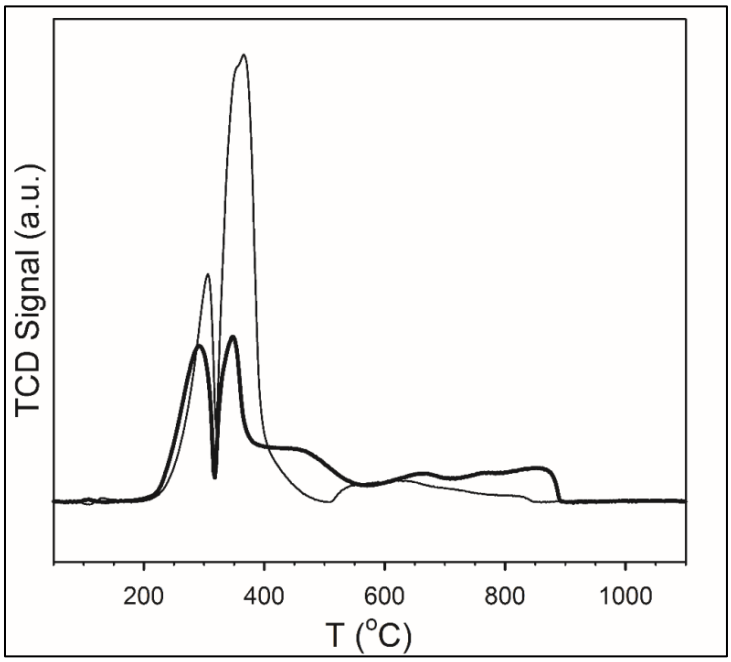

Figure 3.2: TPR profiles of 15%Co/SiO_2 catalysts, including catalysts calcined in (light line) air or (bold line) nitric oxide.

Figure 3.2 compares the reduction profiles of the 15% Co/SiO_2 catalyst, with the light line being that of a standard air-calcined catalyst and the bold corresponding to the catalyst calcined in nitric oxide. For standard air-calcined catalysts, weakly interacting SiO_2 leads to larger cobalt oxide particles than those observed on strongly interacting Al_2O_3 [15]. In agreement with this, the profile of the air-calcined catalyst displays primarily two sharp peaks, with the first one corresponding to the reduction of Co_3O_4 to CoO and the second being larger particles of CoO to Co^0, very much like the reduction of bulk Co_3O_4 [14,15]. On the other hand, the nitric oxide calcination lends itself to producing much smaller particles [10-13], which

interact more strongly with the support, such that the profile displays a decrease in the sharp low-temperature peak (i.e., larger particles) and a significant increase in peaks corresponding to smaller, more strongly interacting particles. The H_2 chemisorption/pulse reoxidation results confirm that smaller, less reducible, particles are formed after activating the nitric oxide-calcined catalyst. Since one goal is to examine the possibility of reverse spillover (where the hydroxyl groups on the support can affect the activated metal surface coverage), it is of interest to use a catalyst with smaller particles in greater interaction with the support. Thus, the catalyst calcined in nitric oxide was selected.

3.3.3 Competitive Desorption

After reduction, the plug flow reactor was cooled to 100 $^{\circ}$C while under H_2/D_2 mixture to allow for the H/D atoms to be chemisorbed to the cobalt surface before starting the TPD. The reactor was then held at 100 $^{\circ}$C with neon flow to prevent any false outcomes due to the retention of physisorbed or weakly bound hydrogen or deuterium. The temperature was then increased to desorb the chemisorbed H/D and sweep the evolved H_2, D_2, and HD into the sampling bag. The neon flow was decreased during this time to keep hydrogen isotopes in the bag concentrated enough to allow for sampling, especially in the case of the desorbed gas obtained from the reduced CoO. CoO serves as a reference, since the cobalt particles are not supported.

The H/D ratios presented in Tables 3-5 were calculated from the amounts determined for each injection based on the calibration curves:

$$H_2 = y = 5.02\ x - 12.37$$

$$HD = y = 4.88x - 13.85$$

$$D_2 = y = 4.55x - 11.65$$

where *y* is the peak area and *x* is the calculated amount in µL. Once the amounts are obtained the H/D ratio is calculated. Therefore, if a negative isotopic effect is obtained seen the ratio would be less than 1 and vice versa.

The total amount of neon collected in the bag was 225 mL, based on a flow rate of 5 mL/min. and time-on-stream of 45 min during desorption. Taking Table 3.3 injection 1 as an example,

Table 3.3: The isotope effect for the reduced CoO catalyst.

CoO		
Injection	Approach 1	Approach 3
1	1.04	0.98
2	1.04	0.99
3	1.02	0.98
4	1.02	0.99

subtracting the amounts above of H_2 (4.3 µl), HD (5.9 µL), D_2 (3.9 µL) given from each calibration curve, from the total injection volume (0.5 mL), and the ratio of H-D/Ne is 3.0 e^{-2} from the 0.5 mL injection. If the total amount of gas in the bag were 225 mL, then

$$Ne_{total} = 225ml - (225 * 3.0\ e^{-2}) = 218.6\ mL$$

The H_2, HD, D_2 amounts can be found from their percentages in Table 3 injection 1 from the remaining volume in the bag.

$$H_2 = (225\ mL - 218.6\ mL) * 0.3 = 1.9\ mL$$

$$HD = (225\ mL - 218.6\ mL) * 0.4 = 2.6\ mL$$

$$D_2 = (225\ mL - 218.6\ mL) * 0.3 = 1.8\ mL$$

From here, given the following equation based on [15], the H-D uptake can be calculated:

$$\text{H-D uptake (moles/g}_{cat}) = \text{calibration value/(catalyst weight} \times 24.5\ \text{L/mole})$$

The H_2 is 3.1 µmol/g_{cat}, HD is 4.2 µmol/g_{cat}, and D_2 2.9 µmol/g_{cat}, and the total H-D adsorbed is 10.2 µmol/g_{cat}. The H-D uptake value was expected to be low due to the low surface area for CoO before reduction. For this reason, CoO was used instead of Co_3O_4 to help prevent sintering, and allowing enough adsorption of H_2 and D_2 to occur upon the reduced metal.

CoO was set as a control for the difference experimental approaches to obtain, if any, isotopic preferences on the reduced metal surface. The first approach, a 48-h equimolar competitive reduction, leads to no isotopic preference on the metal surface. The bag containing the stripped hydrogen/deuterium molecules from the reduced cobalt metal, was then taken from the system after the TPD. Several injections were made to ensure the homogeneity of H_2, HD, and D_2 in the bag. As shown in Table 3, approach 1, the standard deviation was low for all the injections. This exact approach was repeated three times for the CoO to ensure the results were consistent, where all the runs averaged out as shown on Table 3 approach 1. Duplicating this

approach confirmed the initial results, where no isotopic preference was noted, and ensured that the fixed bed system and analytical setup were sound.

The reason for the different experimental approaches was to mimic the studies presented earlier [4-8], in an attempt to explain the NKIE seen during CO hydrogenation. The first approach mentioned displayed results for a competitive reduction only; however, many of these papers did not reduce the catalyst in a competitive manner. Two more approaches were then designed to mimic the changeover from H_2 to D_2 and vice versa. Again the CoO was used as a control in an attempt to see preferential partitioning in the metal surface only. Unlike the first approach, where the metal is covered with equimolar H and D atoms, the other two approaches allow for entropy to play a role. Once the cobalt surface was completely covered with H or D atoms by running a 44-hour reduction at 350 $^{\circ}$C, the four hour competitive reduction occurred. The four-hour competitive reduction at 350 $^{\circ}$C with a 15-sccm flow, allowed for at least 24 reactor turnovers. If entropy were greater than the partitioning preference on the surface of the cobalt metal, then there would be no bias seen on the reduced cobalt surface. CoO again displayed no isotopic preference for H or D as displayed in Table 3 approach 3.

The next step was to include actual supported cobalt FT catalysts, where two common supports for cobalt catalysts are SiO_2 and Al_2O_3. The idea was to run all three experimental approaches for each of the supported catalysts and if a preference is observed, it would be due to the support. Since the CoO displayed no partitioning preference on any of the approaches, the difference would be caused by exchange on the surface of the support. The first approach did not show any partitioning preferences by any of the catalysts. The second and third approaches, however, displayed a small preference. The bias on both of the supported catalysts leaned toward the gas used during the 44-h reduction. The second experimental approach was to reduce

the supported catalysts under H_2 for 44 hours and both catalysts resulted in an h/d ratio greater than 1 (Table 3.4 and 5 approach 2). Whereas when the same catalysts were reduced under D_2 for 44 hours H/D is less than 1 (Table 3.4 and 3.5: Approach 3).

Table 3.4: The isotope effect for the reduced 25% Co/Al_2O_3 catalyst.

25%Co/Al_2O_3			
Injection	Approach 1	Approach 2	Approach 3
1	1.03	1.16	0.93
2	1.04	1.16	0.93
3	1.05	1.13	0.90
4	1.01	1.12	0.87

Table 3.5: The isotope effect for the reduced 15% Co/SiO_2 catalyst.

15%Co/Si			
Injection	Approach 1	Approach 2	Approach 3
1	0.98	1.05	0.94
2	0.99	1.05	0.96
3	1.00	1.06	0.96
4	1.00	1.05	0.96

3.4 Conclusions

From the initial 48-h competitive H_2/D_2 reduction no isotopic preference was observed after carrying out TPD on the activated CoO, 25%Co/Al_2O_3, and the 15% Co/SiO_2 catalysts. Understanding that no isotopic effect exists upon the cobalt metal, the negative kinetic isotope effect found during CO hydrogenation will not be affected by preferential isotopic partitioning on the metal surface. However, a slight isotopic preference upon the 25% Co/Al_2O_3 and 15% Co/SiO_2 was identified, depending on which gas was used during the 44 hour reduction, H_2 or

D_2, prior to the 4 hour treatment in H_2/D_2. Given the control experiment of Co, and the number of reactor turnovers, this slight isotopic preference must be caused by the Al_2O_3 and SiO_2 supports. This effect, whereby a slight positive isotopic effect was observed when the first treatment occurred using H_2 and a slight negative effect was similarly observed with D_2, could be caused by a minor H/D exchange with the hydroxyl groups on the support [16]. Since the isotopic preference is small and only seen on the supported cobalt catalysts, it seems that neither preferential partitioning of H or D on the surface of cobalt nor reverse spillover from the alumina support contributes to measurements of the negative kinetic isotopic effect during CO hydrogenation.

Chapter 4 : Nickel

Adapted with permission from W.D. Shafer, G. Jacobs, J.P. Selegue, B.H. Davis, *An Investigation of the Partitioning of Dissociated H_2 and D_2 on Activated Nickel Catalysts*. Catal. Lett. **2013** 143:1368-1373. Copyright 2013 Springer International Publishing.

4.1 Introduction

Heterogeneous supported nickel catalysts are commonly used in several different types of chemical processes, including steam reforming of methane or light alcohols to produce syngas (e.g., $CH_4 + H_2O \rightarrow 2CO + 2H_2$, $C_2H_5OH + 3H_2O \rightarrow 2CO_2 + 6H_2$) [1,2] methanation ($CO + 3H_2 \rightarrow CH_4 + CO_2$) [3], hydrogenation [4], and water gas shift ($H_2O + CO \rightarrow CO_2 + H_2$) [5]. Nickel is a relatively inexpensive metal, an attractive feature from the standpoint of industry. However, a significant challenge is that nickel catalysts tend to deactivate due to metal sintering[6] and/or high rates of carbon formation [7]. Measures have been undertaken by several research groups in attempts to inhibit carbon deposition. This includes the use of smaller nickel particles that avoid ensembles required for carbon formation [8,9]. Using dopants such as alkali metals to suppress the Boudouard reaction. [10] Metal oxides (e.g., lanathana, magnesia, etc.) aimed at mitigating acidity [11] or modifying CO adsorption [12], or applying supports with O-mobility that can assist in cleaning carbon from the catalyst as it is formed [13].

A key to understanding these issues and possibly in developing more coke-resistant catalysts may lie in better understanding of what occurs during the catalytic mechanism at the active metal sites. Isotopically labeled hydrogen has been used in a variety of experiments by introducing it through CD_4, D_2, and D_2O [14-17] From the data, and assuming hydrogen is

related to the rate-determining step, the application of isotopes may shed light on the mechanistic pathways. While kinetic isotope effect studies are critically important, none of the studies to date have examined the possibility of a contribution from the preferential partitioning of hydrogen and deuterium on the surface of nickel metal particles. The nickel metal surface, after reduction, could conceivably play a role in the apparent ratios obtained from isotopic studies. The current investigation seeks to quantify the effect, if any, of H/D partitioning on the surface of nickel. If the impact were low, then it would lend greater credibility to the KIE measurements observed in the literature.

4.2 Experimentation

4.2.1 Catalyst Preparation

Nickel nitrate (100 g) were dissolved at room temperature in 600 mL of deionized water. Ammonium hydroxide was added to the dark green mixture to create a 3 M solution. The system was then heated to a boil and held for approximately two hours; a light green solid precipitated from the solution. The cake was then filtered and washed several times with deionized water.

The 25%Ni/Al_2O_3 catalyst used is a commercial catalyst, and it was ground and sieved to the 45 -100-µm particle size range.

4.2.2 BET Surface Area and Porosity Measurements

The surface area, pore volume, and average pore radius of each specific nickel catalyst was measured. Approximately 0.3–0.4 g of sample was weighed and loaded into a 3/8″ o.d. sample tube. Nitrogen was used as the adsorption gas and sample analysis was performed at the

boiling temperature of liquid nitrogen. The sample was evacuated at ambient temperature overnight to approximately 6.7 Pa. The physisorption results were quantified using the Barrett, Joyner, Halenda (BJH) desorption model, which provides a relationship between the amount of the adsorbate lost and each pore emptying step of the desorption process.

4.2.3 Temperature-Programmed Reduction

The samples (Figure 4.1) were first ramped to 350 $^{\circ}$C in pure Ar to drive off any residual

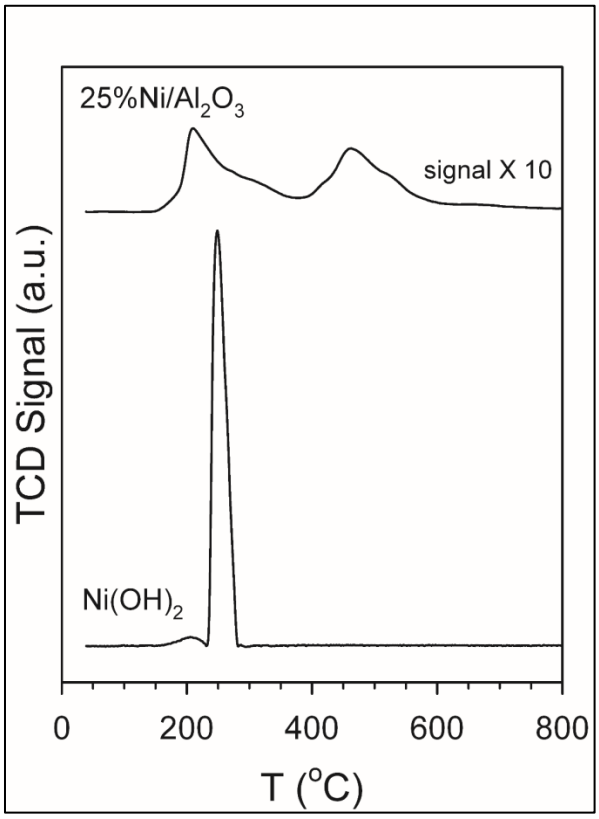

Figure 4.1: A TPR profile for the nickel oxide and the 25% Ni/Al_2O_3

H_2O from the sample, prior to cooling to 50 °C to begin the TPR. The test was performed using 10%H_2/Ar mixture referenced to Ar at a flow rate of 30 cm^3/min. (sccm). The sample was heated to 800 °C at a ramp rate of 10 ºC/min.

4.2.4 Hydrogen Chemisorption by TPD

Hydrogen chemisorption was conducted using temperature-programmed desorption (TPD). The catalyst sample was activated using a flow of 10 cm^3/min of H_2 mixed with 20 cm^3/min of argon at 350 °C for 10 h and then cooled under flowing H_2 to 50 °C. The sample was held at 100 °C under flowing argon to remove and/or prevent adsorption of weakly bound species prior to increasing the temperature slowly to 350 °C. The TPD spectrum was integrated and the number of moles of desorbed hydrogen determined by comparing its area to the areas of calibrated hydrogen pulses. The loop volume was first determined by establishing a calibration curve with syringe injections of nitrogen into a helium flow. Dispersion calculations were based on the assumption of a 1:1 H:Ni stoichiometric ratio and a spherical nickel cluster morphology.

4.2.5 Reduction and Desorption using the H_2/D_2 Mixture

(1) Each nickel catalyst was reduced under 15 sccm of the 1:1 H_2/D_2 mixture. The bed was heated at 1 °C /min to 350 °C and held for 48 h. The system was then cooled to 100 °C at 1 °C /min., at which point neon was introduced and the fixed bed system held at this condition for one hour. The reactor was then heated to 350 °C under 15 mL/min of flowing neon. The hydrogen/deuterium remaining on the catalyst desorbed and was collected in the hydrogen-specific gasbag using neon as the carrier gas.

(2) The nickel catalyst was heated to 350 °C and held for 44 h under 15 sccm of H_2 flow. After 44 h of flow, an uninterrupted switch occurred to allow the 1:1 H_2/D_2 to flow for four hours at the same temperature. The system was cooled to 100 °C at 1 °C /min, and neon was introduced. The fixed bed system was held at this condition for one hour and heated to 350 °C under 15 mL/min of neon. The hydrogen/deuterium remaining on the catalyst desorbed and was collected in a hydrogen-specific gasbag using neon as the carrier gas.

(3) The nickel catalyst was heated to 350 °C and held for 44 h under 15 sccm of D_2 flow. After the 44 h period the D_2 flow was stopped and the H_2/D_2 mixture was introduced at the same flow rate of 15 sccm for 4 h. The system was cooled to 100 °C at 1 °C /min. and neon was introduced and the fixed bed system held at this condition for one hour. The reactor was heated to 350 °C under 15 mL/min of neon. The hydrogen/deuterium remaining on the catalyst was desorbed and collected into the hydrogen-specific gasbag using neon as the carrier gas.

4.3 Results

4.3.1 Surface Area Measurements

One of the main reasons for supporting nickel on alumina is that the interaction between the metal and support tends to stabilize small nickel particles. This provides a relatively high available surface of Ni. The large surface area for the Ni/Al_2O_3 is due primarily to the alumina where the nickel particles are small enough to fit in the alumina pores without causing

significant blocking of the pores. As seen by the BET results (Table 4.1), the activation of unsupported NiO results in a catalyst having a relatively low surface area.

Table 4.1: Summary of BET surface area and porosity measurements.

Catalyst ID	BET SA (m^2/g)	Average Single Point Pore Volume (mL/g)	Average Pore Radius (nm)
$Ni(OH)_2$	17.2	0.096	11.1
$Ni(OH)_2$ (duplicate)	17.1	0.094	11.0
Ni/Al_2O_3	145	0.199	2.6

4.3.2 TPR and Hydrogen Chemisorption / Pulse Reoxidation

The TPR profiles (Figure 1) show that the decomposition of the hydroxyl groups from $Ni(OH)_2$ occurs rapidly in the first small peak at around 200 $^{\circ}$C. Based upon the literature, nickel oxide reduction to the metallic state is observed at temperatures of 523 K to 350 $^{\circ}$C [18]. Richardson et al. also confirmed a reduction temperature for NiO at 350 $^{\circ}$C using TGA [19]. The reduction temperature for nickel in this work was set at 350 $^{\circ}$C, which should reduce the nickel in the oxide, and the Ni/Al_2O_3, also confirmed by the data from pulse reoxidation measurements in Table 4.3. A comparison between Tables 4.2 and 4.3 reveals that, despite the

Table 4.2: Hydrogen chemisorption by TPD with pulse reoxidation after hydrogen reduction for 10 h at 350 ^{o}C.

Catalyst ID	H_2 desorbed per g_{cat} (mol/g_{cat})	% Disp.*	Diam.* (nm)
Ni from H_2-activated $Ni(OH)_2$	20.4	0.40	255

* 100% reduction to Ni^0 was assumed.

Table 4.3: Hydrogen chemisorption by TPD with pulse reoxidation over 25%Ni/Al_2O_3 after hydrogen reduction for 10 h at 350 °C.

H_2 desorbed per g_{cat}	Uncorrected %Disp:	Uncorrected Diam (nm):	O_2 uptake:	% Reduction:	Corrected %Disp:	Corrected Diam (nm):
138*	6.5	15.5	1356**	63.7%	10.2	9.8

* µmol H_2 desorbed/g_{cat}, ** µmol O_2 consumed/g_{cat}.

lower Ni content, the 25% Ni/Al_2O_3 catalyst had an active site density of more than 6 times that of the activated NiO catalyst. This is attributed to the much larger size of the Ni^0 particles of the activated NiO catalyst relative to the 25%Ni/Al_2O_3 catalyst (i.e., ~255 nm assuming complete reduction versus 9.8 nm, respectively).

4.3.3 Competitive Desorption

The activated NiO catalyst was first tested, in order to serve as a basis of comparison with the Ni/alumina catalyst – where hydrogen exchange with the support could occur. The H/D ratios were calculated from the amounts determined for each injection based on the calibration curves as displayed on the previous chapter. H_2 is 5.9 µmol/g_{cat}, HD is 9.9 µmol/g_{cat}, D_2 7.2 µmol/g_{cat}, and the total H-D adsorbed is 23.0 µmol/g_{cat}. This value is close to the value calculated from the TPD of $Ni(OH)_2$ given in Table 2.

The value for µmol/g_{cat} for pure nickel was expected to be low, based on both the low H_2 TPD measurement and the low BET surface area for the $Ni(OH)_2$ catalyst. This simply means that the nickel particle sizes are large and a large fraction of the nickel metal is not on the surface but rather is situated within the core of the particle and inaccessible to hydrogen. The

density of exposed metallic Ni surface sites, though low, was adequate to produce a good signal during chromatography.

In examining the effect of pretreatments with H_2 or D_2 prior to treatment with the H_2/D_2 mixture, activated nickel oxide, unlike the case of cobalt that was previously run,21 does display a slight dependency on the conditions. When scheme 2 was employed, where 44 hours of H_2 was flowed prior to 4 h treatment with the 50%/50% mixture of H_2/D_2, Ni displayed a slight but detectable preference for the hydrogen over deuterium. This effect was also displayed in scheme 3, where for 44 h D_2 was flowed over the metal prior to 4 h of the 50%/50% H_2/D_2 mixture, and deuterium was preferred over hydrogen. In the latter case, where H_2/D_2 was flowed over the metal competitively for 48 hrs., there was no isotopic preference and the ratio was essentially unity. A similar slight isotopic preference with H_2 (or D_2) pretreatment prior to running the 50%/50% H_2/D_2 mixture was observed in our previous work on cobalt only in the case of the alumina-supported cobalt catalyst.[21] This was suggested to be due to exchange with hydroxyl groups on the alumina. One possible explanation is that, unlike cobalt, residual nickel hydroxide could still be present following activation. To probe this possibility, TPR was conducted on a larger amount of Ni oxide (Figure 6). A small peak was indeed detected above the main reduction peaks, verifying that a residual of NiO was present and could be responsible for the slight exchange.

Similarly, when using solely the 50%/50% H_2/D_2 mixture, no isotopic preference was observed for the case of 25%Ni/Al_2O_3 (Scheme 1 of Table 4.4). However, the slight isotopic

Table 4.4: The H/D ratio of Ni^0 under different schemes.

Ni			
Injection	Scheme 1	Scheme 2	Scheme 3
1	1.04	1.15	0.89
2	1.03	1.17	0.91
3	1.06	1.18	0.84
4	1.03	1.12	0.85
Average	1.04	1.15	0.87
STD	0.02	0.03	0.03

effect with H_2 or D_2 treatments prior to running the H_2/D_2 mixture was exacerbated when alumina support was added as a component to the catalyst. This is observed in the slight swings in the H/D ratio for schemes 2 and 3, which are slightly greater than the case of activated NiO.

4.4 Conclusions

The overall scope of this work was to display the isotopic affect for the nickel metal and alumina-supported nickel. There have been several competitive isotopic studies done with Ni and Ni/Al_2O_3. None of these specifically looked into the possibility of isotopic preference during adsorption. Given the results of this work, no hydrogen isotopic preference on the surface of the metal was observed for either a hydrogen-activated NiO catalyst, or an-alumina supported 25%Ni catalyst. Therefore the results of KIE investigations in the literature are likely not due to preferential partitioning of either hydrogen or deuterium on the active metallic Ni sites.

A slight isotopic preference was observed for both the activated NiO and 25%Ni/alumina catalysts when a H_2 (or D_2) pretreatment was carried out for 44 h prior to flowing the 50%/50% H_2/D_2 mixture. This was likely due to exchange with hydroxyl groups on

either residual NiO (i.e., in the case of activated NiO catalyst) or alumina (in the case of the supported Ni catalyst).

Chapter 5 : Ruthenium

Adapted with permission from W.D. Shafer, V.R.R. Pendyala, G. Jacobs, J. Selegue, B.H. Davis, in: Fischer-Tropsch Synthesis, *Catalysts, and Catalysis: Advances and Applications*, eds. B.H. Davis and M.L. Occelli, CRC Press, Taylor & Francis Group, Boca Raton, Florida, **2015.**

5.1 Introduction

Renewed focus on supported ruthenium FTS catalysts can be attributed in part to interest in biomass conversion [12-14]. Given that ruthenium displays the highest FTS activity, this would make way for higher CO/H_2 conversions and hydrocarbon productivities. In addition some work done with ruthenium in a batch reactor [15] under oxidizing conditions displays the ability of a ruthenium catalyst to work under an oxidizing environment. This could also be useful for the biomass-to liquids (BTL) process [13, 14]. Another attribute of ruthenium is its ability to produce a higher alpha product [11, 12, and 16]. The main drawback of Ru is that it is very expensive for commercial use. Nonetheless, Ru is a very good model catalyst for mechanistic studies due to its high reducibility. This is in contrast to cobalt, where an unreduced fraction of cobalt oxide may be present in the working catalyst, especially if a strong interaction between cobalt and the support is present (e.g., cobalt/alumina) [17-25].

One way to advance a catalyst system is to develop understanding of the catalytic cycle. A key factor in determining the mechanism is to understand the rate-determining step (RDS) [26-29]. One technique that sheds light on the RDS is by identifying whether a kinetic isotope effect occurs once elements in reactants are isotopically substituted (e.g., ^{12}C in CO to ^{13}C, or H_2 to D_2 [30, 31]). A KIE only occurs in elementary steps that are kinetically relevant (e.g., the

RDS). Mechanistic studies to date have suggested that the RDS in FTS is controlled by CO hydrogenation. [32, 33] The underlying assumption in these studies is that H* and D* will be equally partitioned on the surface. If this assumption is not true, then this facet must be considered and accounted for in any KIE investigation involving H_2-D_2 switching.

The current work probes the relative H/D coverages on the active ruthenium metal surface through a series of competitive adsorption experiments using an equimolar mixture of H_2 and D_2 to determine if any preferential partitioning occurs that may, in turn, affect the interpretation of KIE investigations.

5.2 Experimental

5.2.1 Catalyst preparation

The 7.0% Ru/NaY was synthesized as such: NaY zeolite (Sigma-Aldrich, having a measured BET surface area of 730 m^2/g) was used as the support for the ruthenium catalyst. The catalyst was prepared by incipient wetness impregnation (IWI), with ruthenium chloride (KFK Furuya Metal Co., Ltd. Japan) as the precursor. Two impregnation steps were used, each to load 3.5% of Ru by weight. Between each step, the catalyst was dried overnight at 100 $^{\circ}C$. After the second impregnation/drying step, the catalyst was calcined under airflow at 350 $^{\circ}C$ for 4 h. The ruthenium zeolite catalyst has a measured BET surface area of 517.7 m^2/g.

The 1.0% Ru/Al_2O_3 was synthesized as such: Catalox 150 γ-alumina (having a measured BET surface area of 150 m^2/g) was used as the support for the catalyst. The catalyst was also prepared by IWI method by using ruthenium nitrosyl nitrate (Alfa Aesar) precursor. Once the catalyst was dried overnight at 100 $^{\circ}C$, it was subsequently calcined at 350 $^{\circ}C$ for 4 h in flowing air. The one percent ruthenium catalyst has a measured BET surface area of 140.6 m^2/g.

5.2.2 BET surface area and porosity measurements

The surface area, pore volume, and average pore radius of each ruthenium catalyst were measured using a Micromeritics Tri-Star 3000 gas adsorption analyzer system. Approximately 0.3-0.4 g of sample were weighed and loaded into a 3/8″ o.d. sample tube. Nitrogen was used as the adsorption gas and sample analysis was performed at the boiling temperature of liquid nitrogen. The sample was evacuated at ambient temperature overnight to approximately 6.7 Pa. The physisorption results were quantified using the Barrett, Joyner, Halenda (BJH) desorption model, which provides a relationship between the amount of the adsorbate lost and each pore emptying step of the desorption process.

5.2.3 Temperature-Programmed Reduction

The ruthenium catalysts (Figure 5.1) were first ramped to 350 ºC in pure Ar to remove

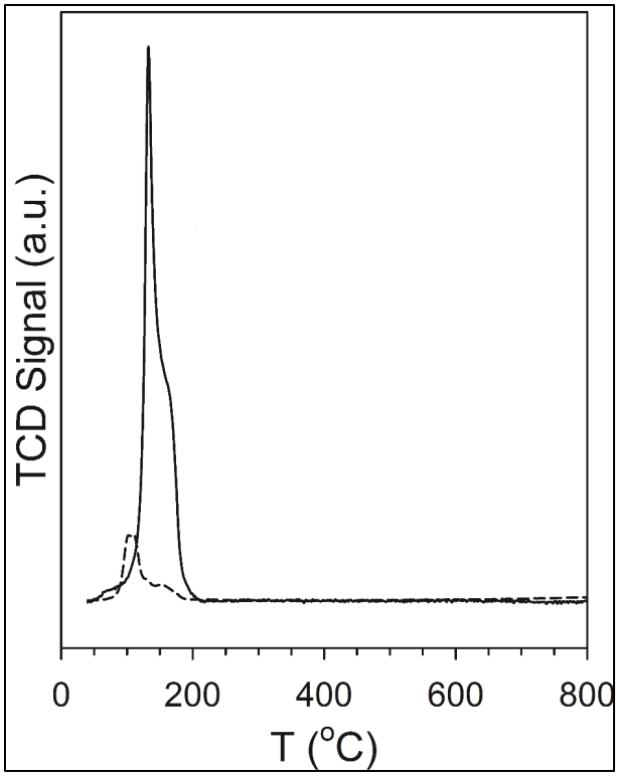

Figure 5.1**:** TPR profiles of supported ruthenium catalysts. 7% Ru/NaY (solid line), and 1% Ru/Al_2O_3 (dotted line).

residual H_2O from the sample, prior to cooling to 50 ºC to begin the TPR. The test was performed using 10% H_2/Ar mixture referenced to Ar at a flow rate of 30 cm^3/min (sccm). The sample was heated to 800 ºC at a ramp rate of 10 ºC/min.

5.2.4 Hydrogen Chemisorption by TPD

Hydrogen chemisorption was conducted using temperature-programmed desorption (TPD) with the Zeton-Altamira AMI-200 instrument. The catalyst sample was activated using a flow of 10 cm^3/min of H_2 mixed with 20 cm^3/min of argon at 350 $^{\circ}$C for 10 h and then cooled under flowing H_2 to 100 $^{\circ}$C. The sample was held at 100 $^{\circ}$C under flowing argon to remove and/or prevent adsorption of weakly bound species prior to increasing the temperature slowly to

350 °C. The TPD spectrum was integrated and the number of moles of desorbed hydrogen determined by comparing its area to the areas of calibrated hydrogen pulses. The loop volume was determined by establishing a calibration curve with syringe injections of nitrogen into a helium flow. Dispersion calculations (Table 5.1) were based on the assumption of a 1:1 H:Ru stoichiometric ratio and a spherical ruthenium cluster morphology.

Table 5.1: Hydrogen chemisorption by TPD with pulse reoxidation after hydrogen reduction for 10 h at 350 °C.

Catalyst	H_2 desorbed (μmol/g_{cat})	Dispersion* (%)	Diameter* (nm)
1% Ru/Al_2O_3	22	44	3.5
7% Ru/NaY	15.8	4.6	33.7

* 100% reduction to Ru^0 was assumed.

5.2.5 Reduction and Desorption using the H_2/D_2

Twenty grams of catalyst (i.e., either 1% Ru/Al_2O_3 catalyst or 7.1% Ru/NaY) were loaded into the plug flow reactor. The following three separate experimental approaches were used for each catalyst:

(1) The ruthenium catalyst was reduced under 15 sccm of the 1:1 H_2/D_2 mixture. The bed was heated at 1 °C /min to 623 K and held for 48 h. The system was then cooled to 100 °C at 1 °C /min., at which point neon gas flow was switched on and the fixed bed system was held at this condition for 1 h. The reactor was then heated to 350 °C under 5 mL/min of flowing neon. The hydrogen/deuterium remaining on the catalyst was desorbed

and collected in the hydrogen-specific gasbag using neon as the carrier gas.

(2) The ruthenium catalysts were heated to 350 °C and held for 44 h under 15 sccm of H_2 flow. After 44 h of flow, an uninterrupted switch occurred to allow the 1:1 H_2/D_2 to flow for 4 h at the same temperature. The system was cooled to 100 °C at 1 °C /min and the gas flow was switched to neon. The fixed bed system was held at this condition for 1 h. The reactor was heated to 350 °C under 5 mL/min of neon. The hydrogen/deuterium remaining on the catalyst desorbed and was collected in a hydrogen-specific gasbag using neon as the carrier gas.

(3) The ruthenium catalyst was heated to 350 °C and held for 44 h under 15 sccm of D_2 flow. After the 44 h period, the D_2 was stopped and the H_2/D_2 mixture was introduced at the same flow rate of 15 sccm for 4 h. The system was then cooled to 100 °C at 1 °C /min, gas flow was switched to neon, and the fixed bed system held at this condition for 1 h. The reactor was heated to 350 °C under 5 mL/min of neon. The hydrogen/deuterium remaining on the catalyst was desorbed and collected into the hydrogen specific gasbag using neon as the carrier gas.

5.3 Results and Discussion:

5.3.1 Surface Area Measurements

The BET surface area measured by adsorption of nitrogen was found to be 141 m^2/g for the 1% Ru/Al_2O_3 catalyst. A weight percentage loading of 1% ruthenium is equivalent to 1.3%

by weight RuO_2. If the Al_2O_3 is the only contributor to the area, then the area of the Ru/Al_2O_3 catalyst should be 0.987 x 150 m^2/ g = 148 m^2/g. The actual measure of surface area is approximately that of the calculated value, suggesting that pore blocking should not be a significant problem. The porosity results from the BJH adsorption tests are given in Table 1. For the case of the NaY-supported ruthenium catalysts, if NaY is the sole contributor to the surface area, the value should be close to 0.908 × 730 m^2/g = 662 m^2/g. Because the surface area of the catalyst is lower (518 m^2/g) than the expected value of 663 m^2/g, the result suggests that a fraction of the RuO_2 clusters were large enough to cause some pore blocking of the zeolite.

5.3.2 TPR and Hydrogen Chemisorption / Pulse Reoxidation

The reducibility of the supported Ru catalysts was investigated by temperature programmed reduction (TPR) experiments, and the profiles are represented in Figure 1. Both supported Ru catalysts samples display a sharp reduction peak at ~ 105-125 °C, with a shoulder on the higher temperature side of the main peak, and these are attributed the reduction of Ru species to metallic Ru (i.e., Ru^0). The activation temperature of the present study is sufficiently high to ensure complete reduction of the Ru species to Ru^0.

The hydrogen chemisorption method is used to determine the dispersion and indirectly the crystallite size of ruthenium on Al_2O_3 and NaY supports and the results are presented in Table 5.1. The NaY supported Ru (7% Ru/NaY) catalyst exhibited lower average dispersion and larger average crystallite size than the alumina supported Ru (1% Ru/Al_2O_3) catalyst. These results suggest that a significant fraction of Ru was of sufficient size to remain external to the micropores of the catalyst.

5.3.3 Competitive Desorption

The H/D ratios presented in Tables 5.2 and 5.3 were calculated from the amounts

Table 5.2: The isotope effect for the reduced 7% Ru/NaY catalyst.

Injection	Approach 1	Approach 2
1	0.95	0.97
2	0.96	0.97
3	0.94	0.97
4	0.95	0.95
Average	0.95	0.96
STD	0.01	0.01

Table 5.3: The isotope effect for the reduced 1% Ru/Al_2O_3 catalyst.

Injection	Approach 1		Approach 2	Approach 3
	Fresh	Repeat		
1	0.93	0.93	0.97	0.90
2	0.93	0.91	0.97	0.94
3	0.95	0.94	0.97	0.91
4	0.92	0.93	0.96	0.93
Average	0.93	0.93	0.97	0.92
STD	0.01	0.01	0.01	0.02

determined for each injection based on the calibration curves, again as noted in Chp3 with cobalt. The H_2 is 3.3 μmol/g_{cat}, HD is 5.5 μmol/g_{cat}, D_2 is 4.0 μmol/g_{cat}, and the total H-D adsorbed is 12.8 μmol/g_{cat}. This value is close to the value calculated from the TPD of 7% Ru/NaY given in Table 5.1. The amount of adsorbed gas (μmol/g_{cat}) calculated from the calibration curve is close to the amount calculated from the hydrogen chemisorption experiment. This indicates that relatively the same amount of ruthenium was reduced in both methods. To define the isotopic partitioning effect over the supported Ru catalysts, three different approaches were followed as mentioned in the experimental section. The reason for the different experimental approaches was to mimic the studies presented earlier [33, 35−38] in an

attempt to better understand the inverse kinetic isotope effect (IKIE) observed during CO hydrogenation. The first approach, a 48 h equal H/D molar competitive reduction, showed a small, but measurable, isotopic partitioning preference for D on the ruthenium metal surface of the Ru/NaY catalyst. Several injections were made to ensure adequate reproducibility. As shown in Table 5.3, for approach 1 the standard deviation was very small for all the injections.

Two other approaches were designed to parallel the change over from H_2 to D_2 and vice versa. Again, reduced Ru/NaY was used as a control in an attempt to learn if preferential partitioning occurred for the metal surface only. Once the ruthenium surface was completely covered with H or D atoms following a 44 h reduction at 350 $^{\circ}$C, the 4 h reduction procedure with the equimolar mixture occurred. This 4 h reduction at 350 $^{\circ}$C with a 15-sccm flow allowed for at least 24 reactor turnovers. Similar to the 50%/50% H_2/D_2 mixture reduction, H_2 or D_2 pre-reduced Ru/NaY followed by exposure to the 50%/50% H_2/D_2 mixture exhibited preferential partitioning for D, as shown in Table 2. However, when H_2 was used as the reducing gas prior to the 50%/50% H_2/D_2 mixture, the result was closer to unity, whereas when D_2 was used as the reducing gas prior to the 50%/50% H_2/D_2 mixture, the result was further from unity. These findings suggest that some exchange with hydroxyl groups of the support occurs.

Similar trends were observed for the case of 1% Ru/Al_2O_3 (Table 5.3). Our previous work with cobalt and nickel catalysts did not display virtually any isotopic partitioning [39, 40], but the present study for the supported ruthenium catalysts reveal an isotopic partitioning effect in favor of D. To further confirm that the observed effect was correct, this approach was repeated two times over the 1% Ru/Al_2O_3 to ensure the results were consistent and as shown in Table 3 the values indicate an IKIE. Duplicating this approach confirmed the initial results, demonstrating reproducibility.

Cobalt [39] and nickel [40] catalysts yielded no partitioning isotopic effect, whereas, supported ruthenium catalysts resulted in preferential partitioning isotopic effect on the surface ruthenium. This preference to a higher D* surface coverage was not contingent upon the reduction pretreatment utilized (i.e., H_2, H_2/D_2, or D_2) prior to final treatment with the 50%/50% H_2/D_2 mixture. . As can be seen from the data in Tables 3 and 4, all three approaches exhibited a greater amount of deuterium on the surface of the active ruthenium metal. The dependence of the rate-determining step, termination by hydrogen, centers on the assumption that there are equivalent coverages of H and D on the surface. The current results indicate that preferential partitioning on the surface should be considered when a KIE study involving H_2/D_2 switching is carried out.

5.4 Conclusions:

For all three approaches studied, an isotopic preference for D was observed indicating that some H/D partitioning occurs for the hydrogen pool. The overall isotope effect is relatively minor but should be accounted for in assessing the inverse kinetic isotope effect that is obtained and reported during CO hydrogenation. Both Bell and Kellner [35] and Jia et al. [41] have reported that a possible higher surface coverage of D could be a cause for the inverse kinetic isotopic effect seen during CO hydrogenation.

Chapter 6 : Iron

Adapted with permission from W. D. Shafer, V. R. R. Pendyala, M. K. Gnanamani, G. Jacobs, J. P. Selegue, S. D. Hopps, G, A. Thomas, B. H. Davis, Isotopic Apportioning of Hydrogen/Deuterium on the Surface of an Activated Iron Carbide Catalyst. Catal. Lett. **2015**, 145:1683–1690.

6.1. Introduction

The FT reaction [1-4] is at the heart of XTL processes for producing clean fuels from biomass, coal, natural gas, and has the potential to provide an alternative route for the utilization of CO_2. Iron is still one of the main metal catalysts used in the FT process industrially as a means of producing clean fuel from coal. One reason for the industrial usage of iron as an FT metal is low cost due to the high abundance of iron compared to other active metals. Another advantage for the utilization of iron carbide as the active component is its capability of converting low H_2/CO ratio syngas. This makes the iron a good choice for CTL and BTL processes (i.e., from coal and biomass, respectively) as the H_2/CO ratios from the gasification process are often less than unity. To compensate for the low syngas ratios, the iron catalyst is active toward the water-gas-shift (WGS) reaction, which adjusts the H_2/CO to favorable levels for carrying out FTS.

FT synthesis is now over 90 years old and yet the mechanism is still under scrutiny [5-8]. Numerous isotopic tracer studies have been conducted in attempts to shed light on the mechanism [8]. One technique was to label the reactants - CO by means of ^{13}C [9-12], ^{14}C [13-15] or ^{18}O [16], and then monitor the outcome of the isotope in the products by incorporating it into the carburization step or through switching experiments during reaction. Another approach

is to switch to D_2 [17-20] during a steady state period or to run H_2/D_2 [21] experiments competitively. From these experiments, several different mechanisms have been proposed for FT synthesis, with the enol and carbide mechanisms being the two more popular schemes to date [8]. Past work has offered some insight regarding the nature of the rate-determining step, where FT displayed an inverse kinetic isotopic effect (IKIE) [22-28]. Several papers on the mechanism, both theoretical [29-31] and experimental [32-34], have been published as mentioned previously, attempting to establish a full picture for the FT mechanism.

All of the isotopic work with the H_2/D_2 switching experiments focused on the mechanism of CO hydrogenation in an attempt to understand the KIE [28,35,and 36]. The present work probes H/D partitioning on the surface of iron carbide, which could potentially affect any interpretation of a KIE. Therefore, this work examines whether an isotopic preference occurs toward one isotope (H/D) and assesses whether it is sufficiently large to impact the interpretation of the IKIE based on the mechanism displayed during CO hydrogenation. Unlike cobalt [37] and nickel [38], ruthenium [39] seems to display a very slight preference for D resulting in a slightly higher surface coverage of deuterium. A similar result was obtained in the current investigation of iron carbide.

6.2. Experimental

6.2.1 Catalyst Preparation

The precipitated iron catalyst was prepared using a ferric nitrate solution obtained by dissolving iron (III) nitrate monohydrate (1.17M) in deionized water. A controlled flow of the iron nitrate mixture was added to the precipitation vessel together with a stream of ammonium hydroxide (14.8M) that was added at a rate to maintain a pH of 9.0. The slurry was recovered

using a vacuum filter and the solids were washed twice with deionized water. The final filter cake was dried for 24 h in an oven at 110 °C, followed by calcination at 350 °C in flowing air for 4 h.

6.2.2 Catalyst Characterization

6.2.2.1 BET Surface Area and Porosity Measurements

The surface area, pore volume, and average pore radius of the iron oxide catalyst (α–Fe_2O_3) was measured using a Micromeritics Tri-Star 3000 gas adsorption analyzer system. Approximately 0.3-0.4 g of sample was weighed and loaded into a 3/8″ o.d. sample tube. Nitrogen served as the adsorption gas, and sample analysis was performed at the boiling temperature of liquid nitrogen (-196 °C). Before testing, the temperature was gradually ramped to 160 °C and the sample was evacuated overnight to approximately 6.7 Pa. The physisorption results were quantified using the Barrett, Joyner, Halenda (BJH) desorption model, which provides a relationship between the amount of the adsorbate lost and each pore emptying step of the desorption process (Table 6.1).

Table 6.1: ET surface area, and pore characteristics of the iron catalyst.

Catalyst	BET surface area (m^2/g)	Single point pore volume (cm^3/g)	Average pore radius (nm)
α-Fe_2O_3	43.2	0.2033	9.41

6.2.2.2 Temperature Programmed Reduction (TPR) of CO

Carbon monoxide (Figure 1) temperature-programmed reduction (TPR) was conducted with the Zeton-Altamira AMI-200 instrument. The TPR was performed using 10% CO/He mixture (referenced to helium) at a flow rate of 30 cm^3/min. The catalyst samples were heated from 50 to 525 °C using a heating ramp rate of 10 °C /min and held for 1 h. A liquid nitrogen trap was used to continuously remove the CO_2 produced.

6.2.2.3 XRD Analysis

Powder X-ray diffractograms (XRD) of Fe_2O_3 and passivated (i.e., at room temperature under flowing 1% O_2 in nitrogen) iron carbide catalysts were recorded using a Philips X'Pert diffractometer with monochromatic Cu Kα radiation (λ - 1.5418). XRD scans were taken over the range of 2θ from 10 to 90°. The scanning step was 0.01, the scan speed was 0.0025 s^{-1}, and the scan time was 4 s.

6.2.3 Reduction and Desorption using the H_2/D_2 Mixture

Forty grams of iron oxide (Fe_2O_3) were loaded into the plug flow reactor and carburized at 400 °C for 24 h. After calcination, the following five separate experimental approaches were set up to run for each catalyst:

(1) The system was allowed to cool to 35 °C after which 15 sccm of the 1:1 hydrogen/deuterium isotopic mixture was introduced. The temperature was then ramped to 130 °C and held for a period of 48 h. After a period of 1 h, the effluent was passed into a sampling bag to check for methane. Following the 48 h period the system was then cooled to 35 °C and held for

1 h. Once 35 °C was reached, the H_2/D_2 isotopic mixture was replaced with neon for 1 h allowing for 10-15 turnovers. Lastly, the inert gas flow was decreased to 5 sccm and the system was heated from 35 °C to 130 °C and held for 15 min and during this time the effluent was sent to a hydrogen specific Tedlar bag.

(2) The system was allowed to cool to 35 °C after which 15 sccm of pure hydrogen was introduced. The temperature was then ramped to 130 °C and held for a period of 48 During this time, pure hydrogen was passed across the catalyst bed at 15 sccm for 44 h, followed by 4 h of the 1:1 hydrogen/deuterium isotopic mixture. After 1 h at 130 °C, the effluent was passed into a sampling bag to check for methane. Following the 48 h period the system was then cooled to 35 °C and held for 1 h. Once 35 °C was reached, the isotopic hydrogen mixture was replaced with neon for 1 h allowing for 10-15 turnovers. Lastly, the gas flow was decreased to 5 sccm and the system was heated from 35 °C to 130 °C and held for 15 minutes and during this time the effluent was sent to a hydrogen specific Tedlar bag.

(3) The system was allowed to cool to 35 °C after which 15 sccm of pure hydrogen was introduced to the catalyst. The temperature was then ramped to 130 °C and held for a period of 48 h. During this time, pure deuterium was passed across the catalyst bed at 15 sccm for 44 h, followed by 4 h using the hydrogen/deuterium (1:1) isotopic mixture. After 1 h at 130 °C, the effluent was passed into a bag to check for methane. Following

the 48 h time period the system was then cooled to 35 °C and held for 1 h. Once 35 °C was reached, the isotopic hydrogen mixture was replaced with neon for 1 h allowing for 10-15 turnovers. Lastly, the gas flow was decreased to 5 sccm and the system was heated from 35 °C to 130 °C and held for 15 min and during this time the effluent was sent to a hydrogen specific Tedlar bag.

(4) The system was then allowed to cool to 35 °C, and once the temperature was reached the 1:1 hydrogen/deuterium isotopic mixture was passed across the catalyst at 15 sccm. After 30 min, a 1 mL needle was placed inline of the effluent flow and 100 μl sample was taken and immediately injected on the GC-TCD. The temperature of the catalyst bed was gradually increased to 130 °C, and during this time the effluent was analyzed by GC-TCD seven times.

(5) The system was then cooled to 130 °C, and neon was allowed to flow through the system at 15 sccm for 1 h, after which a vacuum of 30 inches of water was applied to the fixed-bed system and held for 10 min. The vacuum was then shut off and the system was slowly pressurized to atmospheric pressure with the H_2/D_2 isotopic mixture over a period of 1 h. Once the system was pressurized, neon was allowed to flow at 5 sccm. This was to enable the H_2/D_2 that remained in the system to be sent to the hydrogen specific Tedlar bag.

6.3. Results

6.3.1 Surface Area Measurements

BET surface area and pore size distribution results of α-Fe_2O_3 catalyst are shown in Table 1. The BET surface area for the α-Fe_2O_3 catalyst was found to be 43.2 m^2/g.

Table 6.1. BET measurements for the α-Fe_2O_3 catalyst

Catalyst	**BET surface area (m^2/g)**	**Single point pore volume (cm^3/g)**	**Average pore radius (nm)**
α-Fe_2O_3	43.2	0.2033	9.41

6.3.2 Temperature Programmed Reduction α-Fe_2O_3 using Carbon Monoxide (CO-TPR)

Considering that the aim of this work was to study the surface partitioning of H/D on the active carbide, no promoters or supports were used. An appropriate temperature was needed to sufficiently carburize the iron oxide. CO-TPR was used to investigate the carburization behavior of catalysts in a CO atmosphere. The CO-TPR profile of α-Fe_2O_3 catalyst is shown in Figure 6.1.

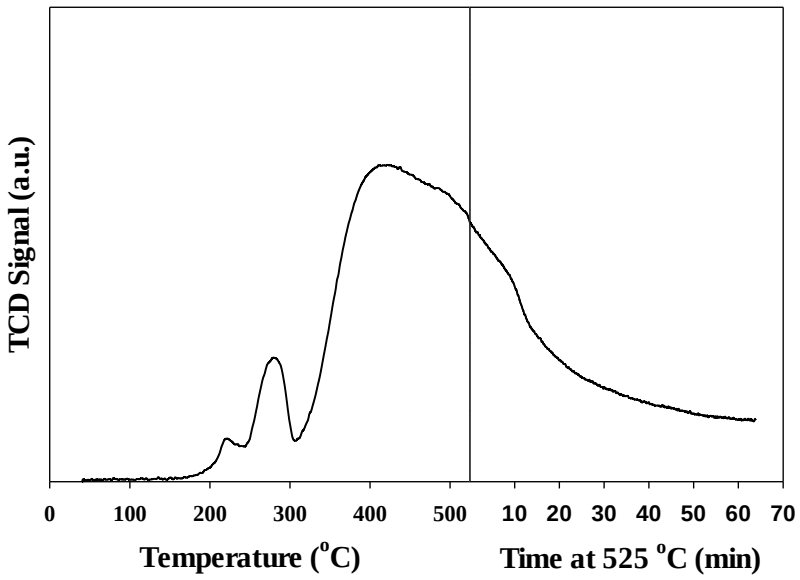

Figure 6.1: Temperature programmed reduction of CO (CO-TPR) profile of α-Fe_2O_3 catalyst.

The profile displays two primary reduction/carburization peaks. Furthermore, a very weak peak below 250 °C is also detected, which could be ascribed to the reduction of hematite (α-Fe_2O_3) to magnetite (Fe_3O_4) and the first major peak is located in the temperature range of 250–300 °C. These peaks are associated with reduction of Fe_2O_3 to lower oxides (i.e., Fe_3O_4 and a defect-laden form of this oxide) prior to carburization. The peaks are fully consistent with our previous CO-TPR XANES/EXAFS results [40-42]. The second peak is located in the temperature range of 350–525 °C. This could be ascribed to the carburization of iron magnetite to iron carbide [43-45]. Based on the CO-TPR data, the iron oxide was sufficiently carburized under the CO pretreatment conditions followed in this work.

6.3.3 X-ray Diffraction (XRD) Analysis

To confirm the formation of iron carbide (Fe_5C_2) phase following the carburization of *α-Fe_2O_3*, the X-ray diffraction (XRD) technique was utilized. XRD patterns of as prepared and carburized α-Fe_2O_3 catalyst are shown in Figure 6.2. The iron oxide (α-Fe_2O_3) catalyst was

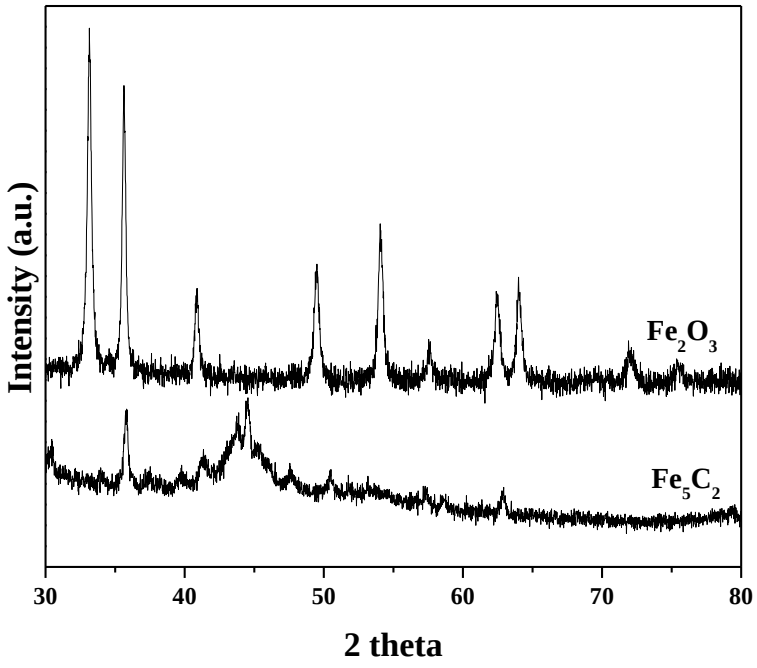

Figure 6.2: X-ray diffraction patterns of iron oxide and iron carbide.

carburized under similar conditions as used in TPD experiments (400 °C for 24h at ambient pressure), with the exception that the samples were further passivated at room temperature by using 1%O_2/N_2 for two hours before being submitted for XRD. The as-prepared catalyst displayed the XRD lines characteristic of α-Fe_2O_3 at 33, 37, 41, 49, 62, and 64 ° respectively, whereas the carburized catalyst exhibited diffraction lines corresponding to the Hägg (Fe_5C_2) iron carbide phase.

6.3.4 Analysis

The H/D ratios presented in Table 6.2 were calculated from the amounts determined for

Table 6.2: The isotope effect for the reduced iron catalyst.

α-Fe_2O_3								
H/D ratio	Approach 1			Approach 2	Approach 3	Approach 4		Approach 5
Injection	1	2	3			(°C)	1	
1	0.95	0.94	0.93	0.96	0.94	35	1.02	1.06
2	0.96	0.94	0.93	0.97	0.94	55	0.95	1.06
3	0.95	0.94	0.92	0.97	0.93	65	0.94	1.06
4		0.93	0.93	0.96	0.93	88	0.93	1.05
5			0.93			115	0.93	1.06
6						125	0.93	
7						130	0.93	
Average	0.95	0.94	0.93	0.97	0.93		0.95	1.06
STD	0.01	0.00	0.00	0.00	0.00		0.03	0.00

each injection based on the calibration curves as displayed in Chapter 3. The partitioning isotope effect in this study is defined as the total amount of desorbed H_2 divided by the total amount of desorbed D_2. When the H/D ratio is greater than 1, the partitioning isotope effect is normal; in contrast, if an inverse isotopic effect is obtained, the ratio would be less than 1.

The total amount of neon collected in the bag was 225 ml, based on a flow 5 mL/min and time on-stream of 45 min during desorption. Combined with the calibration curves given for each specific gas, the amount of each gas was quantified for the entire run from the amount injected on the GC. The results from the given calculations will allow the overall H/D ratio to

be taken into account followed by the determination of an overall H/D preference for each separate approach.

6.3.5 Isotopic Partitioning

Prior to each isotopic partitioning experiment, the Fe_2O_3 was carburized at 400 $^{\circ}$C, based on the results from TPR of carbon monoxide. Before performing any of the approaches, additional measures were taken to ensure the existence of the iron carbide phase, and that the desorption process does not interfere with the reaction of the iron catalyst. Excessive temperatures above 300 $^{\circ}$C produced significant methane compared to the amount of H_2 in the bag filled. The aim was to find a temperature where H/D could be found in the Tedlar gasbags without producing any methane. From this analysis, 130 $^{\circ}$C was chosen because of the formation of methane was not observed in the effluent during the adsorption process.

Figure 6.3 displays three different chromatograms, and the figure on the far left

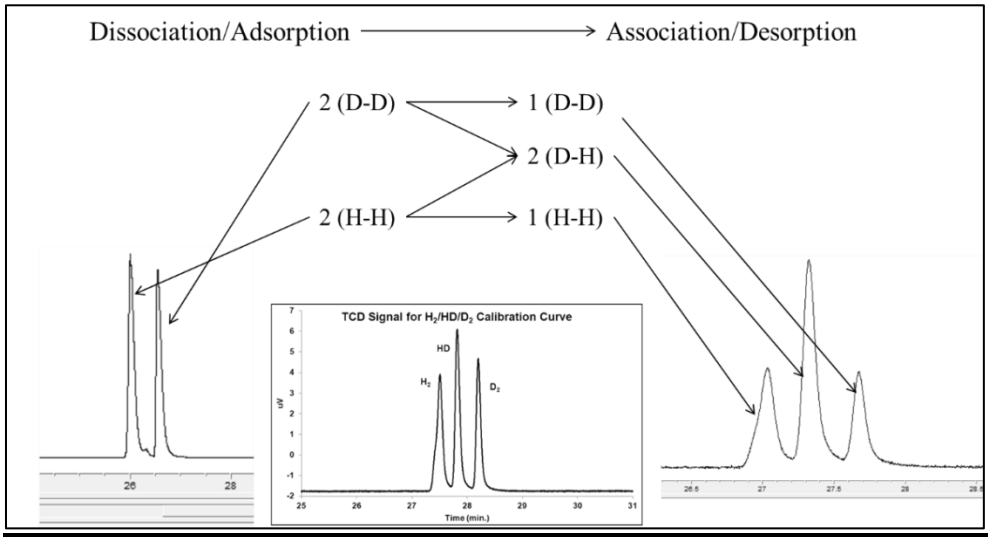

Figure 6.3: Displays the dissociative adsorption and recombinative desorption of the H_2/D_2 close to equilibrium.

represents the feed sample (no HD is present). The middle one is the feed gas mixture (H_2:HD:D_2 are at a 1:1:1 ratio), which was purchased from Cambridge Isotope Laboratories to construct calibration curves; and, the far right image is a chromatogram of the effluent at 35 $^{\circ}$C where H_2:HD:D_2 are at 1:2:1 ratios. These three chromatograms display the following:

1) HD is present in the effluent and not in the feed demonstrating that the H_2/D_2 mixture is desorbing from the surface in a dissociative manner.
2) Since the effluent displays H_2:HD:D_2 ratios of 1:2:1 compared to that of the feed, this means that when the hydrogen (or deuterium) is dissociated, the H (or D) combines with either deuterium or hydrogen.
3) Since the HD peak is twice the others, the H_2/D_2 completely exchanged.

The results indicate that dissociative adsorption is occurring without methane being formed and that associative desorption is statistically random.

The first three approaches were carried out for elongated activation periods to ensure bed saturation before the system was cooled and filled with neon. After the period where only neon flowed through the system, the Tedlar bag was then placed online after the reactor to capture all the desorbed hydrogen/deuterium. Again, the bag was checked to ensure that no methane was present that could interfere with an interpretation of the results. As shown in Table 2, results for the first three approaches displayed a very slight isotopic preference toward deuterium (H/D < 1) . Unlike the results given for cobalt [37] and nickel [38], the slight partitioning preference noted seems to be independent of all three separate approaches utilized

in the experimentation, as also displayed with ruthenium work [39]. The first approach was conducted several times to ensure reproducibility.

6.4. Discussion

Several early studies attempted to distinguish the KIE for methane and FT synthesis differences with inconclusive results. Jungers et al. [46-47] performed the H_2/D_2 switching experiment over a nickel catalyst, finding that CO hydrogenation occurred more rapidly with D_2. Others, through separate experimentation, came to the same conclusions [48-49]. However, due to the complicated nature of the FT mechanism, others observed no isotopic preference [24-27], and still others reported a positive KIE [25]; however, many of these studies were directed at the hydrogenation of CO to CH_4.

The complications that have arisen from the H_2/D_2 switching experiments, in an attempt to describe the route of CO hydrogenation, not only give unclear results involving the nature of the rate-determining step (RDS), but also through exhibiting no KIE, demonstrate that H_2 might possibly not be involved in the RDS. Given these conflicting results for the kinetic switching with CO hydrogenation and given complications of the FT synthesis, doubts as to whether this type of experiment could be used to describe the RDS and whether hydrogen plays a role in the RDS of CO hydrogenation.

In an attempt to shed light on this, Wilson [36] listed the likely kinetic steps involved in the hydrogenation of CO to CH_4.

$$H_2 \overset{K_H'}{\rightleftharpoons} (H_2)_g \overset{K_H''}{\rightleftharpoons} 2H_g \qquad (1)$$

$$CO \rightleftharpoons CO_g \rightleftharpoons C_s + O_g \qquad (2)$$

$$C+H \overset{k_1}{\underset{(K_1)}{\rightleftharpoons}} CH \overset{k_2}{\underset{(K_2)}{\rightleftharpoons}} CH_2 \overset{k_3}{\underset{(K_3)}{\rightleftharpoons}} CH_3 \longrightarrow CH_4 \qquad (3)$$

Wilson used an argument from Ozkai, who suggested that the KIE may not solely be affected by the rate-determining step but also by the available concentration of the isotopic material [35]. Wilson then illustrated that the role hydrogen played in the FT process is not only driven by kinetics, but could also be affected by isotopic concentrations (e.g., surface coverage of H or D). In short, the KIE displayed during hydrogenation of CO can potentially be explained as a combination of thermodynamic effects (for the dissociated H/D on the surface), and the kinetic effects (for CO hydrogenation) [23]. To our knowledge, all of the work that has been done experimentally has focused solely on the kinetics of CO hydrogenation. Before the hydrogen can be incorporated into a C-H(D) bond, H_2 (D_2) needs to be dissociatively adsorbed onto the surface of the active sites. Although most recent studies for the H_2/D_2 switching studies display similar results to those of Jungers et al. [46,47], the difficulties need to be addressed. Thus, determining the significance of isotopic partitioning upon the active metal for H_2/D_2 adsorption is necessary, and the main purpose for this work. The results indicate that preferential adsorption of D_2 is not the reason for the IKIE for FT synthesis with an iron carbide catalyst.

6.5. Conclusions

In the case of iron carbide, and as observed for ruthenium [37], but unlike those of cobalt [38], nickel [39], there is a very slight higher coverage of deuterium on the surface of the iron carbide. Since the overall isotopic preference of all 5 approaches utilized are close to 1, this leads to the conclusion that the differences displayed for the KIE, observed during CO hydrogenation, could be only slightly complicated by the adsorption of hydrogen/deuterium, but remain primarily due to the kinetics of CO hydrogenation.

Chapter 7 : Final Remarks, Observations, and Future Thoughts

7.1 Concluding Remarks

Evidence from the experimental results indicates that the thermodynamic step of competitive adsorption displayed very little to no KIE for all four metals analyzed. Hence, even though hydrogen undergoes several steps in the formation of hydrocarbons from CO, the thermodynamics of adsorption have no effect in the overall KIE for CO hydrogenation. Two different concluding remarks result from competitive hydrogen adsorption experiments:

1) Since competitive adsorption does not affect CO hydrogenation, KIE work utilizing H_2/D_2 switching experiments can be used to focus solely on the KIE for converting CO to aliphatic products.
2) Theoretical results that display KIE for adsorption have not agreed, as of yet, with experimental results for competitive hydrogen adsorption.

7.1.1 First Remark

As mentioned, the elucidation of equimolar competitive partitioning for hydrogen/deuterium display that relatively no KIE is present in the adsorption process. Thus, the atomic coverage across the active FT metal would essentially be uniform, allowing equivalent molar amounts of H/D atoms to incorporate into the chain growth during CO hydrogenation. Provided, if the IKIE is solely from the kinetics of CO hydrogenation, (i.e., summing up all the series of small steps between) then 3 observations may exist:

1) As a primary KIE, the change in rates of CO conversion observed indicate that hydrogen plays a role in the rate-determining step.
2) The IKIE itself reveals the larger difference in ZPE's are in the transaction states.
3) In accordance with the Hammond's postulate, the overall process for CO hydrogenation is very exothermic, revealing the transition state to be closer in energy to the reactants.

If hydrogen is involved in the RDS, as observed, then based upon the second observation and Figure 1.16, where the ratio between the X-H and X-D is $\sqrt{2}$, as noted in Table 7.1 [1], and X is

Table 7.1: A table of vibration frequencies, adapted from Nakamoto et al. [1]

	ν_H		ν_D	$\nu_H/\sqrt{2}$
H_2	4430	D_2	3134	3132.48
CH	3000	CD	2200	2121.32
MH	2250	MD	1591	1590.99
	2120		1520	1499.07
	2000		1414	1414.21
	1850		1360	1308.15
	1700		1202	1202.08

(M,H,D, or C) from the vibrational calculations from equation 12 should indicate an IKIE.

Considering this, the difference in the frequencies is again a result of the spring force constant, due to the chances in mass of the bound atoms. In addition, if A and A' are bigger than

B and B', where A/A' = B/B', then $\Delta A > \Delta B$. Hence, the mass is inversely proportional to the frequency, and one would expect M-H(D) < C-H(D); therefore ΔM-H(D) < ΔC-H(D). Provided this is the case, one could conclude, with the hypothesis from section 1.4.1, that where the KIE is dependent upon ZPE, the CO hydrogenation would yield a larger difference in ZPEs in the products of C-H (C-D) (as stated in the second observance). Applying the actual terminal frequencies for the C-H, C-D, M-H, and M-D to equation 1.14 (section 1.4.1) yields an overall KIE for CO hydrogenation ranging from 0.76 – 0.86 k_H/k_D. This very rudimentary calculation then leads to the conclusion, as proposed in the previous mechanistic schemes, that CO hydrogenation very well could itself display an IKIE, where the limitations are the differences in the C-H and C-D bonds during formation.

7.1.2 Second Remark

The proposed theoretical observations given herein both agree [2] and disagree [3] with previous calculations. Regardless, the experimental data provided by the current work disagree with the attempts to calculate the KIE though vibrational theory [2, 3]. Whereas most of the attempts through calculations, including this one, display a defined KIE based upon the differences in activation energy through ZPE vibration frequencies of H_2 (D_2) and M-H (D), experimentally no KIE exists for the competitive adsorption of hydrogen and deuterium for cobalt and nickel, and a very slight IKIE exists for iron and ruthenium.

The purpose of this work was to expound on the adsorption process experimentally, in the hopes to further the present knowledge, for the tremendously complicated adsorption process. However, this did not occur and in turn a new piece was uncovered; i.e., the difference noted between the calculated/experimental values. The unexpected deviation from the

theoretical work could simply mean that the vibrational factor (the difference in ZPE for the reactants and transition states) is not the only influence. Given these are very simple diatomic molecules, adsorbed onto a metal surface, the measurable vibrational frequencies for only the pseudo-stable reactant and final states should be easily measured. Yet surface complications of hydrogen adsorption can arise from, to name a few [4]:

1) direct repulsion reactions;
2) lateral mobility (at elevated temperatures);
3) induced site heterogeneity;
4) through-metal indirect interactions;
5) coverage-dependence of heat of adsorption.

Regardless, these surface properties mentioned are for hydrogen adsorption alone. Adding deuterium only complicates the matter for theoretical calculations, surface entropy, exchange rates, readsorption of the HD species, etc. All of these factors could play a role in why the attempts to uncover a KIE for competitive hydrogen/deuterium adsorption did not agree with the experimental evidence displayed here.

7.2 Future Work

The current work was specifically meant to reveal the competitive surface coverage of hydrogen/deuterium and how this could potentially affect CO hydrogenation; now that we can experimentally describe how the effect is noted, future work can be focused upon KIE for CO hydrogenation.

The future work mentioned specifically targets the reactor and instrument setup's ability in regard to the isotopic separation on metals. Now that the separation of H_2/HD/D_2 is possible, attempting to uncover an exchange rate for the actual FT process for H_2/D_2 through solvent interference might also be possible [5]. Work has already begun using a cobalt catalyst, as a mean to understand the effects brought by the use of solvents such as C_{30} oil, hexadecane, where H_2/D_2 exchange rates are greatly reduced. These rates are then recovered with a washing of pentane, reviving the concept using a supercritical reactor with liquid pentane as a means to wash the catalyst and yield a more productive reactor.

This exchange rate could also be utilized by looking at the iron as well. Does a certain level of coking impede hydrogen-exchange rates? An overall scope could be noted, where say 3 catalysts (no K, 1.4 K, and 5 K) from a base 100Fe5.1Si catalyst could be carburized at different temperatures to see if the level of carburization impedes the exchange rate as H_2 and D_2 are passed across the catalyst.

This work could be extended outside of FT metals, where other processes/observances that display a hydrogen KIE on the metal could be probed. Metals such as ceria, platinum, and zirconia are common metal supports [6] for the WGS process that can affect the KIE. Observances such as spillover can be probed for effects, as seen on Rh [7, 8].

Lastly, in light of the separation of the H_2/D_2 products, we hope to separate of the isotopically abundant mixtures of methane (i.e., CH_4 – CDH_3 – CD_2H_2, etc.). If this could be accomplished, the previous statistical approaches given by the results from the mass spectra during online analysis could be overcome. This could be a beneficial direction to turn without relying on any statistical operations from online mass spectra fragmentation patterns.

7.3 Closing Remarks

An extraordinary amount of work and insight has been brought to the FT process over the more than 90 years since its discovery. The current work is a small piece of the puzzle, performed in an attempt to uncover a mechanism for the process as a whole. Nevertheless, more work will be required to fully disclose a mechanistic route for the entire FT process.

Appendix 1: List of Abbreviations

1. ASF – Anderson-Shulz-Flory
2. BPD – Barrels Per Day
3. BTL – Biomaterials to Liquid's
4. CTL – Coal to Liquids
5. FID – Flame Ionization Detector
6. FT – Fischer Tropsch
7. GTL – Gas to Liquids
8. IKIE – Inverse Isotopic Effect
9. KIE – Kinetic Isotope Effect
10. NKIE – Normal Kinetic Isotope Effect
11. RDS – Rate Determining Step
12. RTS – Raw materials to Liquids
13. SV – Space Velocity
14. TOS – Time On Stream
15. TPR – Temperature Programmed Reduction
16. TPD – Temperature Programmed Desorption
17. TCD – Thermal Conductivity Detector
18. VLE – Vapor Phase Equilibrium
19. WGS – Water Gas Shift
20. XRD – X-Ray Diffraction
21. ZPE – Zero Point Energy

References

Chapter 1

1. Taylor, H., *Paul Sabatier 1854-1941*. J. Am. Chem. Soc., **1944**, 66, 1615–1617.
2. A. G. Morachevskii, Paul Sabatier (to 150th Anniversary of His Birthday) *Russian Journal of Applied Chemistry*, **2004**, 77, 1909-1912.
3. The Nobel Prize in Chemistry 1912: Paul Sabatier http://www.nobelprize.org/nobel_prizes/chemistry/laureates/1912/ (assessed 7/22/15).
4. P. Sabatier, How I Have Been Led to the Direct Hydrogenation Method by Metallic Catalysts, *Industrial and Engineering Chemistry*, **1926**, 18**,** 1005–1008.
5. W. Zerong, *Comprehensive Organic Name Reactions and Reagents 3*, John Wiley & Sons, Inc. New York City, New York, **2010.**
6. P. Sabatier, J. B. Senderens, *Direct Hydrogenation of Oxides of Carbon in Presence of Various Finely Divided Metals.* Compt. Rend., **1902,** 134, 689-691.
7. P. Sabatier, J. B. Senderens, *Decarbonization of Carbon Monoxide*. Bull. Soc. Chim., 1903, 29, 294.
8. W. D. Bancroft, A. B. George, *Hydrogenation of Benzene with Nickel and Platinum*. J. Phys. Chem., **1931**, 35, 2219.
9. P. Sabatier, J. B. Senderens, *New Synthesis of Methane.* Compt. Rend., **1902**, 134, 514-516.
10. P. Sabatier, Paris Et. Liege Librairie Polytechnique, *CH.* Beranger, Editeur Pairs, 15, Rue Des saints-Peres, 15 Liege, 21, Rue De La Regence, La Catalyse En Chimie Organique **1920,** 21, 1-387.
11. Sabatier, P. and Mailhe, A., Ann. Chim. Phys., **1908**, 10, 527.

12. F. Fischer and H. Tropsch "Process for the production of paraffin-Hydrocarbon with more than one carbon atom." **1930,** FT patent 1746464.

13. A. N. Stranges, *A History of the Fischer-Tropsch Synthesis in Germany 1926-45*, Studies in Surface Science and Catalysis, **2007**, 163, 1-27.

14. R. B. Anderson. *Forty Years With The Fischer-Tropsch Synthesis 1944-1984,* Studies in Surface Science and Catalysis, **1984**, 19, 457–461.

15. F. Fischer, H. Tropsch, *Synthesis of Petroleum at Atmospheric Pressure From Gasification Products of Coal*, Brennst-Chem, **1926**, 7, 97-104.

16. F. Fischer, H. Tropsch, *Development of the Benzene Synthesis from Carbon Monoxide and Hydrogen at Atmospheric Pressure,* Brennst-Chem, **1930**, 11, 489-500.

17. "Documents on German Foreign Policy 1918-1945", Series C, Vol. 5, United States, Government Printing Office, Washington **1966**, document № 490, 853-862.

18. "Principles to Govern the Treatment of Germany in the Initial Control Period," no. 848, The Conference of Berlin (The Potsdam Conference), 1945, Foreign relations of the United States, Diplomatic Papers (17 vols., Washington, DC, 1949-1964-1968), 2, **1960**, 750-3, on 752.

19. "Multilateral: German industries," United States Treaties and Other International Agreements, part I, 1951 (35 vols., Washington DC, 1950-84): 2 **1952**, 962-72, on 963.

20. "Multilateral: Incorporation of Germany into European Community of Nations," United States Treaties and Other International Agreements, part II, 1952 (35 vols., Washington DC, 1958-84), 3, **1954,** 2714-22, 2716.

21. Historical Milestones http://www.sasol.com/about-sasol/company-profile/historical-milestones, assessed (07/27/15).

22. Department of State, Office of the Historian:MILESTONES: 1969–1976 Oil Embargo, 1973–1974 U.S., https://history.state.gov/milestones/1969-1976/oil-embargo (assessed 07/27/15).

23. German document Retrieval Project: http://www.fischer-tropsch.org/DOE/germ_doc_ret_proj/report.pdf (assessed 07/28/15).

24. The German Document Retrieval Project http://www.fischer-tropsch.org/DOE/germ_doc_ret_proj/overview.pdf (assessed 07/28/15).

25. Archival Procedures for the German Document retrieval Project http://www.fischer-tropsch.org/DOE/germ_doc_ret_proj/procedures.pdf (assessed 07/29/15).

26. M. E. Dry, *The Fischer-Tropsch (FT) synthesis processes, Handbook of Heterogeneous Catalysis (2nd Edition)* **2008**, 6, 2965-2994.

27. J. L. Casci, M.C. Lok, M.D. Shannon, *Fischer–Tropsch catalysis: The basis for an emerging industry with origins in the early 20th Century,* Catalysis Today **2009**, 145, 38-44.

28. C. H. Bartholomew, *History of cobalt catalyst design for Fischer-Tropsch synthesis* American Institute of Chemical Engineers, Spring National Meeting, New Orleans, LA, United States, Mar. 30-Apr. 3, **2003** , 2884-2897.

29. B. H. Davis, *An overview of Fischer-Tropsch synthesis at the U.S. Bureau of Mines*, American Institute of Chemical Engineers, Spring National Meeting, New Orleans, LA, United States, Mar. 30-Apr. 3, **2003**, 2789-2797.

30. Gas-to-Liquids (GTL) http://www.shell.com/global/future-energy/natural-gas/gtl.html, (assessed 07/31/15).

31. Gas-To-Liquids Plants face challenges in the U.S market. http://www.eia.gov/todayinenergy/detail.cfm?id=15071, (assessed 07/31/15).

32. Gas-to-Liquids: Transforming Natural Gas into Super clean Fuels, http://www.chevron.com/deliveringenergy/gastoliquids/,(assessed 07/31/15).

33. Davis, Burtron H. Clean fuels from coal: The path to 1972, Preprints of Symposia - American Chemical Society, Division of Fuel Chemistry **2003**, 48(1), 141-143.

34. Zhang, Yongoing; Davis, Burtron H. Indirect coal liquefaction - where do we stand?, From Preprints - American Chemical Society, Division of Petroleum Chemistry **1999**, 44(1), 20-24.

35. Coal To Liquids http://energy.gov/fe/science-innovation/clean-coal-research/coal-liquids, (assessed 08/1/15).

36. Clean Coal :Carbon capture, utilization and storage, http://www.sasol.co.za/innovation/new-energy/clean-coal, (assessed 08/1/15).

37. Biomass To liquids (BTL), http://www.biofuelstp.eu/btl.html, (assessed 08/1/15).

38. Biomass To liquids (BTL), http://www.velocys.com/our_products_applications_btl.php, (assessed 08/1/15).

39. Coal and Biomass to Liquids, http://energy.gov/fe/coal-and-biomass-liquids,(assessed 08/1/15).

40. C. Higman, M. van der Burgt, *Gasification*, Gulf Professional Publishing. Houston TX, Copyright. **2008,** 1-456.

41. P. A. Nikrityuk, B. Meye, *Gasification Processes: Modeling and Simulation*, Wiley-VCH, New York NY, **2014**, 1-360.

42. G. Jacobs, A. Crawford, L. Williams, P.M. Patterson, B.H. Davis, *Low temperature water-gas-shift: comparison of thoria and ceria catalysts,* Applied Catalysis, A: General **2004**, 267(1-2), 27-33.

43. M. Martinelli, G. Jacobs, U.M. Graham, W.D. Shafer, D.C. Cronauer, J.A. Kropf, C.L. Marshall, S. Khalid, C.G. Visconti, L. Lietti, B.H. Davis, *Water-gas-shift: Characterization and testing of nanoscale YSZ supported Pt catalysts*. Appl. Catal., A: Gen. **2015**, 497, 184-197.

44. Water Gas Shift and Hydrogen Production : Water Gas Shift http://www.netl.doe.gov/research/coal/energy-systems/gasification/gasifipedia/water-gas-shift,(assessed 08/3/15).

45. J. Scherzer, A. J. Gruia, *Hydrocracking Science and Technology* **1996**, Marcell Dekker INC., New York NY,

46. J. Yang, W.D. Shafer, V.R.R. Pendyala, G. Jacobs, D. Chen, A. Holmen, B.H. Davis, *Fisher-Tropsch Synthesis: Using Deuterium as a Tool to Investigate Primary Product Distribution* Catal. Lett. **2014**, 144(3), 524-530.

47. B. Shi, B.H. Davis, *Fischer-Tropsch synthesis: accounting for chain-length related phenomena.* Appl. Catal., A: Gen. **2004**, 277(1-2), 61-69.

48. B.H. Davis, *Fischer–Tropsch synthesis: current mechanism and futuristic needs*. Fuel Proc. Tech., **2001** 71, 157-166.

49. A. Tuxen, S. Carenco, M. Chintapalli, C. Chuang, C. Escudero, E. Pach, P. Jiang, F. Borondics, B. Beberwyck, A.P. Alivisatos, G. Thornton, W.F. Pong, J. Guo, R. Perez, F. Besenbacher, M. Salmeron, *Size-Dependent Dissociation of Carbon Monoxide on Cobalt Nanoparticles.* J. Am. Chem. Soc. **2013**, 135, 2273-2278.

50. Y. Qi, J. Yang, D. Chen, A. Holmen, *Recent Progresses in Understanding of Co-Based Fischer–Tropsch Catalysis by Means of Transient Kinetic Studies and Theoretical Analysis*. Catal. Lett. **2015,** 145, 145-161.

51. G. Jacobs, B. H. Davis, *Applications of isotopic tracers in Fischer–Tropsch synthesis.* Catal Sci Technol., **2014** 4, 3927-3944.

52. R. B. Anderson, R.A. Friedel, H. H. Storch. *Fischer-Tropsch Reaction Mechanism Involving Stepwise Growth of Carbon Chain*. J. Chem. Phys. **1951**, 19, 313.

53. G.V. Schulz, Z Phys. Chem , **1935**, 30, 379.

54. P.J. Flory, *Molecular Size Distribution in Linear Condensation Polymers*, J. Am. Chem. Soc., **1936,** 58, 1877-1885.

55. M. E. Dry, *The Fischer–Tropsch process: 1950–2000.* Catal. Today, 71, **2002**, 227–241.

56. D.R. Milburn, V. R. K. Chary, B.H. Davis, *Promoted iron Fischer-Tropsch catalysts: characterization by nitrogen sorption*, Appl. Catal., A: Gen. **1996**, 144, 121-132.

57. M. Luo, H. Hamdeh, B.H. Davis, *Potassium promoted iron Fischer-Tropsch Synthesis catalyst activation study with Mossbauer spectroscopy* Preprints - American Chemical Society, Division of Petroleum Chemistry **2007**, 52, 73-76.

58. V.R.R. Pendyala, G. Jacobs, M. K. Gnanamani, Y. Hu, A. MacLennan, B.H. Davis, *Selectivity control of Cu promoted iron-based Fischer-Tropsch catalyst by tuning the oxidation state of Cu to mimic K Applied Catalysis*, A: Gen. **2015**, 495, 45-53.

59. O. Rachid, A. H. Singleton, J. G. Goodwin Jr, *Comparison of patented Co F–T catalysts using fixed-bed and slurry bubble column reactors*, Appl. Catal. A: Gen., **1999,** 186, 129-144.

60. G. Jacobs, T. K. Das, Y. Zhang, J. Li, G. Racoillet, B. H. Davis, *Fischer–Tropsch synthesis: support, loading, and promoter effects on the reducibility of cobalt catalysts* Appl. Catal. A: Gen. **2002,** 233, 263–281.

61. E. Iglesia, S.C. Reyes, R.J. Madon, *Transport-Enhanced a-Olefin Readsorption Pathways in Ru-Catalyzed Hydrocarbon Synthesis*. J. Catal., **1991**, 129, 238-256.

62. R.J. Madon, E. Iglesia, *The Importance of Olefin Readsorption and H_2/CO Reactant Ratio for Hydrocarbons Chain Growth on Ruthenium Catalysis.* J. Catal., **1993**, 139, 576-590.

63. E.W. Kuipers, I.H. Vinkenburg, H. Oosterbeek, *Chain Length Dependence of α-Olefin Readsorption in Fischer-Tropsch Synthesis.* J. Catal., **1995**, 152, 137-146.

64. C.H. Zhang, Y. Yang, T.B. Teng, T.Z. Li, Zheng, H.W. Xiang, Y.W. Li, *Study of an iron-manganese Fischer–Tropsch synthesis catalyst promoted with copper.* J. Catal. **2006**, 237, 405-415.

65. B. Shi, B.H. Davis, *Fischer-Tropsch synthesis: The paraffin to olefin ratio as a function of carbon number.* Catal. Today **2005**, 106, 129-131.

66. B. Shi, L. Wu, Y. Liao, C. Jin, A. Montavon, *Explanations of the formation of branched hydrocarbons during Fischer-Tropsch synthesis by alkylidene mechanism.* Topics in Catal. **2014**, 57, 451-459.

67. B. Shi, B.H. Davis, *Fischer-Tropsch Synthesis: Evidence for Chain Initiation by Ethene and Ethanol for an Iron Catalyst.* Topics in Catal. **2003**, 26, 157-161.

68. A. Tuxen, S. Carenco, M. Chintapalli, C.-Hao Chuang,. C. Escudero, E. Pach, P. Jiang, F. Borondics, B. Beberwyck, A. P. Alivisatos, G. Thornton, W.-Fa. Pong, J. Guo, R.

Perez, F.G. Besenbacher, M. Salmeron, *Size-Dependent Dissociation of Carbon Monoxide on Cobalt Nanoparticles*. J. Am. Chem. Soc. **2013**, 135, 2273−2278.

69. M.E. Bridge, C.M. Comrie, R.M. Lambert, *Chemisorption Studies on Cobalt single Crystal Surface, I. Carbon monoxide on Co(OOO1).* Surf. Sci., **1977**, 67, 393.

70. E.D. Williams, W.H. Weinberg, *The Geometric Structure of Carbon Monoxide Chemisorbed on the Ruthenium (001) Surface at Low Temperatures*. Surf. Sci. **1979,** 82, 93.

71. G. Ertl, M. Neumann, K.M. Streit, *Chemisorption of CO on the Pt (111).* Surface, Surf. Sci. **1977**, 64, 393.

72. K. Christmann, O. Schober, G. Ertl, , *Adsorption of CO on a Ni(111) surface*. J. Chem. Phys. **1974**, 60, 4719-4724.

73. H. Ohtani, M.A.V. Hove, G.A. Somorjai, *LEED intensity analysis of the surface structures of Pd(111) and of CO adsorbed on Pd(111) in a (√3 × √3)R30° arrangement*. Surf. Sci., **1987**, 187, 372-386.

74. P.A. Thiel, E.D. Williams, J.T. Yates Jr., W.H. Weinberg, *The chemisorption of Co on Rh(111).* Surf. Sci., **1979** 84, 54-64.

75. J. Lauterbach, R.W. Boyle, M. Schick, W.J. Mitchell, B. Meng, W.H. Weinberg, *The adsorption of CO on Ir(111) investigated with FT-IRAS.* Surf., Sci., **1996**, 350, 32-44.

76. H. Papp, *The chemisorption of carbon monoxide on a Co(0001) single crystal surface; studied by LEED, UPS, EELS, AES and work function measurements.* Surf. Sci., **1983**, 129, 205-218.

77. H. Pfnür, D. Menzel, F.M. Hoffmann, A. Ortega, A.M. Bradshaw, *High resolution vibrational spectroscopy of CO on Ru(001): The importance of lateral interactions*. Surf. Sci., **1980**, 93, 431-452.

78. J.P. Biberrian, M.A. Van Hove, *A new model for CO ordering at high coverages on low index metal surfaces: A correlation between LEED, HREELS and IRS: II. CO adsorbed on fcc (111) and hep (0001) surfaces*. Surf., Sci., **1984**, 138, 361-389.

79. G.T.K.K. Gunasooriya, *Combined Theoretical and Experimental Study of CO Adsorption and Reactivity Over Platinum and Cobalt*, National University of Singapore, Singapore, **2014**.

80. J.J.C. Geerlings, M.C. Zonnevylle, C.P.M. de Groot, *Studies of the Fischer-Tropsch reaction on Co(0001).* Surf. Sci., **1991**, 241, 302-314.

81. G.A. Beitel, A. Laskov, H. Oosterbeek, E.W. Kuipers, *Polarization Modulation Infrared Reflection Absorption Spectroscopy of CO Adsorption on Co(0001) under a High-Pressure Regime.*, J. Phys. Chem., **1996**, 100, 12494-12502.

82. G.A. Beitel, C.P.M. de Groot, H. Oosterbeek, J.H. Wilson, *A Combined in-Situ PM-RAIRS and Kinetic Study of Single-Crystal Cobalt Catalysts under Synthesis Gas at Pressures up to 300 mbar*, J. Phys. Chem. B **1997,** 101, 341, 4035-4043.

83. E. Patanou, E.Z. Tveten, D. Chen, A. Holmen, E.A. Blekkan, *Microcalorimetric studies of H_2 and CO on Co/γ-Al_2O_3 catalysts for Fischer–Tropsch synthesis*. Catal. Today, **2013**, 214, 19-24.

84. B. H. Davis, *Fischer–Tropsch Synthesis: Reaction mechanisms for iron catalysts*, Catal. Today, **2009**, 141, 25–33.

85. R. C. Brady III and R. Pettit, *Mechanism of the Fischer-Tropsch reaction. The chain propagation step.* J. Am. Chem. Soc., **1981**, 103, 1287–1289.

86. R. C. Brady III, R. Pettit, *Reactions of diazomethane on transition-metal surfaces and their relationship to the mechanism of the Fischer-Tropsch reaction*. J. Am. Chem. Soc., **1981**, 102, 6181–6182.

87. P. M. Maitlis and V. Zanotti, Organometallic Models for Metal Surface Reactions: Chain Growth Involving Electrophilic Methylidynes in the Fischer–Tropsch Reaction. Catal. Lett., **2007**, 122, 80–83.

88. P. M. Maitlis, H. C. Long, R. Quyoum, M. L. Turner, Z.-Q. Wang, *Heterogeneous catalysis of C–C bond formation: black art or organometallic science?* Chem. Commun., **1996**, 1, 1–8.

89. B. E. Mann, M. L. Turner, R. Quyoum, N. Marsih and P. M. Maitlis, Demonstration by ^{13}C NMR Spectroscopy of Regiospecific Carbon−Carbon Coupling during Fischer−Tropsch Probe Reactions, J. Am. Chem. Soc., **1999**, 121, 6497–6498.

90. J. Gaube and H. F. Klein, *Studies on the reaction mechanism of the Fischer–Tropsch synthesis on iron and cobalt.* J. Mol. Catal. A, **2008**, 283, 60–68.

91. R. A. van Santen, A. J. Markvoort, I. A. W. Filot, M. M. Ghouriab, E. J. M. Hensen, *Mechanism and microkinetics of the Fischer–Tropsch reaction,* Phys. Chem. Chem. Phys. **2013**, 15, 17038.

92. M. Ojeda, R. Nabar, A. U. Nilekar, A. Ishikawa, M. Mavrikakis, E. Iglesia, *CO activation pathways and the mechanism of Fischer–Tropsch synthesis,* J. of Catal. **2010**, 272, 287–297.

93. Kummer, J. T.; Podgurski, H. H.; Spencer, W. B.; Emmett, P. H. *Mechanism studies of the Fischer-Tropsch synthesis. The addition of radioactive alcohol,* J. Am. Chem. Soc., **1951**, 73, 564-569.

93. J. T. Kummer, W. Dewitt, P. H. Emmett, *Some Mechanism Studies on the Fischer-Tropsch Synthesis Using C^{14}.* J. Am. Chem. Soc., **1948**, 70, 3632-3643.

94. H.H. Storch, N. Golumbic, R.B. Anderson, *The Fischer–Tropsch and Related Syntheses,* Wiley, New York, NY, **1951**.

95. H. Pichler, H. Schulz, *Neuere Erkenntnisse auf dem Gebiet der Synthese von Kohlenwasserstoffen aus CO und H_2.* Chemie Ingenieur Technik. **1970,** 42, 1162-1174.

96. C. F. Huo, Y. W. Li, M. Beller, H. Jiao, *$HCo(CO)_3$-Catalyzed Propene Hydroformylation. Insight into Detailed Mechanism.* Organometallics **2003**, 22, 4665-4677.

97. O. C. Elvins, A. W. Nash, *Synthetic Fuel From Carbon Monoxide and Hydrogen.* Fuel, **1926**, 5, 263-265.

98. O.C. Elvins, A.W. Nash, *Reduction of Carbon Monoxide*. Nature, **1926**, 118, 154.

99. J. Yang, W.D. Shafer, V.R.R. Pendyala, G. Jacobs, D. Chen, A. Holmen, B.H. Davis, *Fischer–Tropsch Synthesis: Using Deuterium as a Tool to Investigate Primary Product Distribution.* Catal. Lett., **2014**, 144, 524-530.

100. J. Yang, W.D. Shafer, V.R.R. Pendyala, G. Jacobs, W. Ma, D. Chen, A. Holmen, B.H Davis *Fischer-Tropsch Synthesis: Deuterium Kinetic Isotopic Effect for a 2.5% Ru/NaY catalysis.* Top. Catal., **2014**, 57, 508-517.

101. C. M. Masuku, W.D. Shafer, W. Ma, M. K. Gnanamani, G. Jacobs, D. Hildebrandt, D. Glasser, B.H. Davis, *Variation of residence time with chain length for products in a slurry-phase Fischer Tropsch reactor*, J. of Catal. **2012**, 287, 93-101.

102. G. P. Van Der Laan and A. A. C. M. Beenackers, *Kinetics and Selectivity of the Fischer-Tropsch Synthesis: A Literature Review*. Catal. Rev., **1999**, 41, 255–318.

103. A. Steynberg, M. Dry, *Fischer-Tropsch Technology*, Studies in Surface science and Catalysis , **2004**, 152, 1-700.

104. B. Schliebs, J. Gaube, *The Influence of the Promoter K_2CO_3 in Iron Catalysts on the Carbon Number Distribution of Fischer-Tropsch Products*. Berichte der Bunsengesellschaft für physikalische Chemie, **1985,** 89, 68-73.

105. J. Patzlaff, Y. Liu, C. Graffmann, J. Gaube, *Studies on product distributions of iron and cobalt catalyzed Fischer–Tropsch synthesis* Appl. Catal. A, **1999,** 186, 109.

106. G.A. Huff Jr, C.N. Satterfield, *Evidence for two chain growth probabilities on iron catalysts in the Fischer-Tropsch synthesis* J. Catal., **1984**, 85, 370-379.

107. X. Zhan, B.H. Davis, Two Alpha Fischer-Tropsch Product Distribution. A role for Vapor-Liquid Equilibrium? Pet. Sci. Technol., **2000**, 18, 103.

108. A.P. Raje, B.H. Davis, Effect of Vapor−Liquid Equilibrium on Fischer−Tropsch Hydrocarbon Selectivity for a Deactivating Catalyst in a Slurry Reactor Energy Fuels, **1996**, 10, 552.

109. E. Iglesia, S.C. Reyes, R.J. Madon, Transport-Enhanced a-Olefin Readsorption Pathways in Ru-Catalyzed Hydrocarbon Synthesis. J. Catal. **1991**, 129, 238-256.

110. R.J. Madon, E. Iglesia, The Importance of Olefin Readsorption and H_2/CO Reactant Ratio for Hydrocarbon Chain Growth on Ruthenium Catalysts. J. Catal., **1993**, 139, 576-590.

111. R.J. Madon, S.C. Reyes, E. Iglesia, *Primary and Secondary reaction pathways in Runtehnium-catalyzed hydrocarbon synthesis.* J. Phys. Chem. **1991**, 95, 7795-7804.

112. T.P. Wilson, *Comments on heterogeneous methanation: Absence of H_2/D_2 kinetic isotope effect on Ni, Ru, and Pt*. J. Catal. **1979**, 60, 167-168.

113. M. Ojeda, A. Li, R. Nabar, A.U. Nilekar, M. Mavrikakis, E. Iglesia, *Kinetically Relevant Steps and H_2/D_2 Isotope Effects in Fischer−Tropsch Synthesis on Fe and Co Catalysts.* J. Phys. Chem. C. **2010**, 114, 19761-19770.

114. R.A. Dalla Betta, M. Shelef, *Heterogeneous Methanation: Absence of H_2-D_2, Kinetic Isotope Effect on Ni, Ru, and Pt.* J. Catal., **1977**, 49, 383-385.

115. M .Shelef, R.A. Dalla Betta, *Reply to comments on heterogeneous methanation: Absence of H_2/D_2 kinetic isotope effect on Ni, Ru, and Pt*, J. Catal. **1979**, 60, 169-170.

116. P.F.M.T. van Nisselrooij, J.A.M. Luttikholt, R.Z.C. van Meerten, M.H.J.M. de Croon, J.W.E. Coenen, *Hydrogen/deuterium kinetic isotope effect in the methanation of carbon monoxide on a nickel-silica catalyst.* Appl. Catal., **1983**, 6, 271-281.

117. E.W. McKee, *Interaction of hydrogen and carbon monoxide on platinum group metals* J. Catal. 1967, 8, 240-249.

118. C.S. Kellner, A.T. Bell, *Evidence for H_2/D_2 Isotope Effects on Fischer-Tropsch Synthesis over Supported Ruthenium Catalysts*. J. Catal. **1981**, 67, 175-185.

119. L. Luyten, J.C. Jungers, *La cinétique de la synthèse catalytique du méthane sur le nickel*. Bull. Soc. Chim. Belg. **1945**, 54, 303-318.

120. J. Nicolai, M. d'Hont, J.C. Jungers, *La synthèse du méthane à partir d'anhydride carbonique et d'hydrogène sur le nickel.* Bull. Soc. Chim. Belg. **1946**, 55, 160-176.

121. T. Mori, H. Masuda, H. Imai, A. Miyamoto, Y. Murakami, Shokubai, 1980, 22, 7.

122. M.M. Sakharov, E.S. Dokukina, Kinet. Katal. ,**1961**, 2, 710.

123. R.A. Dalla Betta, M. Shelef, *Heterogeneous Methanation: Absence of H_2-D_2, Kinetic Isotope Effect on Ni, Ru, and Pt.* J. Catal. **1977**, 49, 383-385.

124. B. Shi, J. Chunfen, *Inverse kinetic isotope effects and deuterium enrichment as a function of carbon number during formation of C–C bonds in cobalt catalyzed Fischer–Tropsch synthesis.* J. Appl. Catal A: Gen. **2011**, 393, 178-183.

125. Nakamoto, K., *Infrared Spectra of Inorganic and Coordination Compounds*., **1978,** Wiley, New York, NY.

126. A.P Baddorf, V Jahns, D.M Zehner, H Zajonz, D Gibbs. *Relaxation and Thermal Expansion of Ru(0 0 0 1) between 300 and 1870 K and the Influence of Hydrogen* Surf. Sci. **2002**, 498, 74-82.

127. B. Hammer, *Coverage dependence of N_2 dissociation at an N, O, or H precovered Ru(0001) surface investigated with density functional theory.* Phys. Rev. B. **2001**, 63, 205423.

128. T. A. Jachimowski, W. H. Weinberg, *Direct reaction of gas-phase atomic hydrogen with chemisorbed hydrogen on Ru(001), J. Chem. Phys.* **1994**, 101, 10997-11003.

129. M. Y. Chou, J. R. Chelikowsky, *First-principles study of hydrogen adsorption on Ru(0001): Possible occupation of subsurface sites.* Phys. Rev. Lett. **1987**, 59, 1737-1740.

130. J. Schulz, E. Taglauer, P. Feulner, D. Menzel, *Position analysis of light adsorbates by recoil detection: H on Ru(001).* Nucl. Instrum. Methods Phys. Res. Sect. B **1992**, 64, 588-592.

131. H. Conrad, R. Scala, W. Stenzel and R. *Unwin Adsorption of hydrogen and deuterium on Ru(001)* J. Chem. Phys. **1984**, 81, 6371-6378.

132. M. Y. Chou, J. R. Chelikowsky, *Theoretical study of hydrogen adsorption on Ru(0001): Possible surface and subsurface occupation sites*. Phys. Rev. B: Condens. Matter Mater. Phys. **1989**, 39, 5623-5631.

133. M.V. Arena, E.D. Westre, D.E. Brown, J. Kutzner, S.M. George, *Surface diffusion of hydrogen on a stepped Ru(001) surface.* Surf. Sci. **1995**, 325, 151-162.

134. Y.-K. Sun, W.H. Weinberg, *Determination of the absolute saturation coverage of hydrogen on Ru(001)* Surf. Sci. **1989**, 214, L246-L252.

135. M. Sokolowski, T. Koch, H. Pfnür, *Ordered structures and phase diagram of atomic hydrogen chemisorbed on ruthenium (001).* Surf. Sci. **1991**, 243, 261-272.

136. H. Shi, K. Jacobi *Hydrogen vibrations on the Ru(001) surface revisited*. Surf. Sci. **1994**, 313, 289-294.

137. M.A. Barteau, J.Q. Broughton, D. Menzel, *Determination of hydrogen atom binding sites on Ru(001) by HREELS.* Surf. Sci. **1983**, 133, 443-452.

138. J.T. Yates Jr., C.H.F. Peden, J.E. Houston, D.W. Goodman, *Subsurface penetration of chemisorbed hydrogen isotopes into the Ru(0001) crystal surface.* Surf. Sci. **1985**, 160, 37-45.

139. C.H.F. Peden, D.W. Goodman, J.E. Houston, J.T. Yates Jr., *Subsurface hydrogen on Ru(0001): Quantification by Cu titration*. Surf. Sci. **1988**, 194, 92-100.

140. M. Lindroos, H. Pfnür, D. Menzel, *Investigation of a disordered adsorption system by electron reflection: H/Ru(001) at intermediate coverages.* Surf. Sci. **1987**, 192, 421-437.

141. J. Lapujoulade, K. S. Neil. *Chemisorption of Hydrogen on the (111) Plane of Nickel.* J. Chem. Phys. **1972**, 57, 3535-3545.

142. K. Christmann, O. Schober, G. Ertl, M. Neumann. *Adsorption of hydrogen on nickel single crystal surfaces*. J. Chem. Phys. **1974**, 60, 4528-4540.

143. K. Christmann, R. J. Behm, G. Ertl, M. A. Van Hove, W. H. Weinberg. *Chemisorption geometry of hydrogen on Ni(111): Order and disorder.* J. Chem. Phys. **1979**, 70, 4168-4184.

144. J. N. Russell Jr., I. Chorkendorff, A.-M. Lanzillotto, M. D. Alvey, J. T. Yates Jr. *Angular distributions of H_2 thermal desorption: Coverage dependence on Ni(111).* J. Chem. Phys. **1986**, 85, 6186-6191.

145. A. D. Johnson, K. J. Maynard, S. P. Daley, Q. Y. Yang, and S. T. Ceyer. *Hydrogen embedded in Ni: Production by incident atomic hydrogen and detection by high-resolution electron energy loss*, Phys. Rev. Lett. **1991**, 67, 927-930.

146. Aubrey T. Hanbicki, S. B. Darling, D. J. Gaspar, S. J. Sibener, *Influence of steps on the interaction between adsorbed hydrogen atoms and a nickel surface*. Chem. Phys. **1999**, 111, 9053-9057.

147. G.F.A. Van De Walle, H. Van Kempen, P. Wyder, C.J. Flips, *Scanning tunneling microscopy and (scanning) tunneling spectroscopy on stepped Ni(111)/H*. Surf. Sci. **1987**, 181, 27-36.

148. A. Winkler, K.D. Rendulic, *Adsorption kinetics for hydrogen adsorption on nickel and coadsorption of hydrogen and oxygen.* Surf. Sci. **1982**, 118, 19-31.

149. G. X. Cao, E. Nabighian, X. D. Zhu, *Diffusion of Hydrogen on Ni(111) over a Wide Range of Temperature: Exploring Quantum Diffusion on Metals.* Phys. Rev. Lett. **1997**, 79, 3696-3999.

150. H. Okuyama, T. Ueda, T. Aruga, and M. Nishijima, *Overtones of H vibrations at Ni(111): Formation of delocalized states.* Phys. Rev. B. **2001**, 63, 233403.

151. H. Premm, H. Pölzl, A. Winkler, *Dynamics and kinetics of subsurface absorption and desorption for the system hydrogen (deuterium)–Ni(111).* Surf. Sci. **1998**, 401, L444-L451.

152. S. Wright, J. F. Skelly, A. Hodgson, *Energy disposal during desorption of D_2 from the surface and subsurface region of Ni(111).* Faraday Discuss. **2000**, 117,133-146.

153. H. Yang, J. L. Whitten, *Dissociative adsorption of H_2 on Ni(111).* J. Chem. Phys. **1993**, 98, 5039-5049.

154. G. Kresse, J. Hafner, *First-principles study of the adsorption of atomic H on Ni (111), (100) and (110).* J. *Surf. Sci.* **2000**, *459*, 287-302.

155. H. Kaji, K. Kakitani, Y. Yagi, A. Yoshimori, *Vibrational States and Atomic Arrangement of Hydrogen Adsorbed Ni (111) Surface. Shinku,* **2002**, *45*, 258-261.

156. H. Zheng, B. K. Rao, S. N. Khanna, and P. Jena, *Electronic structure and binding energies of hydrogen-decorated vacancies in Ni.* Phys. Rev. B. **1997**, 55, 4174-4181.

157. Castellani, N. J.; Le´gare´, P.; Demangeat, C.; Pick, S. *Surf. Sci.* **1996**, *352-354*, 148.

158. X. Sha, B. Jackson, *Ab initio and transition state theory studies of the energetics of H atom resurfacing on Ni(1 1 1).* Chem. Phys. Lett. **2002**, 357, 389-396.

159. Y. Itsumi, D. E. Ellis, *Electronic bonding characteristics of hydrogen in bcc iron: Part I. Interstitials.* J. Mater. Res. **1996**, 11, 2206-2213.

160. L. Hammer, H. Landskron, W. Nichtl-Pecher, A. Fricke, K. Heinz, K. Müller, *Hydrogen-induced restructuring of close-packed metal surfaces: H/Ni(111) and H/Fe(110),* Phys. Rev. B: Condens. Matter Mater. Phys. **1993**, 47, 15969-15972.

161. Ch. Minot, C. Demangeat, *The iron–hydrogen system: Lattice location of hydrogen, heat of formation, and hydrogen–hydrogen binding energy* J. Chem. Phys. **1987**, 86, 2161-2167.

162. W. Moritz, R. Imbihl, R. J. Behm, G. Ertl, T. Matsushima, *Adsorption geometry of hydrogen on Fe(110).* J. Chem. Phys. **1985**, 83, 1959-1968.

163. Pietro Cremaschi, Hong Yang, Jerry L. Whitten *Ab initio chemisorption studies of H on Fe(110).* Surf. Sci. **1995**, 330, 255-264.

164. E. A. Kurz, J. B. Hudson, *The adsorption of H_2 and D_2 on Fe(110): I. Helium scattering as a probe of adsorption.* Surf. Sci. **1988**, 195, 15-30.

165. E. A. Kurz, J. B. Hudson *The adsorption of H_2 and D_2 on Fe(110): II. Angle resolved thermal desorption spectroscopy and kinetic mechanism.* Surf. Sci. **1988**, 195, 31-42.

166. A.M. Baró, W. Erley. *The chemisorption of hydrogen on a (110) iron crystal studied by vibrational spectroscopy (EELS).* Surf. Sci. **1981**, 112, L759-L764.

167. R. Imbihl, R.J. Behm, K. Christmann, G. Ertl, T. Matsushima, *Phase transitions of a two-dimensional chemisorbed system: H on Fe(110).* Surf. Sci. **1982**, 117, 257-266.

168. W. Nichtl-Pecher, J. Gossmann, L. Hammer, K. Heinz, K. Müller, *Adsorption of hydrogen on Fe(110) at cryogenic temperatures investigated by low energy electron diffraction.* J. Vac. Sci. Technol. A. **1992**, 10, 501-507.

169. K. Christmann, *Interactions of hydrogen with solid surfaces*, Sur. Sci. R., **1988**, 9, 1-163

170. C. H. Bartholomew, Hydrogen adsorption on supported cobalt, iron, and nickel. Catal. Lett., **1990**, 7, 27-52.

Chapter 3

1. Z. X.-Guang, X. Y.-Sheng, G. X.-Xia. *EHMO calculations for the chain growth process in Fischer-Tropsch synthesis on supported group VIII metals*. J. Mol. Catal. **1988**, 43, 381− 394.
2. M. Zhuo, K. F. Tan, A. Borgna, M. Saeys, *Density Functional Theory Study of the CO Insertion Mechanism for Fischer−Tropsch Synthesis over Co Catalysts.* J. Phys. Chem. C **2009**, 113, 8357−8365.
3. M. E. Dry, *The Fischer-Tropsch process - commercial aspects*. Catal. Today, **1990**, 6, 183−206.
4. P. Winslow, A. T. Bell, *Studies of the surface coverage of unsupported ruthenium by carbon- and hydrogen-containing adspecies during CO hydrogenation.* J. Catal. **1985**, 91, 142−154.
5. C. S. Kellner, A. T. Bell, *Evidence for H_2D_2 isotope effects on Fischer-Tropsch synthesis over supported ruthenium catalysts.* J. Catal. **1981**, 67, 175−185.
6. M. Ojeda, A. Li, R. Nabar, A. U. Nilekar, Manos Mavrikakis, E. Iglesia, *Kinetically Relevant Steps and H_2/D_2 Isotope Effects in Fischer−Tropsch Synthesis on Fe and Co Catalysts.* J. Phys. Chem. C. **2010**, 114, 19761−19770.
7. S. Zheng, Y. Liu, J. Li, B. Shi, *Deuterium tracer study of pressure effect on product distribution in the cobalt-catalyzed Fischer–Tropsch synthesis.* Appl. Catal., A, **2007**, 330, 63−68.

8. B. Shi, B. H. Davis, *Fischer–Tropsch synthesis: accounting for chain-length related phenomena.* Appl. Catal., A **2004**, 277, 61−69.

9. R. L. Espinoza, J. L. Visagie, P. J. van Berge, F. H. Bolder, US Patent 5,733,839, **1998**.

10. J. R. A. Sietsma, A. J. van Dillen, P. E. de Jongh, K. P. de Jong, *Metal nitrate conversion method*, PCT Int. Appl. WO 2008029177, **2008**.

11. J. R. A. Sietsma, A. J. van Dillen, P. E. de Jongh, K. P. de Jong, *Metal nitrate conversion method*, PCT Int. Appl. WO 2007071899, **2007**.

12. J. R. A. Sietsma, J. D. Meeldijk, J. P. den Breejen, M. Versluijs-Helder, A. Jos van Dillen, P. E. de Jongh, K. P. de Jong, *The Preparation of Supported NiO and Co_3O_4 Nanoparticles by the Nitric Oxide Controlled Thermal Decomposition of Nitrates.* Angew. Chem., Int. Ed. **2007,** 46, 4547−4549.

13. D. C. Cronauer, G. Jacobs, L. Linganiso, A. J. Kropf, J. W. Elam, S. T. Christensen, C. L. Marshall, B. H. Davis, *CO Hydrogenation: Exploring Iridium as a Promoter for Supported Cobalt Catalysts by TPR-EXAFS/XANES and Reaction Testing*. Catal. Lett. **2011**, 141, 968−976.

14. G. Jacobs, Y. Ji, B. H. Davis, D. Cronauer, A. J. Kropf, C. L. Marshall, *Fischer–Tropsch synthesis: Temperature programmed EXAFS/XANES investigation of the influence of support type, cobalt loading, and noble metal promoter addition to the reduction behavior of cobalt oxide particles.* Appl. Catal. A **2007**, 333, 177−191.

15. G. Jacobs, T. K. Das, Y. Zhang, J. Li, G. Racoillet, B. H. Davis, *Fischer–Tropsch synthesis: support, loading, and promoter effects on the reducibility of cobalt catalysts.* Appl. Catal., A **2002**, 233, 263−281.

16. R. Prins, Chem. Rev., *Hydrogen Spillover. Facts and Fiction.* **2012**, 112, 2714-2738.

Chapter 4

1. I. H. Son, S. J. Lee, A. Soon, H.-Seog Roh, H. Lee, *Steam treatment on Ni/γ-Al_2O_3 for enhanced carbon resistance in combined steam and carbon dioxide reforming of methane.* Appl. Catal. B: Env. **2013,** 134-135, 103-109.
2. L. V. Mattos, G. Jacobs, B. H. Davis, F. B. Noronoha, *Production of Hydrogen from Ethanol: Review of Reaction Mechanism and Catalyst Deactivation* Chem. Rev. ,**2012**, 112, 4094-4123.
3. P. Schoubye, *Methanation of CO on some Ni catalysts.* J. Catal. **1969**, 14, 238-246.
4. G. Webb, P.B. Wells, *Asymmetric hydrogenation*, Catal. Today **1992**, 12, 319-337.
5. S. Hilaire, X. Wang, T. Luo, R.J. Gorte, J. Wagner, *Water gas shift reaction for the reformed fuels over Cu/MnO catalysts prepared via spinel-type oxide.* Appl. Catal A: Gen. **2001**, 215, 271-278.
6. J. Sehested, J. A. P. Gelten, I. N. Remediakis, H. Bengaard, J.K. Nørskov, *Sintering of nickel steam-reforming catalysts: effects of temperature and steam and hydrogen pressures.* J. Catal. **2004,** 223, 432-443.
7. V. Y. Bychkov, Y. P. Tyulenin, A. A. Firsova, E. A. Shafranovsky, A. Y. Gorenberg, V. N. Korchak, *Carbonization of nickel catalysts and its effect on methane dry reforming.* Appl. Catal. A: Gen., **2013**, 453, 71-79.
8. J. R. Rostrup-Nielsen, *Sulfur-passivated nickel catalysts for carbon-free steam reforming of methane*. J. Catal. **1984**, 85, 31-43.
9. S. M. de Lima, A. M. da Silva, L. O. O. da Costa, J. M. Assaf, G. Jacobs, B. H. Davis, L. V. Mattos, F. B. Noronha, *Evaluation of the performance of Ni/La_2O_3 catalyst prepared from $LaNiO_3$ perovskite-type oxides for the production of hydrogen through*

steam reforming and oxidative steam reforming of ethanol. Appl. Catal. A: Gen. **2010**, 377, 181-190.

10. F. Frusteri, S. Freni, *Bio-ethanol, a suitable fuel to produce hydrogen for a molten carbonate fuel cell.* J. Power Sources, **2007**, 173, 200-209.
11. M. C. Sanchez-Sanchez, R. M. Navarro, J. L. G. Fierro, *Ethanol steam reforming over $Ni/M_xO_y/Al_2O_3$ (M= Ce, La, Zr, and Mg) catalysts: Influence of support on the hydrogen production.* Int. J. Hydrogen Energy, **2007**, 32,1462-1471.
12. A. N. Fatsikostas, D. I. Kondarides, X. E. Verykios,, *Production of hydrogen for fuel cells by reformation of biomass-derived ethanol*. Catal. Today **2002**, 75, 145-155.
13. N. Laosiripojana, S. Assabumrungrat, S. Charojrochkul, *Steam reforming of ethanol with co-fed oxygen and hydrogen over Ni on high surface area ceria support.* Appl. Catal. A: Gen. **2007**, 327, 180-188.
14. J. Happel, I. Suzuki, P. Kokayeff, V. Fthenakis, *Multiple isotope tracing of methanation over nickel catalyst.* J. Catal. **1980**, 65, 59-77.
15. T. Osawa, Y. Hamano, S. Saga, O. Takayasu, *Hydrogen–deuterium exchange of methane on nickel surface prepared by the reduction of nickel oxide.* J. Mol. Catal. A: Chem. **2009**, 298, 111-114.
16. J. Wei, E. Iglesia, *Isotopic and kinetic assessment of the mechanism of reactions of CH_4 with CO_2 or H_2O to form synthesis gas and carbon on nickel catalysts*. J. Catal. **2004,** 224, 370-383.
17. K. Bhattacharya, U.R. Marwah, D.D. Sood, *Isotopic exchange between hydrogen and water over plain and hydrophobized nickel—chromia catalysts.* J. Catal. **1992**, 134, 399-408.

18. B. Janković, B. Adnađević, S. Mentus, *The kinetic study of temperature-programmed reduction of nickel oxide in hydrogen atmosphere.* Chem. Eng. Sci. **2008**, 63, 567-575.

19. J. T. Richardson, R. Scates, M. V. Twigg, *X-ray diffraction study of nickel oxide reduction by hydrogen.* Appl. Catal. A **2003**, 246, 137-150.

20. G. Jacobs, T. K. Das, Y. Zhang, J. Li, G. Racoillet, B. H. Davis, *Fischer–Tropsch synthesis: support, loading, and promoter effects on the reducibility of cobalt catalysts.* Appl. Catal., A **2002**, 233, 263−281.

21. W. D. Shafer, G. Jacobs, B. H. Davis, *Fischer–Tropsch Synthesis: Investigation of the Partitioning of Dissociated H_2 and D_2 on Activated Cobalt Catalyst.* ACS Catal. **2012**, 2, 1452-1456.

Chapter 5

1. A. T. Bell, *Catalytic Synthesis of Hydrocarbons over Group VIII Metals. A Discussion of the Reaction Mechanism.* Catal Rev Sci Eng. **1981**, 23, 203-232.
2. M. E. Dry, *Practical and theoretical aspects of the catalytic Fischer-Tropsch process* Appl Catal A: Gen. **1996**, 138, 319-344.
3. B. H. Davis, *Fischer–Tropsch Synthesis: Reaction mechanisms for iron catalysts,* Catal. Today, **2009**, 141, 25-33.
4. H. Schulz, *Short history and present trends of Fischer–Tropsch synthesis.* Appl Catal A: Gen, **1999**, 186, 3-12.
5. G. P. van der Laan, A.A.C.M. Beenackers, *Intrinsic kinetics of the gas–solid Fischer–Tropsch and water gas shift reactions over a precipitated iron catalyst.* Appl Catal A: Gen. **2000**, 193, 39-53.
6. W. Keith Hall, R. J. Kokes, P. H. Emmett, *Mechanism Studies of the Fischer-Tropsch Synthesis: The Incorporation of Radioactive Ethylene, Propionaldehyde and Propanol.* J. Am. Chem. Soc. **1960**, 82, 1027-1037.
7. C. F. Huo, J. Ren, Y. W. Li, J. Wang, H. Jiao, *CO dissociation on clean and hydrogen precovered Fe(111) surfaces*. J. Catal. **2007,** 249, 174-184.
8. O. R. Inderwildi, S.J. Jenkins, D. A. King, *Fischer−Tropsch Mechanism Revisited: Alternative Pathways for the Production of Higher Hydrocarbons from Synthesis Gas*. J. Phys. Chem. C **2008**, 112, 1305-1307.
9. F. J. Perez-Alonso, T. Herranz, S. Rojas, M. Ojeda, M.L. Granados, J.L.G. Fierro, J.R. Gancedo, *Evolution of the bulk structure and surface species on Fe–Ce catalysts during the Fischer–Tropsch synthesis.* Green Chem. **2007**, 9, 663-670.

10. A. Y. Khodakov, W. Chu, P. Fongarland, *Advances in the Development of Novel Cobalt Fischer−Tropsch Catalysts for Synthesis of Long-Chain Hydrocarbons and Clean Fuels*. Chem. Rev. **2007** 107, 1692-1744.

11. G. P. van der Laan, A.A.C.M. Beenackers, *Kinetics and Selectivity of the Fischer–Tropsch Synthesis: A Literature Review.* Catal. Rev. Sci. Eng. **1999**, 41, 255-318.

12. C. N. Hamelinck, A. P.C. Faaij, H. den Uil, H. Boerrigter, *Production of FT transportation fuels from biomass; technical options, process analysis and optimization, and development potential.* Energy **2004**, 29, 1743-1771.

13. M. Claeys, E. van Steen, *On the effect of water during Fischer–Tropsch synthesis with a ruthenium catalyst.* Catal. Today **2002**, 71, 419-427.

14. J. Kang, S. Zhang, Q. Zhang, Y. Wang, *Ruthenium Nanoparticles Supported on Carbon Nanotubes as Efficient Catalysts for Selective Conversion of Synthesis Gas to Diesel Fuel.* Angew. Chem. Int. Ed. **2009**, 48, 2565-2568.

15. V. R. R. Pendyala, W.D. Shafer, B.H. Davis, *Aqueous-Phase Fischer–Tropsch Synthesis: Effect of Reaction Temperature on Ruthenium Nanoparticle Catalyst and Comparison with Supported Ru and Co Catalysts.* Catal. Lett. **2013**, 143, 895-901.

16. J.P. Hindermann, G.J. Hutchings, A. Kiennemann, *Mechanistic Aspects of the Formation of Hydrocarbons and Alcohols from CO Hydrogenation*, Catal. Rev. **1993**, 35, 1-127.

17. Vada S, Hoff A, Adnanes E, Schanke D, Holmen A Fischer-Tropsch synthesis on supported cobalt catalysts promoted by platinum and rhenium Topics Catal. **1995**, 2, 155-162.

18. A.M. Hilmen, D. Schanke, A. Holmen, *TPR study of the mechanism of rhenium promotion of alumina-supported cobalt Fischer-Tropsch catalysts*. Catal. Lett. **1996**, 38, 143-147.

19. R.L. Espinoza, J.L. Visagie, P.J. van Berge, F.H. Bolder, U.S. Patent 5,733,839, **1998**.

20. W.J. Wang, Y.W. Chen. *Influence of metal loading on the reducibility and hydrogenation activity of cobalt/alumina catalysts.* Appl. Catal. **1991** 77, 223-233.

21. D. Schanke, A. M. Hilmen, E. Bergene, K. Kinnari, E. Rytter, E. Ådnanes, A. Holmen *Study of the deactivation mechanism of Al_2O_3-supported cobalt Fischer-Tropsch catalysts.* Catal. Lett. **1995**, 34, 269-284.

22. A.M. Hilmen, D. Schanke, K.F. Hanssen, A. Holmen *A Study of the effect of water on alumina supported cobalt Fischer–Tropsch catalyst.* Appl Catal A: Gen **1999**, 186, 169-188.

23. K. M. Cook, S. Poudyal, J. T. Miller, C. H. Bartholomew, W. C. Hecke, *Reducibility of alumina-supported cobalt Fischer–Tropsch catalysts: Effects of noble metal type, distribution, retention, chemical state, bonding, and influence on cobalt crystallite size* Appl Catal A: Gen **2012**, 449, 69-80.

24. G. Jacobs, Y. Ji, B. H. Davis, D. Cronauer, A. J. Kropf, C. L. Marshall, *Fischer–Tropsch synthesis: Temperature programmed EXAFS/XANES investigation of the influence of support type, cobalt loading, and noble metal promoter addition to the reduction behavior of cobalt oxide particles.* Appl. Catal., A **2007**, 333, 177−191.

25. G. Jacobs, T. K. Das, Y. Zhang, J. Li, G. Racoillet, B. H. Davis, *Fischer–Tropsch synthesis: support, loading, and promoter effects on the reducibility of cobalt catalysts* Appl. Catal. A: Gen. **2002,** 233, 263–281.

26. E.F.G. Harrington Chem. Ind. **1946** 183.

27. L.E. McCandlish, *On the mechanism of carbon-carbon bond formation in the CO hydrogenation reaction.* J. Catal. **1983**, 83, 362-370.

28. H. Pichler, H. Schulz, *Neuere Erkenntnisse auf dem Gebiet der Synthese von Kohlenwasserstoffen aus CO und H_2.* Chemie Ingenieur Technik. **1970,** 42, 1162-1174.

29. P. Biloen, W.M.H. Sachtler, *Mechanism of Hydrocarbon Synthesis over Fischer-Tropsch Catalysts Adv.* Catal. **1981,** 30, 165-216.

30. K.R. Krishna, A.T. Bell, *An isotopic tracer study of the deactivation of Ru/Ti0_2 catalysts during Fischer-Tropsch synthesis.* J. Catal. **1991,** 130, 597-610.

31. P. Winslow, A. T. Bell, *Studies of the surface coverage of unsupported ruthenium by carbon- and hydrogen-containing adspecies during CO hydrogenation.* J. Catal. **1985**, 91, 142−154.

32. B.H. Davis, *Fischer–Tropsch synthesis: current mechanism and futuristic needs*. Fuel Proc. Tech. **2001**, 71,157-166.

33. A.P. Raje, B.H. Davis, *Effect of Vapor−Liquid Equilibrium on Fischer−Tropsch Hydrocarbon Selectivity for a Deactivating Catalyst in a Slurry Reactor* Energy Fuels, **1996**, 10, 552-560.

34. C. S. Kellner, A. T. Bell, *Evidence for H_2D_2 isotope effects on Fischer-Tropsch synthesis over supported ruthenium catalysts.* J. Catal. **1981**, 67, 175−185.

35. M. Ojeda, A. Li, R. Nabar, A.U. Nilekar, M. Mavrikakis, E. Iglesia, *Kinetically Relevant Steps and H_2/D_2 Isotope Effects in Fischer−Tropsch Synthesis on Fe and Co Catalysts.* J. Phys. Chem. C. **2010**, 114, 19761-19770.

36. S. Zheng, Y. Liu, J. Li, B. Shi, *Deuterium tracer study of pressure effect on product distribution in the cobalt-catalyzed Fischer–Tropsch synthesis.* Appl Catal A: Gen. **2007**, 330:63-68.

37. B. Shi, B.H. Davis, *Fischer-Tropsch synthesis: accounting for chain-length related phenomena.* Appl. Catal., A: Gen. **2004**, 277, 61-69.

38. W. D. Shafer, G. Jacobs, B. H. Davis, *Fischer–Tropsch Synthesis: Investigation of the Partitioning of Dissociated H_2 and D_2 on Activated Cobalt Catalyst.* ACS Catal. **2012**, 2, 1452-1456.

39. W.D. Shafer, G. Jacobs, J.P. Selegue, B.H. Davis, *An Investigation of the Partitioning of Dissociated H_2 and D_2 on Activated Nickel Catalysts*. Catal. Lett. **2013** 143, 1368-1373.

40. J. Yang, W.D. Shafer, V.R.R. Pendyala, G. Jacobs, D. Chen, A. Holmen, B.H. Davis, *Fisher-Tropsch Synthesis: Using Deuterium as a Tool to Investigate Primary Product Distribution* Catal. Lett. **2014**, 144(3), 524-530.

Chapter 6:

1. M. Luo, H. Hamdeh, B. H. Davis, *Fischer-Tropsch Synthesis: Catalyst activation of low alpha iron catalyst.* Catal. Today **2009,** 140, 127-134.
2. D. Leckel, *Diesel Production from Fischer−Tropsch: The Past, the Present, and New Concepts.* Energy and Fuels **2009**, 23, 2342-2358.
3. F. Fischer, H. Tropsch, *Synthesis of Petroleum at Atmospheric Pressure From Gasification Products of Coal*, Brennst-Chem, **1926**, 7, 97-104.
4. F. Fischer, H. Tropsch, *Development of the Benzene Synthesis from Carbon Monoxide and Hydrogen at Atmospheric Pressure*, Brennst-Chem, **1930**, 11, 489-500.
5. B.H. Davis, *Fischer–Tropsch synthesis: current mechanism and futuristic needs*. Fuel Proc. Tech. **2001**, 71,157-166.
6. A. Tuxen, S. Carenco, M. Chintapalli, C. Chuang, C. Escudero, E. Pach, P. Jiang, F. Borondics, B. Beberwyck, A.P. Alivisatos, G. Thornton, W.F. Pong, J. Guo, R. Perez, F. Besenbacher, M. Salmeron, *Size-Dependent Dissociation of Carbon Monoxide on Cobalt Nanoparticles.* J. Am. Chem. Soc. **2013**, 135, 2273-2278.
7. Y. Qi, J. Yang, D. Chen, A. Holmen, *Recent Progresses in Understanding of Co-Based Fischer–Tropsch Catalysis by Means of Transient Kinetic Studies and Theoretical Analysis*. Catal. Lett. **2015,** 145, 145-161.
8. G. Jacobs, B. H. Davis, *Applications of isotopic tracers in Fischer–Tropsch synthesis.* Catal Sci Technol., **2014** 4, 3927-3944.
9. R. Zhang, X. Hao, Y. Yong, Y. Li *Investigation of acetylene addition to Fischer–Tropsch Synthesis.* Catal Comm. **2011**, 12, 1146-1148.

10. Krishnamoorthy S, Li A, Iglesia E, *Pathways for CO_2 Formation and Conversion During Fischer–Tropsch Synthesis on Iron-Based Catalysts*. Catal. Lett. **2002**, 80:77-86.

11. B. Shi, B.H. Davis, *^{13}C-tracer study of the Fischer–Tropsch synthesis: another interpretation.* Catal. Today **2000**, 58, 255-261.

12. B.E. Mann, M.L. Turner, R. Quyoum, N. Marsih, P.M. Maitlis, *Demonstration by ^{13}C NMR Spectroscopy of Regiospecific Carbon−Carbon Coupling during Fischer−Tropsch Probe Reactions.* J. Am. Chem. Soc. **1999**, 121, 6497-6498.

13. D. Chakrabarti, A. de Klerk, V. Prasad, M.K. Gnanamani, W.D. Shafer, G. Jacobs, D.E. Sparks, B.H. Davis, *Conversion of CO_2 over a Co-Based Fischer–Tropsch Catalyst.* Ind. Eng. Chem. Res. **2015**, 54, 1189-1196.

14. A. Sarkar, R. Keogh, S. Bao, B.H. Davis, *Fischer-Tropsch Synthesis: Reaction Pathways for ^{14}C-Labeled Acetic Acid.* Catal. Lett. **2008,** 120, 25-33.

15. B. Shi, B.H. Davis, *Fischer-Tropsch Synthesis: Evidence for Chain Initiation by Ethene and Ethanol for an Iron Catalyst.* Topics in Catal. **2003**, 26, 157-161.

16. D. Chakrabarti, M.K. Gnanamani, W.D. Shafer, M.C. Ribeiro, D.E. Sparks, V. Prasad, A. de Klerk, B.H. Davis, Abstracts of Papers, 248th ACS National Meeting & Exposition, San Francisco, CA, United States, August 10-14, **2014** , ENFL-566.

17. J. Yang, W.D. Shafer, V.R.R. Pendyala, G. Jacobs, D. Chen, A. Holmen, B.H. Davis, *Fischer–Tropsch Synthesis: Using Deuterium as a Tool to Investigate Primary Product Distribution*. Catal. Lett., **2014**, 144, 524-530.

18. J. Yang, W.D. Shafer, V.R.R. Pendyala, G. Jacobs, W. Ma, D. Chen, A. Holmen, B.H Davis *Fischer-Tropsch Synthesis: Deuterium Kinetic Isotopic Effect for a 2.5% Ru/NaY catalysis.* Top. Catal., **2014**, 57, 508-517.

19. M. K. Gnanamani, G. Jacobs, W. D. Shafer, M. C. Ribeiro, V. R. R. Pendyala, W. Ma, B. H. Davis *Fischer Tropsch synthesis: Deuterium isotopic study for the formation of oxygenates over CeO_2 supported Pt–Co catalysts.* Catal. Comm. **2012**, 25, 12-17.

20. B. Shi, Y. Liao, J.L. Naumovitz, *Formation of 2-alkenes as secondary products during Fischer–Tropsch synthesis*. Appl. Catal. A: Gen **2015**, 490, 201-206.

21. B. Shi, J. Chunfen, *Inverse kinetic isotope effects and deuterium enrichment as a function of carbon number during formation of C–C bonds in cobalt catalyzed Fischer–Tropsch synthesis.* J. Appl. Catal A: Gen. **2011**, 393, 178-183.

22. M. Ojeda, R. Nabar, A. U. Nilekar, A. Ishikawa, M. Mavrikakis, E. Iglesia, *CO activation pathways and the mechanism of Fischer–Tropsch synthesis,* J. of Catal. **2010,** 272, 287–297.

23. M. Ojeda, A. Li, R. Nabar, A. U. Nilekar, Manos Mavrikakis, E. Iglesia, *Kinetically Relevant Steps and H_2/D_2 Isotope Effects in Fischer−Tropsch Synthesis on Fe and Co Catalysts.* J. Phys. Chem. C. **2010**, 114, 19761−19770.

24. R.A. Dalla Betta, M. Shelef, *Heterogeneous Methanation: Absence of H_2-D_2, Kinetic Isotope Effect on Ni, Ru, and Pt.* J. Catal., **1977**, 49, 383-385.

25. M .Shelef, R.A. Dalla Betta, *Reply to comments on heterogeneous methanation: Absence of H_2/D_2 kinetic isotope effect on Ni, Ru, and Pt*, J. Catal. **1979**, 60, 169-170.

26. P.F.M.T. van Nisselrooij, J.A.M. Luttikholt, R.Z.C. van Meerten, M.H.J.M. de Croon, J.W.E. Coenen, *Hydrogen/deuterium kinetic isotope effect in the methanation of carbon monoxide on a nickel-silica catalyst.* Appl. Catal., **1983**, 6, 271-281.

27. E.W. McKee, *Interaction of hydrogen and carbon monoxide on platinum group metals* J. Catal. 1967, 8, 240-249.

28. C. S. Kellner, A. T. Bell, *Evidence for H_2D_2 isotope effects on Fischer-Tropsch synthesis over supported ruthenium catalysts.* J. Catal. **1981**, 67, 175−185.

29. R.A. van Santen, A.J. Markvoort, *Chain Growth by CO Insertion in the Fischer–Tropsch Reaction.* ChemCatChem **2013**, 5, 3384-3397.

30. R.A. van Santen, A.J. Markvoort, M.M. Ghouri, P.A.J. Hilbers, E.J.M. Hensen, *Monomer Formation Model versus Chain Growth Model of the Fischer–Tropsch Reaction.* J. Phys. Chem. C. **2013,** 117, 4488-4504.

31. R.A. van Santen, I.M. Ciobica, E. van Steen, M.M. Ghouri, *Chapter 3 - Mechanistic Issues in Fischer–Tropsch Catalysis.* Adv. Catal. **2011**, 54, 127-187.

32. B. Todic, W. Ma, G. Jacobs, B. H. Davis, D. B. Bukur, *CO-insertion mechanism based kinetic model of the Fischer–Tropsch synthesis reaction over Re-promoted Co catalyst.* Catal. Today **2014**, 228, 32-39.

33. M.K. Gnanamani, G. Jacobs, W.D. Shafer, D. Sparks, B.H. Davis, *Fischer–Tropsch Synthesis: Deuterium Kinetic Isotope Study for Hydrogenation of Carbon Oxides Over Cobalt and Iron Catalysts*. Catal. Lett. **2011**, 141, 1420-1428.

34. M. K. Gnanamani, R. A. Keogh, W.D. Shafer, B. H. Davis, *Deutero-1-pentene tracer studies for iron and cobalt Fischer–Tropsch synthesis.* Appl. Catal. A: Gen. **2011**, 393:130-137.

35. A. Ozaki, Isotopic Studies of Heterogeneous Catalysis, Academic Press, New York, NY, **1977**.

36. T.P. Wilson, *Comments on heterogeneous methanation: Absence of H_2/D_2 kinetic isotope effect on Ni, Ru, and Pt*. J. Catal. **1979**, 60, 167-168.

37. W.D. Shafer, V.R.R. Pendyala, G. Jacobs, J. Selegue, B.H. Davis, in: Fischer-Tropsch Synthesis, *Catalysts, and Catalysis: Advances and Applications*, eds. B.H. Davis and M.L. Occelli, CRC Press, Taylor & Francis Group, Boca Raton, Florida, **2015.**

38. W. D. Shafer, G. Jacobs, B. H. Davis, *Fischer–Tropsch Synthesis: Investigation of the Partitioning of Dissociated H_2 and D_2 on Activated Cobalt Catalyst.* ACS Catal. **2012**, 2, 1452-1456.

39. W.D. Shafer, G. Jacobs, J.P. Selegue, B.H. Davis, *An Investigation of the Partitioning of Dissociated H_2 and D_2 on Activated Nickel Catalysts*. Catal. Lett. **2013** 143:1368-1373.

40. M.C. Ribeiro, G. Jacobs, B.H. Davis, D.C. Cronauer, A.J. Kropf, C.L. Marshall, *Fischer−Tropsch Synthesis: An In-Situ TPR-EXAFS/XANES Investigation of the Influence of Group I Alkali Promoters on the Local Atomic and Electronic Structure of Carburized Iron/Silica Catalysts*. J. Phys. Chem. C **2010**, 114, 7895-7903.

41. M.C. Ribeiro, G. Jacobs, V.R.R.R. Pendyala, B.H. Davis, D.C. Cronauer, A.J. Kropf, C.L. Marshall, *Fischer−Tropsch Synthesis: Influence of Mn on the Carburization Rates and Activities of Fe-Based Catalysts by TPR-EXAFS/XANES and Catalyst Testing.* J. Phys. Chem. C **2011**, 115, 4783-4792.

42. G. Jacobs, A. Sarkar, B.H. Davis, D.C. Cronauer, A.J. Kropf, C.L. Marshall, in: Advances in Fischer-Tropsch synthesis, Catalysts and Catalysis, eds. B.H. Davis and M.L. Occelli, Taylor & Francis, Florida, **2009**, 119-146.

43. C.H. Zhang, Y. Yang, T.B. Teng, T.Z. Li, Zheng, H.W. Xiang, Y.W. Li, *Study of an iron-manganese Fischer–Tropsch synthesis catalyst promoted with copper.* J. Catal. **2006**, 237, 405-415.

44. S. Li, A. Li, S. Krishnamoorthy, E. Iglesia, *Effects of Zn, Cu, and K Promoters on the Structure and on the Reduction, Carburization, and Catalytic Behavior of Iron-Based Fischer–Tropsch Synthesis Catalysts*. Catal. Lett. **2001**, 77, 197-205.

45. Y. Jin, A.K. Datye, *Phase Transformations in Iron Fischer–Tropsch Catalysts during Temperature-Programmed Reduction*. J. Catal. **2000**, 196, 8-17.

46. L. Luyten, J.C. Jungers, *La cinétique de la synthèse catalytique du méthane sur le nickel*. Bull. Soc. Chim. Belg. **1945**, 54, 303-318.

47. J. Nicolai, M. d'Hont, J.C. Jungers, *La synthèse du méthane à partir d'anhydride carbonique et d'hydrogène sur le nickel.* Bull. Soc. Chim. Belg. **1946**, 55, 160-176.

48. T. Mori, H. Masuda, H. Imai, A. Miyamoto, Y. Murakami, Shokubai **1980** 22, 7.

49. M.M. Sakharov, E.S. Dokukina) Kinet. Katal. **1961** 2, 710.

Chapter 7

1. Nakamoto, K., *Infrared Spectra of Inorganic and Coordination Compounds, 3rd ed*. Wiley, New York, NY, **1978**.
2. C. S. Kellner, A. T. Bell, *Evidence for H_2D_2 isotope effects on Fischer-Tropsch synthesis over supported ruthenium catalysts.* J. Catal. **1981**, 67, 175−185.
3. M. Ojeda, A. Li, R. Nabar, A. U. Nilekar, Manos Mavrikakis, E. Iglesia, *Kinetically Relevant Steps and H_2/D_2 Isotope Effects in Fischer−Tropsch Synthesis on Fe and Co Catalysts.* J. Phys. Chem. C. **2010**, 114, 19761−19770.
4. K. Christmann, *Interactions of hydrogen with solid surfaces,* Sur. Sci. R., **1988**, 9, 1-163.
5. D. Chakrabarti, M. K. Gnanamani, W. D. Shafer, M. C. Ribeiro, D. E. Sparks, V. Prasad, A. de Klerk, B. H. Davis, *Fischer–Tropsch Mechanism: $^{13}C^{18}O$ Tracer Studies on a Ceria–Silica Supported Cobalt Catalyst and a Doubly Promoted Iron Catalyst*. *I*nd. Eng. Chem. Res. **2015**, 54, 6438-6453.
6. S. M. Schimming, G. S. Foo, O. D. LaMont, A. K. Rogers ,M. M. Yung, A. D. D'Amico, C. Sievers, *Kinetics of hydrogen activation on ceria–zirconia.* J. Catal. **2015**, 329, 335-347.
7. M. A. Henderson, S. D. Worley, *An infrared study of isotopic exchange during methanation over supported rhodium catalysts: an inverse spillover effect*. J. Phys.. Chem. **1985**, 89, 392-394.
8. D. Panayotov, E. Ivanova, M. Mihaylov, K. Chakarova, T. Spassov, K. Hadjiivanov, *Hydrogen spillover on Rh/TiO2: the FTIR study of donated electrons, co-adsorbed CO and H/D exchange*. Phys. Chem. Chem. Phys. **2015**, 17, 20563-20573.

VITA

Education and Training

Currently working on a PhD in Chemistry 2011 to present
Obtained a M.S. in Chemistry, emphasis on organic/analytical 3.7 GPA
Obtained a B.A. in Chemistry, emphasis on materials chemistry

Current Projects

Water Gas Shift, dehydrocyclization, Fischer-Tropsch, hydrocracking, hydroisomerization, hydrodesulfurization, and other types of heterogeneous catalysis process both in a fixed-bed reactor and a Continuous Stir Tank system.

Past Projects

Polymer Synthesis, Polymer Spinning and Testing, Testing for Conductivity and Strength, Modulus, Elasticity, Polymers with Multiwalled Nano-tubes (MWNT), Conducting, making and testing Li-capacitors, carbon capacitors, other battery additives, Synthesis-resorcinarenes and other like novel like compounds, LCMS/GCMS study on biological materials, and method development.

Current Responsibilities

Manager/co-manager for eight labs; maintain and run 13 instruments: 2 SRI GC/FID-TCD, 2 GC-TCD, 2 micro GC-TCD, GC-MS, 5 GC-FID, GC-FPD including repair and specific analysis from each; safety chair (2009-2015), seed committee chair (2015-present), building and maintaining 23 continuous stir tank reactors (CSTR), 10 fixed bed reactors, the gas lines and tanks responsible for gas delivery. Additional information can be provided if needed.

Instrumentation

GC (TCD, FID, MS), LC (ESI, MS/MS), IR, NMR, SEM

Professional Experience

SCIENTIST I 10/07 - Present
University of Kentucky Center of Applied Energy Research (CAER)

TEACHING/GRADUATE ASSISTANT 8/04 - 7/07
Eastern Kentucky University – Richmond, KY

ELECTRO-CHEMISTRY Researcher 1/04 - 8/04
(CAER)

TCLP (Test **C**ontrol **L**eaching **P**rocess) **LAB ANALYST** 8/03 - 1/04
Test America Corporation - Nashville, TN

ORGANIC MATERIALS Researcher 12/02 - 10/03
(CAER)

HEAD LIFEGUARD / Manager 3/98 - 10/02
Harry C. Lancaster Aquatic Center - Lexington, KY

INFRARED SPECTROMETRY LAB TECHNICIAN 5/0 - 8/00
(CAER)

Publications

1. Azzam, Khalid G., Jacobs, Gary, Shafer, Wilson D., & Davis, Burtron H. (2010). Aromatization of hexane over Pt/KL catalyst: Role of intracrystalline diffusion on catalyst performance using isotope labeling. *J. Catal., 270*(2), 242-248. doi: 10.1016/j.jcat.2010.01.002
2. Azzam, Khalid G., Jacobs, Gary, Shafer, Wilson D., & Davis, Burtron H. (2010). Dehydrogenation of propane over Pt/KL catalyst: Investigating the role of L-zeolite structure on catalyst performance using isotope labeling. *Appl. Catal., A, 390*(1-2), 264-270. doi: 10.1016/j.apcata.2010.10.022
3. Gnanamani, Muthu Kumaran, Hamdeh, Hussein H., Shafer, Wilson D., Sparks, Dennis E., & Davis, Burtron H. (2013). Fischer-Tropsch Synthesis: Effect of Potassium on Activity and Selectivity for Oxide and Carbide Fe Catalysts. *Catal. Lett., 143*(11), 1123-1131. doi: 10.1007/s10562-013-1110-7
4. Gnanamani, Muthu Kumaran, Jacobs, Gary, Hamdeh, Hussein H., Shafer, Wilson D., & Davis, Burtron H. (2013). Fischer-Tropsch synthesis: Moessbauer investigation of iron containing catalysts for hydrogenation of carbon dioxide. *Catal. Today, 207*, 50-56. doi: 10.1016/j.cattod.2012.02.059

5. Gnanamani, Muthu Kumaran, Jacobs, Gary, Shafer, Wilson D., & Davis, Burtron H. (2013). Fischer-Tropsch synthesis: Activity of metallic phases of cobalt supported on silica. *Catal. Today, 215*, 13-17. doi: 10.1016/j.cattod.2013.03.004
6. Gnanamani, Muthu Kumaran, Jacobs, Gary, Shafer, Wilson D., Pendyala, V. R. R., & Davis, Burtron H. (2013). Low temperature water-gas shift reactions over alkali-promoted cobalt carbide catalysts. *Prepr. - Am. Chem. Soc., Div. Energy Fuels, 58*(1), 1310-1311.
7. Gnanamani, Muthu Kumaran, Jacobs, Gary, Shafer, Wilson D., Ribeiro, Mauro C., Pendyala, Venkat Ramana Rao, Ma, Wenping, & Davis, Burtron H. (2012). Fischer Tropsch synthesis: Deuterium isotopic study for the formation of oxygenates over CeO_2 supported Pt-Co catalysts. *Catal. Commun., 25*, 12-17. doi: 10.1016/j.catcom.2012.03.028
8. Gnanamani, Muthu Kumaran, Jacobs, Gary, Shafer, Wilson D., Sparks, Dennis, & Davis, Burtron H. (2011). Fischer-Tropsch Synthesis: Deuterium Kinetic Isotope Study for Hydrogenation of Carbon Oxides Over Cobalt and Iron Catalysts. *Catal. Lett., 141*(10), 1420-1428. doi: 10.1007/s10562-011-0673-4
9. Gnanamani, Muthu Kumaran, Jacobs, Gary, Shafer, Wilson D., Sparks, Dennis E., Hopps, Shelley, Thomas, Gerald A., & Davis, Burtron H. (2013). Low Temperature Water-Gas Shift Reaction Over Alkali Metal Promoted Cobalt Carbide Catalysts. *Top. Catal.*, Ahead of Print. doi: 10.1007/s11244-013-0219-7
10. Gnanamani, Muthu Kumaran, Keogh, Robert A., Shafer, Wilson D., & Davis, Burtron H. (2010). Deutero-1-pentene tracer studies for iron and cobalt Fischer-Tropsch synthesis. *Prepr. Symp. - Am. Chem. Soc., Div. Fuel Chem., 55*(2), 449-450.
11. Gnanamani, Muthu Kumaran, Keogh, Robert A., Shafer, Wilson D., & Davis, Burtron H. (2011). Deutero-1-pentene tracer studies for iron and cobalt Fischer-Tropsch synthesis. *Appl. Catal., A, 393*(1-2), 130-137. doi: 10.1016/j.apcata.2010.11.035
12. Gnanamani, Muthu K., Keogh, Robert A., Shafer, Wilson D., Shi, Buchang, & Davis, Burtron H. (2010). Fischer-Tropsch synthesis: Deuterium labeled ethanol tracer studies on iron catalysts. *Appl. Catal., A, 385*(1-2), 46-51. doi: 10.1016/j.apcata.2010.06.039
13. Gnanamani, Muthu K., Keogh, Robert A., Shafer, Wilson D., Shi, Buchang, Jacobs, Gary, & Davis, Burtron H. (2010). *Fischer-Tropsch synthesis: deuterium labeled ethanol tracer studies on iron catalysts*.
14. Gnanamani, Muthu Kumaran, Linganiso, Linda Z., Jacobs, Gary, Keogh, Robert A., Shafer, Wilson D., & Davis, Burtron H. (2012). Hydroisomerization of n-Hexadecane Over Anion Modified Pt/HfO2 Catalysts. *Catal. Lett., 142*(10), 1180-1189. doi: 10.1007/s10562-012-0882-5
15. Gnanamani, Muthu Kumaran, Ribeiro, Mauro C., Ma, Wenping, Shafer, Wilson D., Jacobs, Gary, Graham, Uschi M., & Davis, Burtron H. (2011). Fischer-Tropsch synthesis: Metal-support interfacial contact governs oxygenates selectivity over CeO_2

supported Pt-Co catalysts. *Appl. Catal., A, 393*(1-2), 17-23. doi: 10.1016/j.apcata.2010.11.019

16. Gnanamani, Muthu Kumaran, Shafer, Wilson D., & Davis, Burtron H. (2012). Deuterium exchange study for hydrogenation of D5-1-pentene (4,4,5,5,5) over conventional cobalt Fischer-Tropsch catalyst. *Catal. Lett., 142*(2), 190-194. doi: 10.1007/s10562-011-0750-8
17. Gnanamani, Muthu Kumaran, Shafer, Wilson D., Sparks, Dennis E., & Davis, Burtron H. (2011). Fischer-Tropsch synthesis: Effect of CO_2 containing syngas over Pt promoted Co/γ-Al2O3 and K-promoted Fe catalysts. *Catal. Commun., 12*(11), 936-939. doi: 10.1016/j.catcom.2011.03.002
18. Gnanamani, Muthu Kumaran, Willauer, Heather D., Hardy, Dennis R., Williams, Frederick W., Shafer, Wilson, & Davis, Burtron H. (2009). Inverse isotope effect in CO_2 hydrogenation: doubly promoted (Cu, K) Fe catalysts. *Prepr. Symp. - Am. Chem. Soc., Div. Fuel Chem., 54*(2), 935.
19. Jermwongratanachai, Thani, Jacobs, Gary, Ma, Wenping, Shafer, Wilson D., Gnanamani, Muthu Kumaran, Gao, Pei,. Marshall, Christopher L. (2013). Fischer-Tropsch synthesis: Comparisons between Pt and Ag promoted Co/Al_2O_3 catalysts for reducibility, local atomic structure, catalytic activity, and oxidation-reduction (OR) cycles. *Appl. Catal., A, 464-465*, 165-180. doi: 10.1016/j.apcata.2013.05.040
20. Jermwongratanachai, Thani, Jacobs, Gary, Shafer, Wilson D., Ma, Wenping, Pendyala, Venkat Ramana Rao, Davis, Burtron H., . . . Marshall, Christopher L. (2013). Fischer-Tropsch Synthesis: Oxidation of a Fraction of Cobalt Crystallites in Research Catalysts at the Onset of FT at Partial Pressures Mimicking 50% CO Conversion. *Top. Catal.*, Ahead of Print. doi: 10.1007/s11244-013-0204-1
21. Jermwongratanachai, Thani, Jacobs, Gary, Shafer, Wilson D., Pendyala, Venkat Ramana Rao, Ma, Wenping, Gnanamani, Muthu Kumaran, . . . Davis, Burtron H. (2013). Fischer-Tropsch synthesis: TPR and XANES analysis of the impact of simulated regeneration cycles on the reducibility of Co/alumina catalysts with different promoters (Pt, Ru, Re, Ag, Au, Rh, Ir). *Catal. Today*, Ahead of Print. doi: 10.1016/j.cattod.2013.10.057
22. Kang, Jungshik, Ma, Wenping, Keogh, Robert A., Shafer, Wilson D., Jacobs, Gary, & Davis, Burtron H. (2012). Hydrocracking and Hydroisomerization of n-Hexadecane, n-Octacosane and Fischer-Tropsch Wax Over a Pt/SiO_2-Al_2O_3 Catalyst. *Catal. Lett., 142*(11), 1295-1305. doi: 10.1007/s10562-012-0910-5
23. Klotz, J. L., Bush, L. P., Smith, D. L., Shafer, W. D., Smith, L. L., Arrington, B. C., & Strickland, J. R. (2007). Ergovaline-induced vasoconstriction in an isolated bovine lateral saphenous vein bioassay. *J Anim Sci, 85*(9), 2330-2336.
24. Klotz, J. L., Bush, L. P., Smith, D. L., Shafer, W. D., Smith, L. L., Vevoda, A. C., . . . Strickland, J. R. (2006). Assessment of vasoconstrictive potential of D-lysergic acid

using an isolated bovine lateral saphenous vein bioassay. *J. Anim. Sci. (Savoy, IL, U. S.), 84*(11), 3167-3175. doi: 10.2527/jas.2006-038

25. Ma, Wenping, Jacobs, Gary, Kang, Jungshik, Sparks, Dennis E., Gnanamani, Muthu Kumaran, Pendyala, Venkat Ramana Rao, Wilson D. Shafer, Robert A. Keogh, Uschi M. Graham, Gerald A. Thomas, Davis, Burtron H. (2013). Fischer-Tropsch synthesis. Effect of alkali, bicarbonate and chloride addition on activity and selectivity. *Catal. Today, 215*, 73-79. doi: 10.1016/j.cattod.2013.03.003
26. Masuku, Cornelius Mduduzi, Shafer, Wilson Davis, Ma, Wenping, Gnanamani, Muthu Kumaran, Jacobs, Gary, Hildebrandt, Diane, . . . Davis, Burtron H. (2012). Variation of residence time with chain length for products in a slurry-phase Fischer-Tropsch reactor. *J. Catal., 287*, 93-101. doi: 10.1016/j.jcat.2011.12.005
27. Pendyala, Venkat Ramana Rao, Gnanamani, Muthu Kumaran, Jacobs, Gary, Ma, Wenping, Shafer, Wilson D., & Davis, Burtron H. (2013). Fischer-Tropsch synthesis: effect of ammonia impurities in syngas feed over a cobalt/alumina catalyst. *Appl. Catal., A, 468*, 38-43. doi: 10.1016/j.apcata.2013.07.060
28. Pendyala, Venkat Ramana Rao, Gnanamani, Muthu Kumaran, Ma, Wenping, Jacobs, Gary, Shafer, Wilson D., & Davis, Burtron H. (2013). Fischer-Tropsch synthesis: Effect of ammonia impurities in syngas feed over cobalt catalyst. *Prepr. - Am. Chem. Soc., Div. Energy Fuels, 58*(1), 1041-1042.
29. Pendyala, Venkat Ramana Rao, Jacobs, Gary, Shafer, Wilson D., Keogh, Robert A., Kang, Jungshik, Sparks, Dennis E., & Davis, Burtron H. (2013). Shape-selective alkylation of biphenyl with propylene using zeolite and amorphous silica-alumina catalysts. *Appl. Catal., A, 453*, 195-203. doi: 10.1016/j.apcata.2012.12.011
30. Pendyala, Venkat Ramana Rao, Shafer, Wilson D., & Davis, Burtron H. (2013). Aqueous-Phase Fischer-Tropsch Synthesis: Effect of Reaction Temperature on Ruthenium Nanoparticle Catalyst and Comparison with Supported Ru and Co Catalysts. *Catal. Lett., 143*(9), 895-901. doi: 10.1007/s10562-013-1076-5
31. Shafer, Wilson D., Jacobs, Gary, & Davis, Burtron H. (2012). Fischer-Tropsch Synthesis: Investigation of the Partitioning of Dissociated H_2 and D_2 on Activated Cobalt Catalysts. *ACS Catal., 2*(7), 1452-1456. doi: 10.1021/cs300269m
32. Shafer, Wilson D., Selegue, John P., Jacobs, Gary, & Davis, Burtron H. (2013). An Investigation of the Partitioning of Dissociated H_2 and D_2 on Activated Nickel Catalysts. *Catal. Lett., 143*(12), 1368-1373. doi: 10.1007/s10562-013-1092-5
33. Smith, Darrin, Smith, Lori, Shafer, Wilson, Klotz, James, & Strickland, James. (2009). Development and Validation of an LC-MS Method for Quantitation of Ergot Alkaloids in Lateral Saphenous Vein Tissue. *J. Agric. Food Chem., 57*(16), 7213-7220. doi: 10.1021/jf901086q
34. Sparks, Dennis, Jacobs, Gary, Gnanamani, Muthu Kumaran, Pendyala, Venkat Ramana, Ma, Wenping, Kang, Jungshik, Wilson D. Shafer, Robert A. Keogh, Ursula M. Graham,

Pei Gao, Davis, Burtron H. (2012). Poisoning of cobalt catalyst used for Fischer-Tropsch synthesis. *Prepr. - Am. Chem. Soc., Div. Pet. Chem., 57*(1), 79-81.

35. Sparks, Dennis E., Jacobs, Gary, Gnanamani, Muthu Kumaran, Pendyala, Venkat Ramana Rao, Ma, Wenping, Kang, Jungshik, Wilson D. Shafer, Robert A. Keogh, Ursula M. Graham, Pei Gao, Davis, Burtron H. (2013). Poisoning of cobalt catalyst used for Fischer-Tropsch synthesis. *Catal. Today*, *215*, 67-72. doi: 10.1016/j.cattod.2013.01.011
36. Yang, Jia, Shafer, Wilson D., Pendyala, Venkat Ramana Rao, Jacobs, Gary, Chen, De, Holmen, Anders, & Davis, Burtron H. (2013). Fischer-Tropsch Synthesis: Using Deuterium as a Tool to Investigate Primary Product Distribution. *Catal. Lett.*, Ahead of Print. doi: 10.1007/s10562-013-1164-6
37. Yang, Jia, Shafer, Wilson D., Pendyala, Venkat Ramana Rao, Jacobs, Gary, Ma, Wenping, Chen, De, Davis, Burtron H. (2013). Fischer-Tropsch Synthesis: Deuterium Kinetic Isotopic Effect for a 2.5% Ru/NaY Catalyst. *Top. Catal.*, Ahead of Print. doi: 10.1007/s11244-013-0207-y
38. Jermwongratanachai, Thani; Jacobs, Gary; Shafer, Wilson D.; Ma, Wenping; Pendyala, Venkat Ramana Rao; Davis, Burtron H.; Kitiyanan, Boonyarach; Khalid, Syed; Cronauer, Donald C.; Kropf, A. Jeremy; et al From Topics in Catalysis (2014), 57(6-9), 479-490. DOI:10.1007/s11244-013- 0204-1
39. Yang, Jia; Shafer, Wilson D.; Pendyala, Venkat Ramana Rao; Jacobs, Gary; Ma, Wenping; Chen, De; Holmen, Anders; Davis, Burtron H. From Topics in Catalysis (2014), 57(6-9), 508-517. DOI:10.1007/s11244-013-0207-y
40. Gnanamani, Muthu Kumaran; Jacobs, Gary; Shafer, Wilson D.; Sparks, Dennis E.; Hopps, Shelley; Thomas, Gerald A.; Davis, Burtron H. From Topics in Catalysis (2014), 57(6-9), 612-618. DOI:10.1007/s11244-013- 0219-7
41. Jermwongratanachai, Thani; Jacobs, Gary; Shafer, Wilson D.; Pendyala, Venkat Ramana Rao; Ma, Wenping; Gnanamani, Muthu Kumaran; Hopps, Shelley; Thomas, Gerald A.; Kitiyanan, Boonyarach; Khalid, Syed; et al From Catalysis Today (2014), 228, 15-21. DOI:10.1016/j.cattod.2013.10.057
42. Yang, Jia; Shafer, Wilson D.; Pendyala, Venkat Ramana Rao; Jacobs, Gary; Chen, De; Holmen, Anders; Davis, Burtron H. From Catalysis Letters (2014), 144(3), 524-530. Language: English, Database: CAPLUS, DOI:10.1007/s10562-013- 1164-6
43. Luo, Mingsheng; Shafer, Wilson D.; Davis, Burtron H. From Catalysis Letters (2014), 144(6), 1031-1041. Language: English, DOI:10.1007/s10562-014-1240-6
44. Pendyala, Venkat Ramana Rao; Shafer, Wilson D.; Jacobs, Gary; Davis, Burtron H. From Catalysis Letters (2014), 144(6), 1088-1095. DOI:10.1007/s10562-014-1247-z
45. Ma, Wenping; Jacobs, Gary; Gao, Pei; Jermwongratanachai, Thani; Shafer, Wilson D.; Pendyala, Venkat Ramana Rao; Yen, Chia H.; Klettlinger, Jennifer L. S.; Davis, Burtron H. From Applied Catalysis, A: General (2014), 475, 314-324. DOI:10.1016/j.apcata.2014.01.016
46. Graham, Uschi M.; Jacobs, Gary; Gnanamani, Muthu K.; Lipka, Stephen M.; Shafer, Wilson D.; Swartz, Christopher R.; Jermwongratanachai, Thani; Chen, Rong; Rogers, Fon; Davis, Burtron H. From ACS Catalysis (2014), 4(6), 1662-1672. DOI:10.1021/cs400965t

47. Gnanamani, Muthu Kumaran; Pendyala, Venkat Ramana Rao; Jacobs, Gary; Sparks, Dennis E.; Shafer, Wilson D.; Davis, Burtron H. From Catalysis Letters (2014), 144(7), 1127-1133. DOI:10.1007/s10562-014- 1263-z
48. Pendyala, Venkat Ramana Rao; Jacobs, Gary; Hamdeh, Hussein H.; Shafer, Wilson D.; Sparks, Dennis E.; Hopps, Shelley; Davis, Burtron H. From Catalysis Letters (2014), 144(9), 1624-1635. DOI:10.1007/s10562-014- 1302-9
49. Gnanamani, Muthu Kumaran; Hamdeh, Hussein H.; Jacobs, Gary; Shafer, Wilson D.; Sparks, Dennis E.; Keogh, Robert A.; Davis, Burtron H. From Abstracts of Papers, 248th ACS National Meeting & Exposition, San Francisco, CA, United States, August 10-14, 2014 (2014),
50. Graham, Uschi M.; Jacobs, Gary; Gnanamani, Muthu K.; Lipka, Stephen M.; Shafer, Wilson D.; Swartz, Christopher; Davis, Burtron H. From Abstracts of Papers, 248th ACS National Meeting & Exposition, San Francisco, CA, United States, August 10-14, 2014 (2014)
51. Chakrabarti, Debanjan; Gnanamani, Muthu K.; Shafer, Wilson D.; Ribeiro, Mauro C.; Sparks, Dennis E.; Prasad, Vinay; De Klerk, Arno; Davis, Burtron H. From Abstracts of Papers, 248th ACS National Meeting & Exposition, San Francisco, CA, United States, August 10-14, 2014 (2014), ENFL-566.
52. Shafer, Wilson D.; Jacobs, Gary; Alvez, Gabriela; Snell, Ryan; Hao, Xianghong; Davis, Burtron H. From Abstracts of Papers, 248th ACS National Meeting & Exposition, San Francisco, CA, United States, August 10-14, 2014 (2014), ENFL-619.
53. Shafer, Wilson D.; Jacobs, Gary; Alvez, Gabriela; Snell, Ryan; Hao, Xianghong; Davis, Burtron H. From Preprints - American Chemical Society, Division of Energy & Fuels (2014), 59(2), 842-843.
54. By Graham, U. M.; Jacobs, G.; Gnanamani, M. K.; Lipka, S. M.; Shafer, W. D.; Swartz, C. R.; Davis, B. H. From Preprints - American Chemical Society, Division of Energy & Fuels (2014), 59(2), 818-820.
55. Chakrabarti, D.; Gnanamani, M. K.; Shafer, W. D.; Ribeiro, M. C.; Sparks, D. E.; Prasad, V.; de Klerk, A.; Davis, B. H. From Preprints - American Chemical Society, Division of Energy & Fuels (2014), 59(2), 825-827.
56. Pendyala, Venkat Ramana Rao; Shafer, Wilson D.; Jacobs, Gary; Graham, Uschi M.; Khalid, Syed; Davis, Burtron H. From Catalysis Letters (2015), 145(3), 893-904. DOI:10.1007/s10562-014- 1462-7
57. Chakrabarti, Debanjan; de Klerk, Arno; Prasad, Vinay; Gnanamani, Muthu Kumaran; Shafer, Wilson D.; Jacobs, Gary; Sparks, Dennis E.; Davis, Burtron H. From Industrial & Engineering Chemistry Research (2015), 54(4), 1189-1196. DOI:10.1021/ie503496m
58. Gnanamani, Muthu Kumaran; Shafer, Wilson D.; Pendyala, Venkat Ramana Rao; Chakrabarti, Debanjan; de Klerk, Arno; Keogh, Robert A.; Sparks, Dennis E.; Davis, Burtron H. From Topics in Catalysis (2015), 58(4-6), 343-349. DOI:10.1007/s11244-015- 0375-z
59. Jacobs, Gary; Martinelli, Michela; Shafer, Wilson D.; Graham, Uschi; Davis, Burtron H. From Abstracts of Papers, 249th ACS National Meeting & Exposition, Denver, CO, United States, March 22-26, 2015 (2015), CATL-27.
60. Martinelli, Michela; Jacobs, Gary; Graham, Uschi M.; Shafer, Wilson D.; Cronauer, Donald C.; Kropf, A. Jeremy; Marshall, Christopher L.; Khalid, Syed; Visconti, Carlo

G.; Lietti, Luca; et al From Applied Catalysis, A: General (2015), 497, 184-197. DOI:10.1016/j.apcata.2014.12.055
61. Ma, Wenping; Jacobs, Gary; Thomas, Gerald A.; Shafer, Wilson D.; Sparks, Dennis E.; Hamdeh, Hussein H.; Davis, Burtron H. From ACS Catalysis (2015), 5(5), 3124-3136. DOI:10.1021/acscatal.5b00023
62. Gnanamani, Muthu Kumaran; Jacobs, Gary; Keogh, Robert A.; Shafer, Wilson D.; Sparks, Dennis E.; Hopps, Shelley D.; Thomas, Gerald A.; Davis, Burtron H. From Applied Catalysis, A: General (2015), 499, 39-46. DOI:10.1016/j.apcata.2015.03.046
63. Chakrabarti, Debanjan; Gnanamani, Muthu Kumaran; Shafer, Wilson D.; Ribeiro, Mauro C.; Sparks, Dennis E.; Prasad, Vinay; de Klerk, Arno; Davis, Burtron H. From Industrial & Engineering Chemistry Research (2015), 54(25), 6438-6453. DOI:10.1021/acs.iecr.5b01402
64. Shafer, Wilson D.; Pendyala, Venkat Ramana Rao; Gnanamani, Muthu Kumaran; Jacobs, Gary; Selegue, John P.; Hopps, Shelley D.; Thomas, Gerald A.; Davis, Burtron H. From Catalysis Letters (2015), 145(9), 1683-1690. Language: English, DOI:10.1007/s10562-015-1587-3
65. Gao, Pei; Graham, Uschi M.; Shafer, Wilson D.; Linganiso, Linda Z.; Jacobs, Gary; Davis, Burtron H. From Catalysis Today (2015), Ahead of Print, DOI:10.1016/j.cattod.2015.07.007
66. Jacobs, Gary; Shafer, Wilson D.; Azzam, Khalid; Davis, Burtron H. From Abstracts of Papers, 250th ACS National Meeting & Exposition, Boston, MA, United States, August 16-20, 2015 (2015), CATL-97.
67. Gnanamani, Muthu Kumaran; Jacobs, Gary; Graham, Uschi M.; Ribeiro, Mauro C.; Noronha, Fabio B.; Shafer, Wilson D.; Davis, Burtron H. From Catalysis Today (2015), Ahead of Print., DOI:10.1016/j.cattod.2015.08.047